SCHOOL OF INDUSTRIAL AND INFORMATION ENGINEERING
MASTER OF SCIENCE IN SPACE ENGINEERING

POLITECNICO
DI MILANO

Technische Universität
München

MASTER THESIS IN SPACE PROPULSION

Prediction of Thermo-Physical Properties of Commercially Available Methane Mixtures

External Supervisors - TUM
Prof. Oskar Haidn
Dr. Nadezda Slavinskaya
Internal Supervisor - PoliMi
Prof. Filippo Maggi

Tiziano Santese
ID 944005

Academic Year 2020-2021

List of Symbols

Acronyms

EoS	Equation of state
FL	Frenkel Line
LCH_4	Liquid methane
LH_2	Liquid Hydrogen
LJ	Lennard Jones
LO_x	Liquid Oxygen
CFD	Computational Fluid-Dynamics
FEM	Finite Element Method
LNG	Liquid Natural Gas
MD	Molecular Dynamics
RP-1	Refined-Petroleum-1
WL	Widom Line

General

α	Dimensionless Helmholtz free energy
α_P	Isobaric thermal expansion coefficient
δ	Reduced density in GERG-2008
ϵ	LJ depth of potential
η	Viscosity coefficient
Γ	Collision rate
γ	Surface tension
λ	Thermal conductivity
μ	Joule-Thomson coefficient
ω	Acentric factor
$\Omega^{(l,m)}$	Reduced collision inegrals
ρ	Density
σ	Diameter of the molecule/LJ parameter
τ	Inverse-reduced temperature in GERG-2008
τ_{rt}	Relaxation time
φ	Potential between two molecules
φ_i	Fugacity coefficient of i-th component
Ξ	Virial
a	Helmholtz free energy
c_P	Isobaric heat capacity
c_v	Specific heat at constant volume
D	Diffusion coefficient
G	Gibbs free energy
$g(r)$	Radial distribution function
k	Boltzmann's constant
k_T	Isothermal compressibility
M	Molar mass
m	Molecular weight
n	Number of molecules per unit volume
N_a	Avogadro number
p	Pressure
R	Universal gas constant
r	I distance
s	Entropy
T	Temperature
V	Volume
w	Speed of sound
x_i	Mole fraction i-th component
Z	Compressibility factor
B,C,D	Second,third,fourth virial coefficient

Superscript and subscript

$\tilde{}$	Quantities per mole
*	Reduced with respect to potential parameters
^{o}	Ideal-gas contribution
^{r}	(superscript) Residual contribution
$_c$	Critical parameter
$_r$	(subscript) Reduced with respect to critical constants

Contents

List of Figures

List of Tables

Abstract

The research for green sources of power is pushing in every technological sector, and methane is an attractive choice for space applications since it could be implemented as a fuel in couple with LO_x, substituting the actual use of LH_2. Since pure methane would be extremely expensive, methane-based mixtures have to be considered. In this work, some of the major challenges regarding the use of these mixtures are faced, trying to understand how they behave at high temperatures and pressures, and what are the potentially dangerous areas on a pressure-temperature diagram. Firstly, a general background of knowledge about gases, liquids and mixtures is given. Secondly, thermodynamic and transport properties for methane mixtures are evaluated in the supercritical region, with a code that implements the recent GERG-2008 EoS, which can grant the highest accuracy for hydrocarbons mixtures; here, ethane, propane, nitrogen, and hydrogen are considered as impurities with a mole fraction up to the 5%. The results are analysed to find the so-called Widom Lines, which are the locus of points in supercritical region, where many properties show pronounced extrema. However, these peaks vanish at higher pressures, and then, to visualize where these extrema are more pronounced, a "Widom Area" is depicted around each Widom Line, and it is defined as a region where strong gradients, above a certain threshold, are found. Many examples for different mixtures are given to underline how even a little amount of impurities can have strong effects on the supercritical behaviour of a mixture.
Lastly, another kind of crossover, present in the supercritical state, is described. Viscosity coefficient and speed of sound are evaluated, to show the presence of a structural rather than a thermodynamic change in fluid atoms that causes a variation in the behaviour of those properties. Transport properties and speed of sound present minima that can be traced up to very high pressures, identifying what is called Frenkel Line, and this is done using a recent prediction method for the evaluation of the viscosity coefficient.

0 Motivation of the work and achievements

In recent years liquid methane is under investigation as a possible fuel for liquid rocket engines. Oxygen/methane is a very attractive propellant combination for this application, as it provides an increment of 50s specific impulse, with respect to the actually used storable propellants, namely liquid oxygen and refined petroleum-1 (RP-1). But this would not be the only advantage; the combination LO_x/LCH_4 may be said to be "space storable", which means that once in space, when temperatures are much lower, depending on the tank pressure, the methane can remain in the liquid state and then be used in any moment, without the need of an expensive cooling system. On this point, it is clear the difference between liquid methane and hydrogen: even though LO_x/LH_2 is the most performing propellant couple actually available on the market, it has many drawbacks; firstly the incredibly low energy density, due to the low atomic mass of the hydrogen, that causes the need of large volume of fuel to get a certain energy budget. But this is not enough, because hydrogen is also extremely difficult to be handled from a thermal point of view since it requires operating temperatures near 20 K that are difficult to reach and keep on the ground and impossible in space.
Then, even if methane has a significantly lower specific impulse than hydrogen, it has the key advantages of an approximately 2.6 times higher energy density, which allows smaller tank volume, and needs less powerful turbopumps thanks to the significantly higher fluid density. Moreover, for methane only passive thermal protection is required, and its boiling rates are significantly lower than for hydrogen. At the same time, if methane is compared with RP-1, they are both space storable, with a comparable fluid density but methane has a higher specific impulse.
Another significant advantage is the absence of risks to human health, in both the production and transportation chain. For this reason, they are often considered "green propellants". This promotes the use of methane also from an environmental point of view, in a period in which every technological sector must adapt its products to sustain the worldwide challenge of a cleaner ecosystem.

Then, what is the actual state of the art of liquid methane in space applications? What are its drawbacks?

Liquid methane and liquid oxygen seem to be the favourite couple for the next generation of engines for all the principal space companies all over the world.
The most advanced example of this technology can be found in the USA, with the *Raptor* engine. It is a family of full-flow staged combustion cycle rocket engines developed by SpaceX, that uses LO_x and LCH_4 and that will power "the super-heavy-lift Starship system", overcoming the actual Merlin, since the Raptor has twice its thrust. Also, Blue Origin has developed its own LNG fueled rocket engine, the *BE-4* that has still to be qualified for flight, and is planned to launch the Vulcan Centaur vehicle, the successor of the AtlasV.
In Europe, LO_x and LCH_4 are going to be employed in future space applications, with the Prometheus engine that is under development by ESA to prepare the next generation of engines to be used with the Ariane-6 (or its successor) and the MIRA-LM10 on which Avio is working for use on the smaller Vega-E.
Also in China, the LNG engine named TQ-12 is being designed by Landscape.

0.1 Objectives

One of the main complications in the design of a LO_x-LCH_4 engine is the fact that the critical parameters of the methane are close to the usual operating conditions of the cooling channels and the injectors of a rocket engine. Since the operating conditions are near to the critical point

of methane, the irregularities in the behaviour of thermodynamic properties (like density, heat capacity, thermal expansion etc.) in the supercritical region can be strong and should be accounted during the heat transfer evaluations. With hydrogen instead, the usual operations occur at temperature and pressure which are always supercritical but much higher than the critical point, and those irregularities are avoided. The irregular behaviour is also avoided if the chamber pressure is kept very high; in this way the critical point and all the irregularities are far away from the operating conditions, as it is done in the Raptor engine (up to 300 bar), the only one fully qualified and operational.

In this work, we are more interested in lower pressure values, that are required in expander cycle engines, where the pressures are limited to values below 80 bar, and in booster engines such the Prometheus which will use pressure up to 100 bar. For this reason, complete knowledge of the behaviour of the methane properties in the interested near-critical and supercritical region is required and will be investigated in this work; in this way more accurate values for thermodynamic properties and transport properties would be accessible for the various analysis that are necessary to prepare the mission: CFD analysis for heat transfer evaluation, FEM for structural design etc.

The interesting intervals of temperature and pressure, where properties show a maximum (or minimum) are defined with the so-called Widom-line (or pseudoboiling-line) [8],[32], and by crossing this line, the properties gradient changes its sign, like it can be observed in subcritical conditions; however these extrema vanish at reduced pressure higher than 3. These lines, the mixture properties and the identification of the area where strong gradients are found will be the primary objective of this work, in order to have a precise knowledge of thermodynamic parameters of methane near the critical area.
Besides, it has to be taken into account that the use of chemical pure methane would lead to extremely high costs for real operations and that the use of already operating liquefied natural gas (LNG) would be significantly more cost-efficient. The analyzed propellant will then include different impurities, which can influence the thermodynamic properties of fuel; in particular light hydrocarbons, nitrogen and hydrogen. No carbon dioxide is taken into account since its triple point parameters are much higher than the triple point values of methane; this means that solid carbon dioxide can be present within liquid or vapour methane depending on the pressure. Carbon dioxide was then excluded from the analysis because, to keep safe the rocket engine, CO_2 should be avoided completely from the fuel, especially for conditions below the carbon dioxide triple point. The GERG-2008 model has been chosen as Equation of State since it is the most suitable to describe hydrocarbons mixtures even beyond the critical point. The whole description is taken from [25].

Another important achievement of this thesis is the evaluation of viscosity, and the use of its behaviour to identify another kind of supercritical crossover, the Frenkel Line. This line describes a structural rather than thermodynamic change in the fluid atoms. It was first described by Frenkel, [14] and then by several other authors. A more recent description is found in [42] by Brazhkin et al.. The relaxation time is introduced to explain how this change affects the fluid properties and how this crossover creates minima in the behaviour of transport properties and speed of sound. If the irregularities in thermodynamic properties that can be found after the critical point disappear at higher pressure, the Frenkel line and its structural transformation can be traced up to indefinitely high pressure values, resulting essential for those applications that work at very high pressure, like the Raptor engine of SpaceX.

0.2 Presentation plan

In general, very limited information can be found in open literature related to the thermodynamic and transport properties of mixtures in supercritical states determining behaviour of propellant and heat transport processes under rocket engine operation conditions.
The present work begins with a wide introduction on the fundamental methods to describe liquids, gases and mixtures and their peculiar features. Subsequently, starting from the chosen EoS, it shows the calculations of several thermodynamic properties for methane-based mixtures in supercritical region, the identification of the extrema's coordinates of those properties, and then the definition of an area, called "Widom Area", where strong gradients are found.
The work is concluded with the evaluation of the viscosity coefficient through a recent prediction method, and both viscosity and speed of sound are used to give the first hint on the localization of the Frenkel line, for methane-based mixtures.

Abstract - Italiano

La ricerca di sorgenti di energia ecosostenibili sta accelerando in ogni settore tecnologico, e il metano è una scelta molto attraente per applicazioni spaziali, in quanto può essere impiegato in coppia con l'ossigeno liquido (LO_x), sostituendo l'idrogeno liquido (LH_2). Poiché l'utilizzo del metano puro sarebbe estremamente costoso, bisogna considerare miscele a base di metano, che contengano altre impurità. In questo lavoro, vengono affrontate alcune delle più grandi problematiche riguardanti l'utilizzo di queste miscele, provando a capire il loro comportamento ad alte temperature e pressioni, e ad individuare le aree potenzialmente pericolose su un diagramma pressione-temperatura. Nella fase iniziale del lavoro, vengono presentati i principi fondamentali per la descrizione di gas, liquidi e miscele. Successivamente, diverse proprietà termodinamiche vengono valutate in stato supercritico per miscele di metano, con frazioni molari fino al 5% di etano, propano, azoto e idrogeno. A tale scopo, è stata scelta la recente equazione di stato GERG-2008 [25], la quale garantisce un'elevata accuratezza per miscele di idrocarburi, anche oltre il punto critico. I risultati sono poi analizzati per trovare le "Widom Lines", ovvero il luogo dei punti nella regione supercritica, in cui alcune proprietà termodinamiche presentano dei massimi o dei minimi. Queste linee indicano una transizione nello stato supercritico del fluido, passando da una struttura simile a quella di un liquido, ad una simile a quella di un gas. Questi picchi tuttavia, anche se ancora individuabili, si affievoliscono a pressioni più elevate, e per definire la regione in cui tali estremi sono associati a forti gradienti, una "Widom Area" è stata individuata attorno a ogni Widom Line, definendola come la regione di piano in cui la variazione di una particolare funzione termodinamica supera una certa soglia.
Infine, viene descritta un'ulteriore transizione nella struttura del fluido, questa volta di carattere dinamico, e non termodinamico, che può essere identificata fino a pressioni molto alte. Questa linea, chiamata "Frenkel line", è associata al comportamento delle proprietà di trasporto, e pertanto, il coefficiente di viscosità è stato calcolato, utilizzando un recente modello di previsione che utilizza la stessa equazione di stato di questo lavoro. I minimi del coefficiente di viscosità e della velocità del suono vengono poi utilizzati per tracciare la Frenkel Line.

Motivazione del lavoro e risultati attesi - Italiano

Negli ultimi anni il metano liquido è oggetto di studio come possibile combustibile liquido per motori a razzo. Ossigeno/metano è una combinazione di propellenti molto interessante per questa applicazione, in quanto fornisce un incremento di impulso specifico di $50s$, rispetto ai propellenti immagazzinabili attualmente utilizzati, ovvero ossigeno liquido e petrolio raffinato-1 (RP-1). Ma questo non sarebbe l'unico vantaggio; la combinazione LO_x/LCH_4 può dirsi "*space-storable*", il che significa che una volta nello spazio, quando le temperature sono molto più basse, a seconda della pressione del serbatoio il metano può rimanere allo stato liquido e quindi essere utilizzato in qualsiasi momento, senza la necessità di un dispendioso sistema di raffreddamento. È quindi evidente la differenza tra il metano e l'idrogeno liquido: sebbene LO_x/LH_2 sia la coppia propellente più performante attualmente disponibile sul mercato, presenta molti inconvenienti; in primo luogo la densità energetica incredibilmente bassa, dovuta alla bassa massa atomica dell'idrogeno, che determina la necessità di grandi volumi di combustibile per ottenere un certo budget energetico. Ma questo non basta, perché l'idrogeno è anche estremamente difficile da gestire dal punto di vista termico, poiché richiede temperature di esercizio prossime ai 20 K, difficili da raggiungere e mantenere a terra e impossibili nello spazio.
Quindi, anche se il metano ha un impulso specifico significativamente inferiore rispetto all'idrogeno, ha come vantaggi chiave, una densità di energia circa 2.6 volte superiore all'idrogeno, che consente un volume del serbatoio più piccolo e richiede una potenza inferiore della turbopompa, grazie alla densità del fluido significativamente più elevata. Inoltre, per il metano è necessaria solo una protezione termica passiva e i suoi tassi di ebollizione sono notevolmente inferiori a quelle dell'idrogeno. Allo stesso tempo, se il metano viene confrontato con l'RP-1, questi sono entrambi *space-storable*, con una densità di fluido comparabile, ma il metano ha un impulso specifico maggiore.
Un altro vantaggio significativo è l'assenza di rischi per la salute umana, sia nella catena di produzione che di trasporto. Per questo motivo viene considerato un propellente "green". Questo fattore sprona all'utilizzo del metano anche da un punto di vista ambientale, in un periodo in cui ogni settore tecnologico deve adattare i propri prodotti per sostenere la sfida mondiale di un ecosistema più pulito.

Quindi qual è l'attuale stato dell'arte del metano liquido in applicazioni spaziali? Quali sono i suoi svantaggi?

Metano liquido e ossigeno liquido sembrano essere la coppia preferita per la prossima generazione di motori per tutte le principali compagnie spaziali di tutto il mondo.
L'esempio più avanzato di questa tecnologia si trova negli USA, con il motore *Raptor*. Si tratta di una famiglia di motori a razzo con ciclo di combustione a stadi a flusso pieno, sviluppati da SpaceX, che utilizza LO_x e LCH_4 e che alimenterà la nuova "super-heavy-lift Starship system", soprassedendo l'attuale Merlin, rispetto al quale può generare più del doppio della spinta. Anche Blue Origin ha sviluppato un proprio motore a razzo alimentato a GNL, il *BE-4* che deve ancora essere qualificato per il volo, e che prevede di lanciare il Vulcan Centaur, il successore dell'AtlasV.
In Europa, LO_x e LCH_4 saranno impiegati nelle future applicazioni spaziali, con il motore Prometheus che è in fase di sviluppo da parte dell'ESA per preparare la prossima generazione di motori da utilizzare con l'Ariane-6 (o il suo successore) e il MIRA-LM10 su cui Avio sta lavorando per l'utilizzo sul più piccolo Vega-E.
Anche in Cina, il motore a GNL denominato TQ-12 è in fase di progettazione ad opera di Landscape.

Obiettivi

Una delle principali complicazioni nella progettazione di un motore LO_x-LCH_4 è il fatto che i parametri critici del metano siano vicini alle normali condizioni operative dei canali di raffreddamento e degli iniettori di un motore a razzo. Poiché le condizioni operative sono vicine al punto critico del metano, le irregolarità nel comportamento delle proprietà termodinamiche (come densità, capacità termica, espansione termica ecc.) nella regione supercritica possono essere forti e dovrebbero essere considerate durante le valutazioni del trasferimento di calore. Con l'idrogeno invece, le normali operazioni avvengono a temperatura e pressione sempre supercritiche ma molto superiori al punto critico, e si evitano quelle irregolarità. Il comportamento irregolare viene evitato anche se la pressione della camera viene mantenuta molto alta; in questo modo il punto critico e tutte le irregolarità sono lontani dalle condizioni di esercizio, come avviene nel motore Raptor (fino a 300 bar), l'unico pienamente qualificato ed operativo.

In questo lavoro si è più interessati a valori di pressione inferiori, che sono richiesti nei motori a ciclo espansore, dove le pressioni sono limitate a valori inferiori a 80 bar, e nei motori booster come il Prometheus che utilizzerà pressioni fino a 100 bar. Per questo motivo è richiesta una conoscenza completa del comportamento delle proprietà del metano nella regione quasi critica e supercritica interessata; in questo modo sarebbero accessibili valori più accurati per le proprietà termodinamiche e le proprietà di trasporto per le varie analisi necessarie per preparare la missione: analisi CFD per la valutazione del trasferimento di calore, FEM per la progettazione strutturale ecc.

Gli intervalli di temperatura e pressione interessati, dove le proprietà mostrano un massimo (o un minimo) sono definiti dalla cosiddetta Widom-line (o pseudoboiling-line) [8],[32], e attraversando tale linea, il gradiente delle proprietà cambia di segno, come osserviamo anche che in condizioni subcritiche; tuttavia questi estremi svaniscono a pressioni ridotte maggiori di 3. Tali linee, le proprietà della miscela e l'identificazione dell'area dove si trovano forti gradienti, saranno l'obiettivo primario di questo lavoro, al fine di avere una conoscenza precisa dei parametri termodinamici delle miscele di metano vicino all'area critica.
Inoltre, si deve tener conto del fatto che l'uso del metano puro comporterebbe costi estremamente elevati per le operazioni reali e che l'uso di gas naturali liquefatti (LNG) già operativi sarebbe significativamente più efficiente in termini di costi. Il propellente analizzato includerà quindi diverse impurità, che possono influenzare le proprietà termodinamiche del combustibile; in particolare idrocarburi leggeri, azoto e idrogeno. Non si tiene conto dell'anidride carbonica poiché i valori del suo punto triplo sono molto più alti dei valori del punto triplo del metano; ciò significa che anidride carbonica solida potrebbe essere presente all'interno del metano liquido o gassoso a seconda della pressione. L'anidride carbonica è stata quindi esclusa dall'analisi perché, per mantenere al sicuro il motore del razzo, la CO_2 dovrebbe essere evitata completamente dal carburante, soprattutto per condizioni al di sotto del punto triplo dell'anidride carbonica.

L'ultimo punto che verrà trattato in questo lavoro è la valutazione della viscosità, e l'analisi del suo andamento per identificare un altro tipo di crossover supercritico, la Frenkel Line. Questa linea descrive un cambiamento strutturale piuttosto che termodinamico negli atomi del fluido. È stato descritto prima da Frenkel, [14] e poi da diversi altri autori; una più recente descrizione del fenomeno può essere trovata nel lavoro di Brazhkin et al. [42] . Il "tempo di rilassamento" viene introdotto per spiegare come questo cambiamento influenzi le proprietà del fluido, e che questo crossover crei minimi nel comportamento delle proprietà di trasporto e nella velocità del suono.
Se le irregolarità nelle proprietà termodinamiche che si possono trovare dopo il punto critico scompaiono a pressioni più elevate, la linea di Frenkel e la trasformazione strutturale che la caratterizza possono essere rintracciate fino a valori di pressione indefinitamente alti, risultando essenziale per

quelle applicazioni che lavorano ad altissima pressione, come il motore Raptor di SpaceX.

Piano di presentazione

In generale, in open-literature si possono trovare informazioni molto limitate relative alle proprietà termodinamiche e di trasporto della miscela in stati supercritici, e queste proprietà determinano l'andamento degli scambi di calore e il comportamento generale del propellente in condizioni di funzionamento del motore a razzo. Questo lavoro comincia presentando i metodi fondamentali per descrivere liquidi, gas e miscele, e le loro caratteristiche peculiari. Successivamente, dopo aver scelto l'equazione di stato più adatta, vengono presentati i calcoli di diverse proprietà termodinamiche per miscele a base di metano in regione supercritica, l'identificazione delle coordinate degli estremi di tali proprietà e la definizione di un'area, chiamata "Widom Area", dove si trovano forti gradienti, vengono presentati.
Il lavoro si conclude con la valutazione del coefficiente di viscosità attraverso un recente metodo di previsione; successivamente la viscosità e la velocità del suono vengono utilizzate per dare un primo indizio sulla localizzazione della Frenkel line, per miscele a base di metano.

1 Background knowledge

1.1 Equation of state

The equation of state and the transport properties of fluids are strongly related to the intermolecular attraction and repulsion of molecules. Those theories that related the macroscopic properties of the fluid to these intermolecular forces are highly developed for dilute gases and less for dense gases or liquids.

For a gas, made up of particles without volume and between which no intermolecular force is considered, the equation of state (EoS) is the well-known perfect gas EoS, presented in Eq. (1).

$$p\tilde{V} = RT \tag{1}$$

However, a highly diluted gas shows deviation from Eq. (1) even at atmospheric pressure. Then, this equation is not accurate to describe a real fluid, since it is based on a too simplified model.

Van Der Waals tried to modify the equation in order to obtain a more realistic representation of a real fluid; his model, in Eq. (2), achieves a quite good description of the gas phase and a qualitative one for the liquid phase.

$$\left(p + \frac{a}{\tilde{V}^2}\right)(\tilde{V} - b) = RT \tag{2}$$

His equation presents two parameters, a accounts for the attractive forces between molecules and b takes into account the volume of the particles. Clearly, this model is only an approximation and gives reasonable results only in a limited range of temperatures and pressures. To extend the validity range up to higher temperatures or to the liquid phase, several modifications or new empirical equations of state have been proposed, some of which will be presented in this discussion in the following sections.

Very often, to measure how much the fluid's behaviour is far from the perfect gas model, the *compressibility factor* is used. It is defined as the ratio $p\tilde{V}/RT$ and is indicated as Z; $Z = 1$ means that there is no interaction between molecules, and the gas is behaving like a *perfect gas*. Instead, a compressibility factor different from 1 means that the interaction forces between molecules are not negligible and play an important role in the behaviour of the fluid; these forces can be attractive or repulsive and will be better described later on. More realistic equations of state are capable of measuring the compressibility factor, namely, the deviation from ideality.

One of the most known relations to describe the EoS of a real fluid is the so-called *Virial Equation of State*, presented in Eq. (3).

$$\frac{p\tilde{V}}{RT} = 1 + B(T)/\tilde{V} + C(T)/\tilde{V}^2 + D(T)/\tilde{V}^3... \tag{3}$$

where the functions B(T),C(T), D(T)... are called *second, third.. Virial Coefficients* and have to be evaluated for different fluids and different conditions. This kind of representation has been widely used in the past decades and the second and third virial coefficients have been tabulated for many components in many temperature conditions.

1.2 Transport Coefficients

Primary importance is given to the capacity of transporting some physical properties through the gas or liquid, and this capability is measured by "*Transport Coefficients*". The main parameters that describe this kind of transfer are:

- Ordinary Diffusion: the transfer of mass, due to a gradient in concentration;

- Viscosity: the transfer of momentum, due to a gradient of velocity;

- Thermal Diffusion: transfer of thermal energy, due to a gradient of temperature.

It has to be noticed that in rigorous models these effects are related to each other; for example, diffusion may also result from a temperature gradient (known as Soret effect), or transfer of energy could result from concentration gradient (Dufour effect). The evaluation of these properties is usually very difficult and a variety of methods has been proposed to predict or calculate their value. However, in an ultra-simplified and completely unrealistic theory, very simple relations can be retrieved, that show a surprisingly good estimation of the transport coefficients.
Let's consider all the molecules as rigid non-attracting spheres with a certain diameter, σ; moreover, it is supposed that all the molecules move with the same speed (it was decided to use the arithmetic mean speed, calculated from the velocity distribution function), $\Omega = (8kT/m\pi)^{1/2}$, where k is the Boltzmann constant, T the temperature and m is the molecule mass. As a further hypothesis, it is considered that all the molecules travel only along with the directions which are parallel to the coordinate axis.

Now in these conditions, it is very easy to evaluate the *collision rate* Γ of a molecule, namely the number of collisions suffered per unit time.

$$\Gamma = \left(\frac{1}{3} + \frac{2}{3}\sqrt{2}\right) n\pi\sigma^2\Omega$$

where n is the total number of molecules considered per unit volume. From the collision rate and the assumption of rigid molecules, the *mean free path* l can be retrieved, namely the average distance that a molecule travels between one collision and the following one.

$$l = \frac{\Omega}{\Gamma}$$

Starting from these relations and with few other considerations, reported in [4], the transport coefficient can be expressed as in Eq. (4),Eq. (5) and Eq. (6).

$$D = \frac{1}{3}\Omega l = \frac{\lambda m}{\rho c_v} \tag{4}$$

$$\eta = \frac{1}{3} nm\Omega l = \rho D \tag{5}$$

$$\lambda = \frac{1}{3} nc_v\Omega l = \frac{c_v\eta}{m} \tag{6}$$

The development of the rigorous kinetic theory to the rigid sphere model brings to this exact same results with slightly different coefficients. Using those values and rewriting some terms, more practical definitions of the three quantities can be given as follows.

$$D = 2.6280 \cdot 10^{-3} \frac{\sqrt{T^3/M}}{p\sigma^2} \tag{7}$$

$$\eta = 2.6693 \cdot 10^{-5} \frac{\sqrt{TM}}{\sigma^2} \tag{8}$$

$$\lambda = 1.9891 \cdot 10^{-4} \frac{\sqrt{T/M}}{\sigma^2} \tag{9}$$

From the above results, some preliminary interdependencies can be understood: diffusion varies as the three-halves power of the temperature and is inversely proportional to the pressure;

viscosity and thermal conductivity are independent of the pressure and increase with the square root of the temperature. All the coefficients are inversely proportional to σ^2, which is linked to the *collision diameter* of the molecule. As it will be shown in the frame of the Chapman-Enskog theory, these are only approximate pressure and temperature dependence for real gases, since no interaction between molecules is considered.

1.3 Intermolecular Potential

Up to this point no interaction has been considered, however it is well known that two molecules attract each other when sufficiently far away and repel each other when close enough.
Then, to leave the simplified model in which molecules have no volume, the description of the interaction of the molecules is required. This is a hard task, and the knowledge of intermolecular forces is obtained from both experimental observation and theoretical considerations. The theory gives the functional form, while experimental data are used to determine the adjustable parameters.
It is clear that the force of interaction, F, is a function of the distance between molecules, r; however, it is usually more convenient to use the interaction potential $\varphi(r)$ rather than the force. These two quantities are linked as follow:

$$\varphi(r) = \int_r^\infty F(r)dr$$

Different intermolecular potential energy functions have been defined, and each of them presents some peculiar features and a different accuracy and complexity. Some of them have to be used for *polar* molecules, namely those molecules that present a partial positive charge on a side of the molecule and a negative partial charge on the other, and some of them instead can be used for *non-polar* molecules, and so molecules without partial charges.

The most used potential for polar molecules is the *Stockmayer Potential*, while for non polar molecules it is widely used the *Lennard-Jones 6-12 potential*; many properties have been evaluated in terms of these two models. In this treatment, since methane is a non-polar molecule, only a couple of potentials suitable for this type of molecules will be presented. It has to be pointed out that all the different potentials that will be discussed, are suitable for simple molecules; long molecules or excited molecules cannot be described by those potentials.

Let's give now a brief description of the types of forces involved; there could be an arbitrary division between *short and long range forces*. Short range forces (or Valence forces) arise when the molecules come close enough to have their electron cloud overlapping. These are repulsive forces that are not very accurately described due to the lack of knowledge, and are usually approximated with an oversimplified form, like the following,[4]:

$$\varphi^{short} = be^{-a(r/a_0)}$$

whose parameters depend on the ionization potentials of the two molecules.
A more detailed description is available for long range forces; these forces are generally divided into three contributions:

- Electrostatic Contributions; due to the interaction of the various multipole moments in the molecules; inside the molecule, there could be charges, dipole moments or quadrupole moments, and all these effects are angular dependent (i.e. depend on the orientation of the molecules).

- Induction contribution; when only one of the two molecules have a net charge, this creates an induced dipole (polar/non-polar interaction).

- Dispersion Contributions; Interaction between two non-polar molecules. The random configuration of electrons can generate a temporary (or instantaneous) dipole, that would generate another instantaneous dipole on the other molecule.

1.4 Equation of State - Low and moderate density

The interest moves now on how the *virial equation of state*, presented in Eq. (3), can be obtained. Moreover, it has to be pointed out that the virial expansion is limited by the convergence of the series, which diverges at about the density of the liquid phase; hence, the primary application of the virial equation is the study of gases at low and moderate density.
There are mainly two ways to obtain the virial equation of state,[4]: one starts from the definition of the partition function and the other is based on the classical mechanics virial theorem; here only the second method is quickly presented.

The *Virial Theorem* states that, for a system of N molecules with mass m, and ignoring internal degrees of freedom of the molecules, the average total kinetic energy of the molecules $\overline{K}$ is equal to the virial Ξ, defined as follow:

$$\overline{K} = \frac{1}{2}\sum_i m v_i^2 = \Xi = -\frac{1}{2}\sum_i \overline{\mathbf{r_i} \cdot \mathbf{F_i}}$$

where for each molecule, $\mathbf{r_i}$ is the position vector and F_i is the force vector; the latter has to account for the force exerted from all the other molecules and for the restraining force of the vessel.
By dividing these two contributions into the virial of intermolecular forces, Ξ_i, and the virial of external forces, Ξ_e, the virial theorem can be rewritten as $\overline{K} = \Xi_i + \Xi_e$; exploiting those terms and rearranging, [4], the product pV can be obtained in terms of the total kinetic and intermolecular potential energy of molecules, as follows:

$$pV = \frac{2}{3}\sum_{i=1}^{N} \overline{\frac{p_i^2}{2m}} - \frac{1}{3}\sum_{i=1}^{N} \overline{\left(\mathbf{r_i} \cdot \frac{\partial \varphi(\mathbf{r^N})}{\partial \mathbf{r_i}}\right)}$$

Since the bar indicates time averages, they can be replaced by averages over an ensemble[1], and by making use of classical probability density, it can be obtained:

$$pV = NkT - \frac{1}{3(N-1)!\lambda^{3N} Z_N}\int W_N(\mathbf{r^N})\left(\mathbf{r_i} \cdot \frac{\partial \varphi(\mathbf{r^N})}{\partial \mathbf{r_i}}\right) d\mathbf{r^N} \tag{10}$$

where $\lambda^2 = h^2/2\pi mkT$, Z_N is the partition function[2], and $W_N(\mathbf{r^N}) = e^{-\varphi(\mathbf{r^N})/kT}$ is the *Boltzmann factor*.
Note that If $\varphi = 0$, it goes to the ideal-gas law.
If it is assumed that the potential energy of the system is the sum of the potential energy of pairs of molecules, $\varphi(\mathbf{r^N}) = \frac{1}{2}\sum_i \sum_j \varphi(r_{ij})$, then the Eq. (10) can be rearranged as:

$$pV = NkT - \frac{2\pi N(N-1)}{3V}\int g(r)\left(\frac{d\varphi}{dr}\right) r^3 dr$$

where $g(r)$ is a pair distribution function; the absence of higher order functions is the result coming from the assumption just made.

[1] Microcanonical ensemble. It is a close group of N molecules, in a fixed volume V, where the energy is related to kinetic motion and intermolecular forces; the energy is conserved.
[2] look at [4] for its definition.

1.4.1 Virial Coefficients

Here, only angle independent potentials are considered. The following discussion is based on the assumption of additivity of forces, already done in the last previous passage; this assumption is generally valid except for molecules that tend to associate and molecules capable of hydrogen bonding.
The virial coefficients can also be evaluated with both the two methods cited previously, but also in this case, only the results coming from the virial theorem are presented, [4], in Eq. (11) and Eq. (12).

$$B(T) = -\frac{2\pi\tilde{N}}{3kT}\int_0^\infty r^3 \frac{d\varphi}{dr} e^{-\varphi(r)/kT} dr \tag{11}$$

$$C(T) = -\frac{4\pi^2\tilde{N}^2}{3kT}\int\int\int (1+f_{12}) f_{23} f_{13} r_{12}^2 r_{23} r_{13} \frac{d\varphi_{12}}{dr_{12}} dr_{12} dr_{23} dr_{13} \tag{12}$$

where, from the work of J.E.Mayer, [18], the force can be considered the one in Eq. (13).

$$f_{ij}(r_{ij}) = [e^{-\varphi_{ij}/kT} - 1] \tag{13}$$

It can be found that the equation of state for a mixture of ν components is described by Eq. (3) where the virial coefficients are given by:

$$B(T)_{mix} = \sum_{\alpha=1}^{\nu}\sum_{\beta=1}^{\nu} B_{\alpha\beta}(T) x_\alpha x_\beta \tag{14}$$

$$C(T) = \sum_{\alpha=1}^{\nu}\sum_{\beta=1}^{\nu}\sum_{\gamma=1}^{\nu} C_{\alpha\beta\gamma}(T) x_\alpha x_\beta x_\gamma \tag{15}$$

where x_1 is the mole fraction of the species 1 in the mixture; the function B_{11} is the second virial coefficient for the pure substance 1; the function B_{12} is the virial coefficient evaluated for a potential function φ_{12} which describe the interaction between the two different species.

1.5 Lennard Jones 6-12 potential

In its simplicity, the *Lennard-Jones 6-12 potential* is a good description of repulsive and attractive forces as function of the intermolecular distance r. However, it has no physical basis and the exponential values are chosen for mathematical convenience. Its mathematical representation is in Eq. (16).

$$\varphi(r) = 4\epsilon_{max}[(\sigma/r)^{12} - (\sigma/r)^6] \tag{16}$$

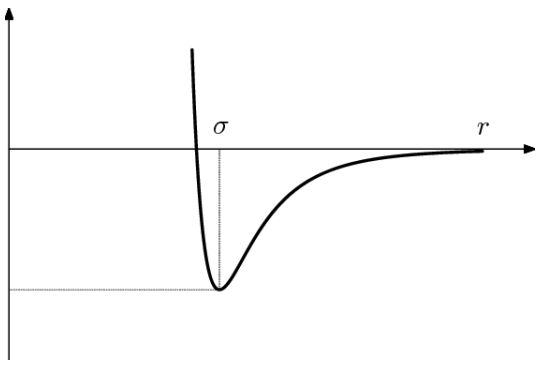

Figure 1: Lennard Jones 6-12 potential

The parameters σ and ϵ have respectively the dimension unit of length and energy and they characterize the chemical species of the molecules involved in the collision. For two distant molecules ($\sigma << r$) the inverse sixth power is dominant and simulate the attraction component; at small distances, ($\sigma >> r$), the inverse twelfth power is more important and simulates the repulsion. This kind of potential describes well the interaction induced dipole - induced dipole between two non-polar molecules. σ is the distance at which the potential becomes zero, while ϵ is the maximum energy of attraction of the two molecules. The trend of the Lennard Jones 6-12 potential is shown in Fig. 1.

As already stated, LJ potential has been used for a wide variety of calculations for both gases and liquids. It is here reported the evaluation of the virial coefficients and some other properties employing this potential.

In the following discussion (taken from [4]), the definition of the following *reduced* quantities helps in simplifying the problem.

$$\begin{cases} r^* = r/\sigma \\ T^* = kT/\epsilon \\ B^* = B/(2/3\pi N_a \sigma^3) = B/b_0 \\ C^* = C/b_0^2 \\ B_k^* = (T^*)^k (d^k B^*/d(T^*)^k) \\ C_k^* = (T^*)^k (d^k C^*/d(T^*)^k) \end{cases}$$

where temperature and molecular distances are adimensionalized with respect to LJ parameters, B and C are second and third virial coefficients and are adimensionalized with respect to $b_0 = 2/3\pi N_a \sigma^3$, with N_a being the Avogadro's number, and B_k^* and C_k^* are the k-th derivatives of the virial coefficients with respect to T^*.

1.5.1 Second Virial Coefficient

Substituting the LJ potential into the Eq. (11), and rearranging with the reduced quantities yields:

$$B^*(T^*) = -\frac{4}{T^*} \int_0^\infty r^{*2} \left(-\frac{12}{r^{*12}} + \frac{6}{r^{*6}}\right) e^{-\frac{4}{T^*}\left(\frac{1}{r^{*12}} - \frac{1}{r^{*6}}\right)}$$

where the exponential term can be expanded as infinite series to integrate the term analytically. The integration has already been done and the solution is presented as infinite series in the following relation:

$$B(T) = b_0 * B^*(T^*) \; ; \qquad B^*(T^*) = \sum_{j=0}^{\infty} b^{(j)} (T^*)^{-(2j+1)/4}$$

where the coefficients $b^{(j)}$ depend only on j.

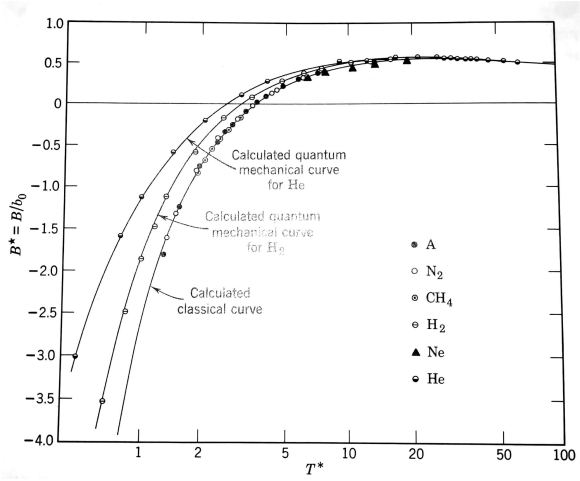

Figure 2: $B^*(T^*)$ evaluated with LJ potential, taken from [4].

It can be shown that the series converges rapidly for reduced temperatures greater than 4 and instead requires more than 30 terms to converge when T^* is lower than 1. In [4], all the values of b_j, the reduced second virial coefficient B^* and its derivatives B_k^* are reported for a range of reduced temperature from 0.3 to 400. In Fig. 2, it is shown the behaviour of B^*: it is negative for reduced temperatures which are lower than the *Boyle temperature*, that is the temperature for which repulsive and attractive forces balance, so B(T) = 0, which occurs approximately at $T^* = 3.42$. This happens because for low temperature, molecules spend longer time in the attractive region of the potential, and this results in a decrease of the pressure, thus a second virial coefficient lower than 0. The opposite occurs for higher temperatures.

Furthermore, it is appreciable the high accuracy of the method when compared with experimental results, shown as dots in Fig. 2.

The derivatives of the second virial coefficient are useful in the evaluation of the deviation from ideality of thermodynamics properties, for example for the evaluation of internal energy, entropy, enthalpy, heat capacity and Joule-Thomson coefficient.

To sum up, in order to evaluate the second virial coefficient, the only information needed is the values of parameters σ and ϵ. These are called *force constants* and are obtained through experimental analysis. They can be found in literature as results of different analyses.
To evaluate the second virial coefficient for mixture, it is only necessary the information about the force constant of the single components and the force constants of the pair of unlike molecules. To do this, if experimental data are unavailable, empirical combining laws are used, for example:

$$\sigma_{\alpha\beta} = \frac{1}{2}(\sigma_\alpha + \sigma_\beta) \qquad \epsilon_{\alpha\beta} = (\epsilon_\alpha \epsilon_\beta)^{1/2} \tag{17}$$

1.5.2 Third Virial Coefficient

Now, substituting the LJ potential into the Eq. (12), and rearranging with the reduced quantities yields:

$$C(T) = b_0^2 C^*(T^*)$$

$$C^*(T^*) = \sum_{j=0}^{\infty} c(j) T^{*-(j+1)/2} \tag{18}$$

but now, c(j) are no more simple functions but complex integrals which have been evaluated in [4] through Kihara's expansion.

Once again all the values for C^* and C_k^* are tabulated, [4]. In Fig. 3 the behaviour of $C^*(T^*)$ is shown along with some experimental results. In general the agreement is not outstanding, in particular for H_2 and He, where quantum effects become important and extremely poor results are observed for elongated molecules. However, it should give quite good result for non-polar spherical molecules, at high temperature and at density such that the correction to the compressibility due to the third virial coefficient is small compared with the one given by the second.

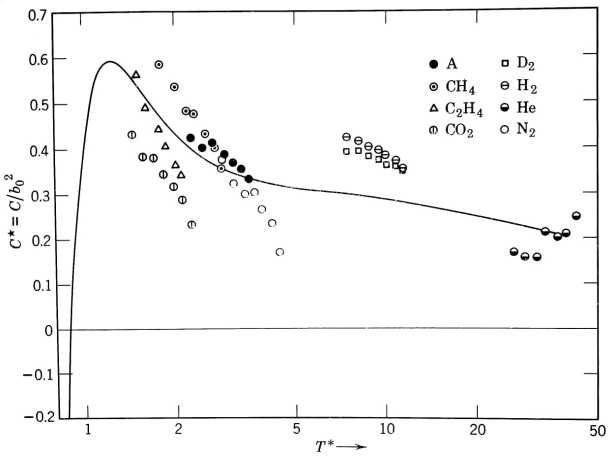

Figure 3: $C^*(T^*)$ evaluated with LJ potential, taken from [4].

No calculations have been made of the third virial coefficient for mixtures, but it can be estimated by making use of the third virial coefficient evaluated with the Square Well potential[3].

[3] Its formulation is reported in [4] Section 3.5 paragraph d

1.5.3 Joule-Thomson coefficient

The Joule-Thomson coefficient is the rate of change of temperature with pressure during an isenthalpic expansion, and it can be related to the EoS as follows:

$$\mu = \left(\frac{\partial T}{\partial p}\right)_H = C_p^{-1}\left[T\left(\frac{\partial V}{\partial T}\right)_p - V\right]$$

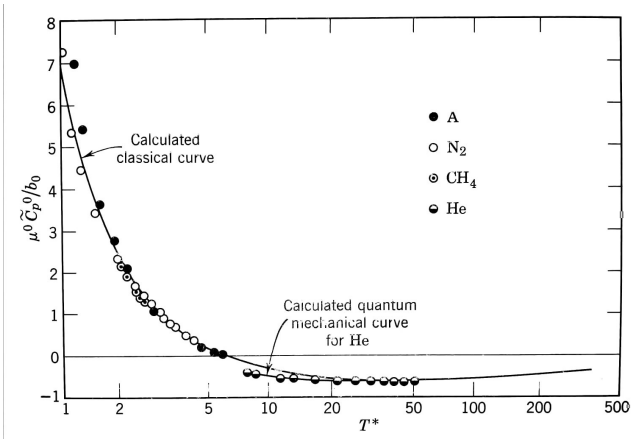

Figure 4: μ_0 evaluated with LJ potential, taken from [4].

This definition can be expanded in powers of 1/V and rewritten in terms of B^* and C^*, as in Eq. (19) from [4], where $\tilde{C}_p^0$ is the zero-pressure molar heat capacity; The first term of the expression is the Joule-Thomson coefficient at zero pressure, μ_0; its behaviour is shown in Fig. 4. It is evident that experimental values perfectly match the theoretical curve.
Values of $B_1^* - B^*$ are tabulated, [4], in order to retrieve the Joule Thomson coefficient at zero pressure; it is also possible to evaluate this quantity for mixtures.

$$\mu = \frac{b_0}{\tilde{C}_p^0}\left[B_1^* - B^*\right] + \frac{b_0^2}{\tilde{V}\tilde{C}_p^0}\left[C_1^* - 2C^* + 2B^{*2} - 2B^* B_1^* + \mu^0 B_2^* R/b_0\right]... \tag{19}$$

For a binary mixture, given μ_0 for each pure component and b_0, B^* and B_1^* for the unlike pair of molecules, the following relation holds:

$$\mu_{mix}^0 = \frac{x_1^2(\tilde{C}_p^0)_1\mu_1^0 + x_2^2(\tilde{C}_p^0)_2\mu_2^0 + 2x_1x_2(b_0)_{12}[(B_1^*)_{12} - (B^*)_{12}]}{x_1(\tilde{C}_p^0)_1 + x_2(\tilde{C}_p^0)_2}$$

1.5.4 Thermodynamic properties

It has been shown up to now, how the virial coefficients can be retrieved starting from the selected intermolecular potential, in this case, the Lennard Jones 6-12. From the evaluation of those coefficients, the deviation from ideality of several thermodynamic properties can be evaluated in terms of reduced virial coefficients, their derivatives and the reduced molar volume $V^* = \tilde{V}/b_0$. The analytic procedure is shown in Appendix B of chapter 3 in [4]; here only the final relation for some properties that will be used later in this work are presented.

1. Heat Capacity at constant pressure

$$\frac{\tilde{C}_p - \tilde{C}_p{}^0}{R} = -\frac{B_2^*}{V^*} + \frac{(B^* - B_1^*)^2 - C^* + C_1^* - 0.5C_2^*}{V^{*2}} + ...$$

2. Heat Capacity at constant volume

$$\frac{\tilde{C}_v - \tilde{C}_v{}^0}{R} = -\frac{2B_1^* + B_2^*}{V^*} - \frac{2C_1^* + C_2^*}{2V^{*2}} + ...$$

3. Speed of Sound

$$c_0^2 = \frac{\gamma^0 RT}{M}\left[1 + \frac{1}{V^*}\left(2B^* + 2(\gamma^0 - 1)B_1^* + \frac{(\gamma^0 - 1)^2}{\gamma^0}B_2^*\right) + ...\right]$$

with $\gamma = \tilde{C}_p/\tilde{C}_v$

1.6 More complex spherically symmetric potentials

Much more realistic and accurate is the "*Modified Buckingham 6-exp potential*", defined in Eq. (20).

$$\varphi(r) = \frac{\epsilon}{1-(6/\alpha)}\left[\frac{6}{\alpha}\exp\left[\alpha\left(1-\frac{r}{r_m}\right)\right]-\left(\frac{r_m}{r}\right)^6\right] \qquad if \;\; r >> r_{max} \tag{20}$$
$$\varphi(r) = \infty \qquad if \;\; r < r_{max}$$

where α is the steepness of the exponential repulsion, r_m is is the value of r at the potential minimum and ϵ is the depth of potential well. r_{max} is the value of r for which $\varphi(r)$ has a spurious maximum. The ratio r_{max}/r_m is given by the smallest root of the trascendental equation:

$$\left(\frac{r_{max}}{r_m}\right)^7 \exp\left[\alpha\left(1-\frac{r_{max}}{r_m}\right)\right] = 1$$

For this potential, the second virial coefficient can be evaluated as:

$$B(T) = b_m B^*(\alpha, T^*)$$

in which $b_m = 2/3\pi\tilde{N}r_m^3$, and $B^*(\alpha, T^*)$ is tabulated, along with the three parameters ϵ, r_m and α in [4].
Even if this potential is more accurate, it is also more complex, and no other virial coefficients have been evaluated yet, leading to a less accurate prediction of thermodynamic properties.

1.7 Chapman-Enskog Theory

What has been said up to now gives a good background of molecular dynamics, explains what are the main parameters to describe the molecule behaviour and what are the different models and capabilities developed in the last century. This knowledge is necessary to introduce one of the most known theories in the field of molecular theory, the Chapman-Enskog Theory.
This model, taken from [4], gives scientific bases to the otherwise phenomenological relations appearing in hydrodynamics, like the Navier–Stokes equations. From it, a relation for each transport coefficient is obtained in terms of molecular properties. The Chapman–Enskog theory is an important step to go from a particle-based description to a continuum hydrodynamical one. The theory is named for Sydney Chapman and David Enskog, who introduced it independently in 1916 and 1917.

They were the first to make modifications to Boltzmann's equation in order to develop a kinetic theory that was valid also for dense gases. Indeed the Boltzmann equation is based on the assumptions that no three-body collisions occur and that the molecules diameter σ is small compared to the average distance between molecules. These assumptions are valid in dilute gases, but not for dense gases.

Enskog and Chapman were able to keep these considerations, based on dilute gases, and expand the theory to dense gases. They stated that, when a gas is compressed, two effects are mainly important:

- "Collisional Transfer of momentum and energy" : which is the exchange of momentum and energy that two molecules feel when they undergo a collision.
- "Change in the number of collision per second" : since σ is no more negligible with respect to the average distance between molecules, the frequency of collisions increases.

By reorganizing Boltzmann's equation to take into account these two contributions, some simple formulations of viscosity and thermal conductivity are found. A detailed treatment of the theory can be found in [4]; here only a few results are reported. The rigorous kinetic theory

relations for the transport properties of a pure substance are presented in Eq. (21),Eq. (22) and Eq. (23).

$$D = \frac{3}{16}\frac{\sqrt{2\pi k^3 T^3/\mu}}{p\pi\sigma^2\Omega^{(1,1)*}} \tag{21}$$

$$\eta = \frac{5}{16}\frac{\sqrt{MkT/(N_a\pi)}}{\sigma^2\Omega^{(2,2)*}} \tag{22}$$

$$\lambda = \frac{25}{32}\frac{\sqrt{MkT/(N_a\pi)}}{\sigma^2\Omega^{(2,2)*}}\frac{c_v}{M/N_a} \tag{23}$$

Where μ is the reduced mass of two colliding particles, [4], while M is the molar mass. In these relations, transport properties have been expressed in terms of the *reduced collision integrals*, $\Omega^{(l,m)}$, which have the physical significance of "deviation of a molecule from the idealized rigid-sphere model". The value of these parameters is the result of complex integrals, and finding the solution is quite long and complex; one of the first calculations was made in [4] where results were summed up in tables as a function of a reduced temperature $T^* = kT/\epsilon$. Several authors have made corrections or modifications to those results, thanks to more recent experimental proofs. In this work the empirical correlation from Neufeld et al. [40] is used, and presented in Eq. (24); here, the collision integrals are evaluated using the Lennard Jones 6-12 potential.

$$\begin{aligned}\Omega^{(l,s)*}(T^*) =& (A/T^{*B}) + [C/\exp(DT^*)] + [E/\exp(FT^*)] + ... \\ &... + [G/\exp(HT^*)] + RT^{*B}\sin(ST^{*W} - P)\end{aligned} \tag{24}$$

This relation contains 12 parameters, but not every collision integral requires all of them. All the parameters are tabulated in [40], as a function of l and n.

Among the relevant results, the Chapman-Enskog theory predicts that the viscosity is independent of density while it does depend on temperature (the predicted behaviour is $\eta \propto T^{1/2}$); it also proposes that η and λ are linked by the isochoric heat capacity, c_v.

Eq. (21),Eq. (22) and Eq. (23) should be compared with the results coming from the simple kinetic theory, presented in Eq. (4),Eq. (5) and Eq. (6).

1.7.1 Limitations of Chapman-Enskog theory

However, the assumptions on which the just presented Chapman-Enskog theory is built limit the applicability of its results.
Firstly, even if some more effects are added to the Boltzmann equation, only binary collisions are taken into account; this means that the theory could have good results for dense gases, but not for liquids, where the density increases a lot, and then the three-body collisions are no more negligible.
Secondly, classical mechanics does not include quantum effects, then low temperature phenomena cannot be described with this model. In [4], 200 K is identified as the threshold temperature above which quantum effects becomes negligible (less than 1% even for hydrogen or helium).
Furthermore, strictly speaking, Chapman-Enskog theory applies only to monoatomic gases (molecules with no internal degrees of freedom, having an interaction potential spherically symmetric) because inelastic collisions occur between molecules with internal degrees of freedom. This means that kinetic energy is no more conserved, although mass and momentum are conserved. Inelastic collisions will cause some deviations in the estimation of the thermal conductivity.

These, and other deviations from reality, create the need for a more precise model, capable of accounting for all the different neglected effects, and many models have been proposed starting from the Chapman-Enskog theory. In this work, one of the most recent prediction methods will be presented for the evaluation of viscosity.

2 Equation of state - Dense gases and Liquids

In the previous section, some basic concepts have been described for a fundamental knowledge of the gaseous state, the evaluation of the compressibility factor and the thermodynamic properties. As stated, the virial expression diverges for densities that are near the density of the liquid state. Here, some theories and empirical models are presented to extend the knowledge for dense gases and liquids.

2.1 The Principle of corresponding states

Originally presented by Van der Waals, this principle is useful to describe the behaviour of dense gases and liquids, reducing the variables utilizing critical constants (or by means of molecular constants in another formulation).
The *critical point* is defined as the point in which the first and the second derivative of the pressure with respect to the volume are zero. The values of pressure, temperature and volume at this point are defined *critical* constants and indicated with a subscript $_c$. The behaviour of a fluid in the proximity of the critical point will be the subject of the next sections. Here, only some definitions are introduced.
With respect to the critical constants, a set of *reduced* variables can be defined in the following way:

$$p_r = p/p_c \qquad T_r = T/T_c \qquad V_r = V/V_c \qquad \rho_r = \rho/\rho_c$$

The empirical *"principle of corresponding states"* is announced in [4] as: "*All substances obey the same equation of state in term of reduced variables*". Since the state of a system can be defined with any two out of the three variables (pressure, temperature and volume), any dimensionless group should be a universal function of any two of the three reduced variables (reduced pressure, temperature or volume). So the compressibility factor could be written as a function of two reduced variables; usually, p_r and T_r are used, since the reduced volume is extremely difficult to be evaluated:

$$p\tilde{V}/RT = F(V_r, T_r) = Z(p_r, T_r) \tag{25}$$

According to the principle, both F and Z should be universal functions; moreover, if the critical point is considered (reduced quantities are equal to 1), it should be true that the critical ratio $p_c\tilde{V_c}/RT_c$, so the critical compressibility factor, is equal to F(1,1), and it should be a universal constant.

Anyway, this is only a rough approximation since it has been noticed from experimental values that the critical ratio is effectively very similar only for similarly-shaped molecules. In [4], the critical ratio is shown for several elements; for spherical non-polar molecules, the critical ratio is approximately equal to 0.292 (methane has it equals to 0.290), hydrocarbons' ratio is approximately 0.267 while polar molecules have a more varying value for the critical ratio.
Hence, it could be expected that the hydrocarbons satisfy a single reduced equation of state, which is different from the reduced EoS for other kinds of molecules. Kamerlingh Onnes realized quite early that substances containing molecules of the same shape should have similar bulk properties, this was named "principle of mechanical equivalence".

From Eq. (25), by multiplying for the critical ratio, it can be obtained that also the reduced pressure should be a universal function of reduced quantities, as in Eq. (26).

$$p_r = \frac{RT_c}{p_c\tilde{V_c}}\frac{T_r}{V_r}F(V_r, T_r) \tag{26}$$

The practical utilization of the principle of corresponding states has been enhanced by the publication of Hougen and Watson's charts of the generalized compressibility and thermodynamic

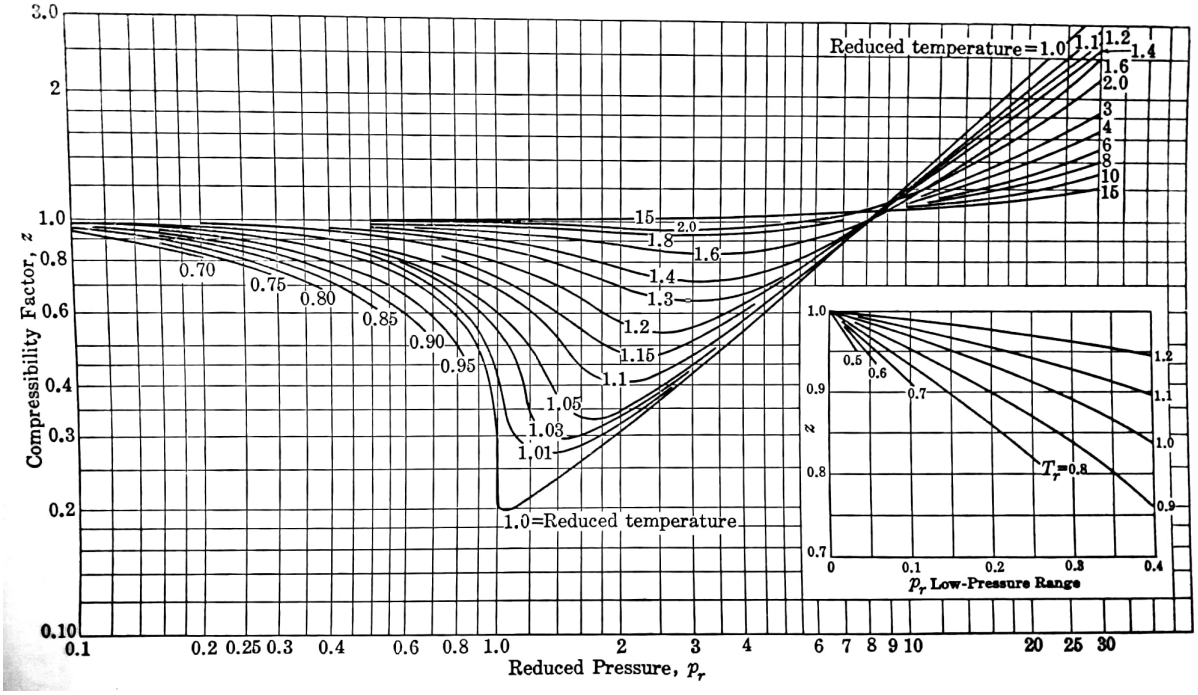

(a) Compressibility factor

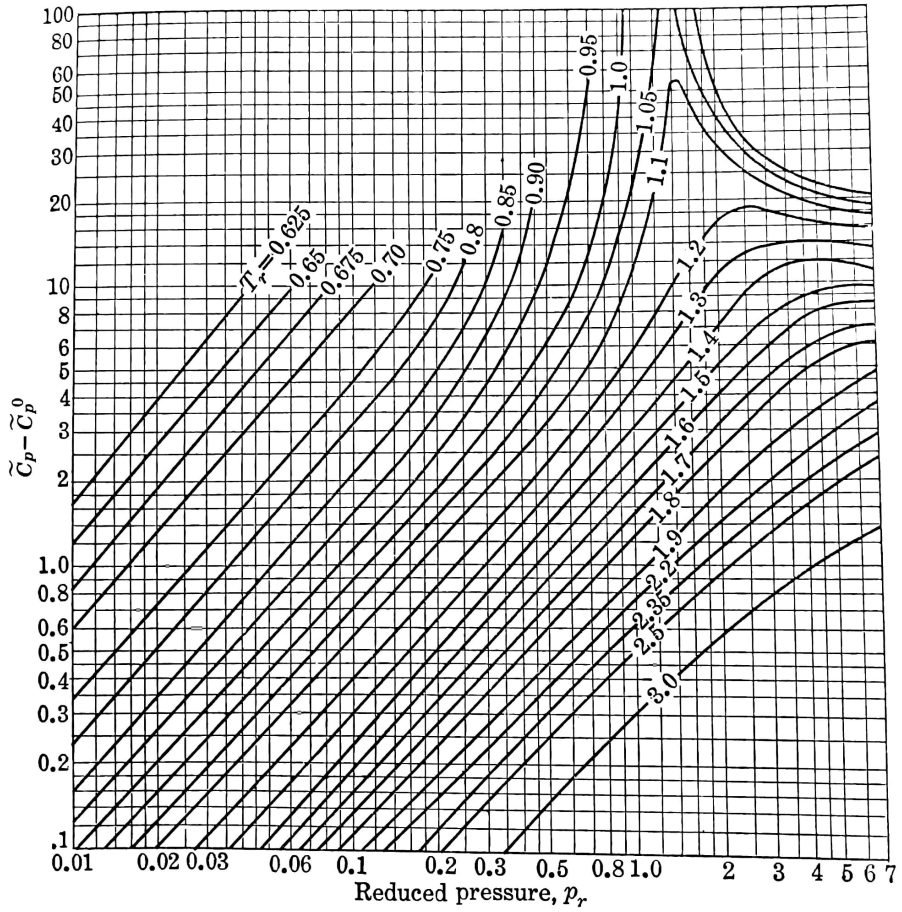

(b) Isobaric heat capacity

Figure 5: Hougen and Watson generalized charts. These graphs are taken from [4]

properties of gases and liquids, [44]. These graphs are plotted as a function of reduced pressure and for different reduced temperatures.
A couple of examples is presented in Fig. 5. Note that all the charts prepared by Hougen and Watson are extrapolated by averaging the data coming from seven gases: H_2, N_2, CO_2, NH_3, CH_4, C_3H_8, C_5H_{12}; since this group is made of many types of molecules, the resulting set of curves cannot be expected to reproduce accurately any of the listed gases. However, those charts remain highly useful in making approximate calculations.
These graphs are often used with mixtures. It is a fair approximation to consider that a mixture behaves as a single component with critical constants equal to the molar averages.

$$(T_c)_{mix} = \sum_i x_i (T_c)_i \qquad (p_c)_{mix} = \sum_i x_i (p_c)_i$$

This treatment of mixtures is rough and applies only to the vapor phase.

2.2 Theoretical development of the principle

Explaining the theoretical nature of the principle of corresponding states is easier with spherical non-polar molecules. In this case, a two parameters potential can be considered, like the Lennard Jones 6-12, which is defined by knowing only ϵ and σ. Treating the motion of molecule with classical mechanics, according to [4], the equation of state of gases may be written as follows:

$$p = kT \frac{\partial}{\partial V} \ln \int e^{-\varphi(\mathbf{r_N})/kT} d\mathbf{r_N} \tag{27}$$

where $\mathbf{r_N}$ contains the position coordinates of all the N molecules. So the pressure depends only on temperature, volume and the two constant parameters. The ϵ and σ can be used to define the following reduced quantities:

$$p^* = p\sigma^3/\epsilon \qquad V^* = \tilde{V}/N_a\sigma^3 \qquad T^* = kT/\epsilon$$

From these considerations, it follows that it is possible to write the reduced pressure as a universal function of the reduced volume and temperature:

$$p^* = p^*(T^*, V^*)$$

where the function depends only on the nature of the potential function. It follows that also the critical quantities reduced by means of molecular parameters are universal constants. Anyway, experimental values show that there is a quite spread between them.
The approximation that reduced critical values are universal constants allows to simply estimate the values of the potential function parameters. For spherical non-polar molecules, obeying the Lennard-Jones potential, approximate relations are found,[4]:

$$\epsilon/k = 0.77 T_c$$

$$b_0 = 0.75 \tilde{V}_c = 18.4 T_c/p_c$$

Several correlations of this kind have been developed, and one of them has been used in the last part of this work.

The simple theory just explained, can be reproduced for elongated molecules or for polar ones. The first case leads to a reduced pressure which is a function of reduced states and l^* (which is the $l^* = l/\sigma$ where l is the length of the molecule); instead in the second case the resulting reduced pressure would be dependent on the reduced states and on μ^* (a parameter defined in the Stockmayer potential for polar molecules and reduced as $\mu^* = \mu/\sqrt{\epsilon\sigma^3}$). Both cases are not of interest in this treatment.

2.3 Empirical equation of state

Many empirical relations have been developed to describe the p-V-T behaviour of gases and liquids and each one of them is specific for particular applications.
For a semi-quantitative understanding of the principal characteristics of the EoS, three models with two adjustable parameters have been defined, namely the Van Der Waals, Berthelot and Dieterici models. Critical properties and virial coefficients are summarized in tables, in [4].
Only the Van der Waals model has been reported here, in Eq. (2), since it will be useful later on.

They are the handiest methods and have quite good results; especially, the critical constant is evaluated by Dieterici surprisingly good, while the second virial coefficient is more accurate in the Berthelot model.
These three two-constants equations can be used for mixtures with the following relations that can be used to define the mixture parameters:

$$a = a_{11}x_1^2 + 2a_{12}x_1x_2 + a_{22}x_2^2$$

$$b = b_{11}x_1^2 + 2b_{12}x_1x_2 + b_{22}x_2^2$$

where a_{ii} and b_{ii} are the pure component parameters, while a_{ij} and b_{ij} can be evaluated with mixing rules, like for example:

$$b_{12}^{1/3} = 0.5(b_{11}^{1/3} + b_{22}^{1/3})$$

$$a_{12} = (a_{11}a_{22})^{1/2}$$

Even if these models are quite useful for fast calculations, more detailed models have to be used for working applications.

2.3.1 Benedict-Webb-Rubin

Benedict, Webb and Rubin generalized the Beattie-Bridgeman model, [4], for both pure substances and mixture. In order to fit the experimentally observed p-V-T data for hydrocarbons up to densities of twice the critical density, eight parameters are necessary to completely define the EoS, as in Eq. (28).

$$p = \frac{RT}{\tilde{V}} + \frac{1}{\tilde{V}^2}\left[RT\left(B_0 + \frac{b}{\tilde{V}}\right) - \left(A_0 + \frac{a}{\tilde{V}} - \frac{a\alpha}{\tilde{V}^4}\right) - \frac{1}{T^2}\left(C_0 - \frac{c}{\tilde{V}}\left(1 + \frac{\gamma}{\tilde{V}^2}\right)e^{-\gamma/\tilde{V}^2}\right)\right] \quad (28)$$

where the eight constants are tabulated in [4] for nitrogen and some hydrocarbons. Moreover, relations are given for the evaluation of those constants for mixtures, using only the mole fraction and the constant for the i-th species.

For mixtures, the eight parameters are assumed to have the form:

$$A_0 = \left[\sum_i x_i (A_0)_i^{1/2}\right]^2 \qquad a = \left[\sum x_i a_i^{1/3}\right]^3$$

$$B_0 = \frac{1}{8}\sum_{ij} x_i x_j \left[(B_0)_i^{1/3} + (B_0)_j^{1/3}\right]^3 \qquad b = \left[\sum x_i b_i^{1/3}\right]^3$$

$$C_0 = \left[\sum_i x_i (C_0)_i^{1/2}\right]^2 \qquad c = \left[\sum x_i c_i^{1/3}\right]^3$$

$$\alpha = \left[\sum x_i \alpha_i^{1/3}\right]^3 \qquad \gamma = \left[\sum x_i \gamma_i^{1/2}\right]^2$$

where subscripts $_i$ and $_j$ stand for pure component parameters.
From these eight constants, some thermodynamic properties can be directly retrieved, like enthalpy, entropy or fugacity. The relations for these quantities are presented in [4]. These relations for the BWR equation of state are valid over the whole range from gas to liquid including the critical region for some hydrocarbons mixtures. Several modifications have been made to this EoS and some of them account for 16 or 32 parameters.

2.3.2 Peng-Robinson

Particular attention is given in this treatment to hydrocarbons for which the Peng-Robinson has been one of the most used, useful also for liquid hydrocarbons. Its formulation is presented in Eq. (29) and taken from [39].

$$P = \frac{RT}{V-b} - \frac{a}{V(V+b)+b(V-b)} \tag{29}$$

where a and b depend on the intermolecular forces of each species. They are defined as follows.

$$b_i = 0.077796\frac{RT_{c,i}}{P_{c,i}}$$

$$a_{c,i}c = 0.457235\frac{R^2T_{c,i}^2}{P_{c,i}}$$

$$\alpha(T_r) = [1 + F(1 - T_r^{0.5})]^2$$

$$a = a_c\alpha(T_r)$$

where F depends on the acentric factor ω and is defined as $F = 0.37464 + 1.54226\omega - 0.26992\omega^2$, while the acentric factor is tabulated for several fluids, [12]. The equation can be also used for mixtures by using the following mixing rules.

$$a_{mix} = \sum_i \sum_j x_i x_j a_{ij}$$

$$a_{ij} = (1 - k_{ij})a_i^{1/2}a_j^{1/2}$$

$$b_{mix} = \sum_i x_i b_i$$

where k_{ij} is the interaction coefficient and depends on each couple of substances involved. It is still object of investigation in many studies, but several data for very numerous couples of substances (including hydrocarbons) are reported in [11].
Also, other more complex mixing rules can be used, as the Wong-Sandler mixing rule, used and explained in [12].

2.3.3 Soave Redlich Kwong

The Soave modification to the Redlich Kwong equation of state is still a cubic equation with a structure very similar to the Peng-Robinson. It is here introduced because it has been partially used in this work.
Its form is presented in Eq. (30).

$$P = \frac{RT}{V-b} - \frac{a}{V(V+b)} \tag{30}$$

This EoS has very accurate results up to the critical region; it has been widely used for liquid, gases and vapor-liquid equilibrium. The two parameters can be directly evaluated for each component from its critical constants and acentric factor.

$$b_i = 0.08664\frac{RT_{c,i}}{P_{c,i}}$$

$$a_i = 0.42727\alpha_i\frac{R^2T_{c,i}^2}{P_{c,i}^2}$$

$$\alpha_i = \left[1 + \left(1 - k_i\sqrt{\frac{T}{T_{c,i}}}\right)\right]^2$$

$$k_i = 0.48508 + 1.5571\omega_i - 0.15613\omega_i^2$$

Mixing rules can be applied, as in Peng Robinson EoS.

2.4 Simple Cell Method

An incredibly good simple theory can be derived starting from the already presented relation from classical mechanics, Eq. (27), and making rough approximations about the "free-volume" and the "lattice energy". The free-volume is the volume in which a molecule is free to move, while the lattice energy is a measure of the cohesive forces that bind ions.
Let's consider molecules as rigid spheres with a diameter equal to σ, and consider all the molecules but one ('*the wanderer*') 'fixed in their equilibrium positions on a regular cubic lattice. With some approximation, and introducing the Van Der Waals coefficient $b = 2\pi N_a\sigma^3/3$, the simplified free volume can be defined as:

$$v_f = 8[(\tilde{V}N_a)^{1/3} - 0.7816(b/N_a)^{1/3}]^3$$

The lattice energy instead, may be supposed to be the negative of the internal energy of vaporization per mole, which could be expressed, following Hildebrand's theory, as a function of $a(T)/\tilde{V}^n$; for many substances, n=1 is a good choice.

$$0.5N_aE(0) = -\Delta\tilde{U}_{vap} = -a(T)/\tilde{V}$$

the function $a(T)$ can be shown to be the coefficient a of Van der Waals.
It should be considered that both the lattice free energy and the free volume depend on both attractive and repulsive forces. In this simplified model, the free volume depends primarily on the repulsive force and lattice energy primarily on the attractive force.
When substituting these simplified expressions into the molecular partition function, rearranging Eq. (27), the Eyring equation of state could be derived, as in Eq. (31).

$$\left(p + \frac{a(T)}{\tilde{V}^2}\right)(\tilde{V} - 0.7816b^{1/3}\tilde{V}^{2/3}) = RT \tag{31}$$

It could be demonstrated that Eyring relation is just a more precise form of Van Der Waals equation of state, accounting for overlapping of rigid spheres. The constant 0.7816 is appropriate for a simple cubic lattice; for a body-centered cubic lattice the constant should be 0.7163, while for face-centered 0.6962.

3 Vapor-Liquid Equilibria and Critical Region

In the previous sections, the equilibrium properties of gaseous and liquid systems have been described. Now, attention is paid to the interaction between liquid and gas, namely the interface between the two states. It will be noticed that, when the temperature is increased up to the critical temperature, a density gradient is generated throughout the vessel, and the distinction between liquid and vapor becomes meaningless.
This behaviour will give the starting point to analyze the two completely homogeneous phases, which exist up to the critical point. In addition, some notions about "retrograde condensation" are introduced.

3.1 Surface Tension

A theoretical treatment of two phases systems must consider the interfacial region and the nature of surface tension. Let's consider a tall box containing liquid and vapor of the same species. From a macroscopic point of view, the density jumps from the liquid value to the vapor value across the interface between the two phases. From a microscopic point of view instead, it must be taken into account that such discontinuity does not exist.
Considering the tall box aligned with the z-axis, and defining properly a dividing surface called *equimolecular dividing surface*, [4], and using the pressure tensor, the surface tension can be defined as in Eq. (32).

$$\gamma = \int (p_0 - p_{xx}(z))dz \tag{32}$$

So the surface tension is the stress acting in the x-direction on a strip of unit area in the yz-plane in addition to the uniform normal pressure, p_0.
Another point of view is to consider the contribution of the surface layer to the thermodynamics functions in a two phases system; in this way, surface tension becomes the one in Eq. (33).

$$\gamma = \left(\frac{\partial A^s}{\partial \alpha}\right)_T = \left(\frac{\partial G^s}{\partial \alpha}\right)_T \tag{33}$$

where A and G are the Helmholtz free energy and the Gibbs free energy, which are equal in the hypothesis of equimolecular dividing surface. The superscript ^{s} stands for surface and indicates the molecules inside the region of transition between solid and gaseous phase. α is the area of the film between the phases.
A more detailed process is carried out in [4], using both the free volume method and the radial distribution function method and comparing analytical and experimental results. Here, a simplified model is presented, that is the Mcleods's equation and the *Parachor*. Mcleod proposed an empirical equation for the surface tension that includes the actual densities of liquid and vapor phases.

$$\gamma = constant \cdot (\rho^l - \rho^v)^4$$

Sudgen has then reformulated this result as in Eq. (34).

$$P = \frac{M\gamma^{1/4}}{\rho^l - \rho^v} \tag{34}$$

where P is called the parachor, and it remains nearly independent of temperature over a wide temperature range; it is tabulated for few substances,[4].Lennard Jones and Corner showed that for simple molecules the parachor is given within the 3.6 per cent of accuracy by the following equation:

$$P = (7.1 \cdot 10^{23})\epsilon^{1/4}\sigma^{5/2}$$

where ϵ and σ are the Lennard-Jones parameters. This suggests that the parachor may provide a sensitive method to obtain the molecular collision diameter.

3.2 Phase-Behaviour of One-Component Systems

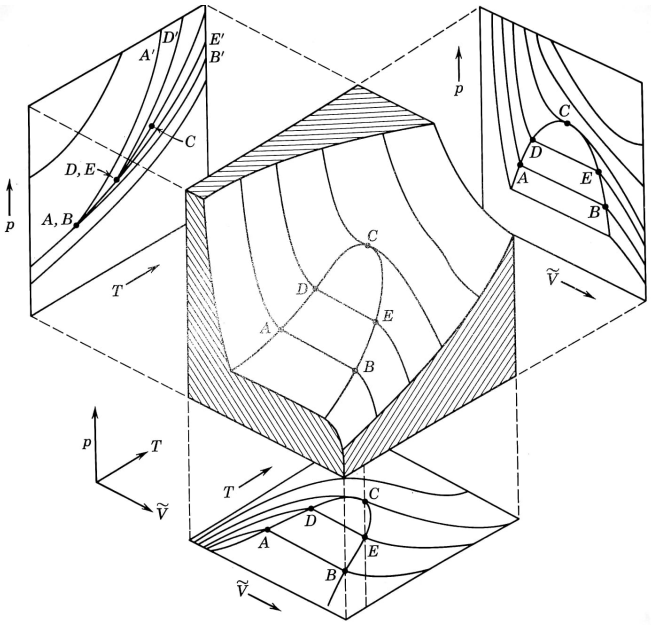

Figure 6: Surface of generic EoS, taken from [4].

The equation of state of a one-component system is a 3-variables equation and can be presented by the surface $p = p(\tilde{V}, T)$, as in Fig. 6. In this figure, the behaviour of the fluid in both liquid and gaseous states is shown. The curve ADCEB is the so-called *coexistence line*; the point C on the tongue-shaped curve is the critical point and it represents the highest pressure and temperature at which two phases can exist and the point for which liquid and vapor phases become indistinguishable. Inside the tongue-shaped region, the system breaks up into a liquid and a vapor phase, which coexist in equilibrium. One side of the curve, the ADC, is called *liquidus*, while the other branch, CEB, is called *vaporus*. What happens in the vicinity of the critical point is the argument of the next subsection.

From this three dimensional view of the EoS, much information is not easily retrieved. Generally, it is split into three 2D representations, as the projections that are shown in Fig. 6. The upper right plot can be obtained by slicing the surface with planes perpendicular to the T-axis. It shows the isotherms on a $p - \tilde{V}$ diagram and the one passing through C is the critical isotherm. Slicing the surface with a plane perpendicular to $\tilde{V}$-axis, the upper left projection can be obtained. It shows the isochores on a p-T diagram; here, the curve (AB)(DE)C is the projection of the tongue-shaped region and is the familiar *vapour pressure curve*. The last projection is the $T - \tilde{V}$ plane which shows the isobars of the system. Each of the three projections is sufficient to reconstruct the whole surface.

From each of these diagrams, the critical point can be found, for example, the critical temperature could be estimated by the analysis of the geometry of the isotherms. From loading a bomb of constant volume instead, it can be shown that the isochores behave differently depending upon whether the overall (gas+liquid) density of loading, $\overline{\rho}$, is less, equal or greater than the critical density; different cases are reported in [4]. Another way is defining a "*rectilinear diameter*" as the arithmetic average of the liquid and vapor densities, and plot all the three densities with varying temperature; the point of intersection of the rectilinear diameter with the coexistence curve gives the critical density and temperature. It has to be pointed out that the equilibrium condition described by the graphs is not always the one obtained from experiments.

Let's consider a vapor that is being compressed; a state of *supersaturation* may occur, namely, the vapor phase is still present even if it should condense, this happens because in order to condense, nuclei should be formed, but for pure substances this process can take a while; this is a *metastable state*. Another example could be the *overexpansion* of a liquid: if a liquid is kept at high pressure and then the pressure is decreased, the liquid would be expected to vaporize but this does not happen immediately and the liquid phase can persist for a considerable length of time. Similarly to condensation, vaporization occurs with the formation of cavities that can form spontaneously or with another gas dissolved in the liquid, and again, this process takes time.

Let us move now to the isotherms that describe these metastable states, even using a very simple EoS like the Van der Waals equation, Eq. (2). This is shown in Fig. 7.
Isotherms below the critical isotherm do not have a horizontal section, as it could be expected for the vapor-liquid equilibrium, but they are S-shaped. For example at temperature T_2 the EoS gives the curved path named with letters DQRSE, instead, the expected equilibrium is represented by the dotted line DE (which indicates the vapor pressure value for T_2). Maxwell suggested that to find the vapor pressure, the dotted line must be chosen such that the area bounded by the line DR and the curve DQR is equal to the area bounded by RE and RSE, in order to have the Gibbs free energy of the liquid phase equals to the one of the vapor phase, when the two phases are in equilibrium.

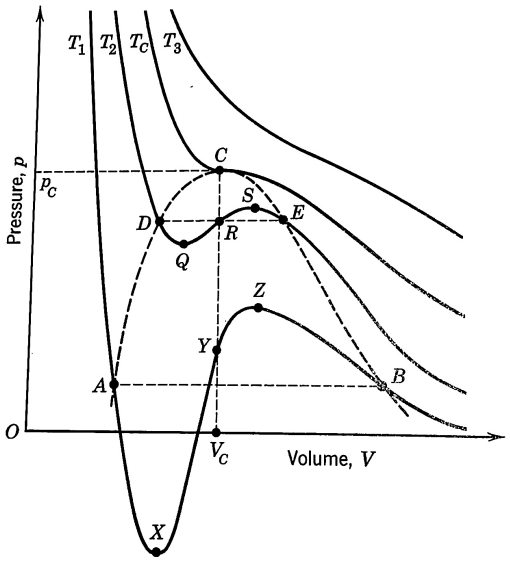

Figure 7: Isotherms of simple analytic EoS, taken from [4].

It is possible to read the portions DQ and SE of the S-shaped analytical curve as representing the metastable states of the fluid, which are experimentally realizable. The segment SE represents the state of supersaturation while DQ corresponds to the overexpansion. The segment QRS has no physical significance.

3.3 Thermodynamic properties in the critical region

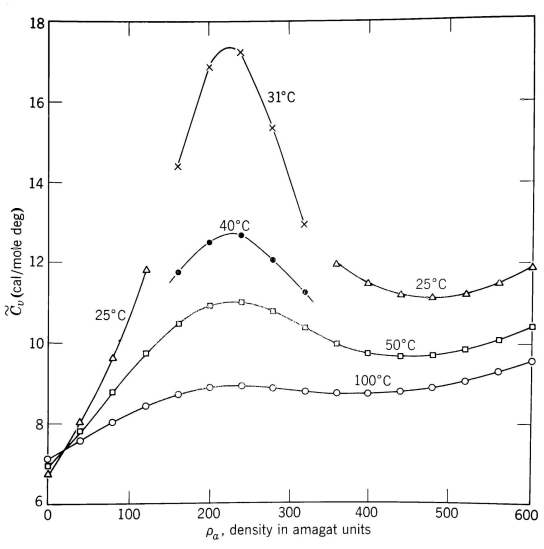

Figure 8: $\tilde{c_v}$ behaviour for CO_2, [4].

It has been noticed that isotherms below the critical point show very different behaviour with respect to isotherms above it. More generally, when a fluid approaches the critical point, significant changes in its properties occur; this is commonly defined as "*transcritical* fluid". When instead, critical temperature and pressure are overcome, the system dynamics is even more complex, and a more detailed treatment will be given later on; in these conditions, fluids are usually referred to as "*supercritical* fluid".
Let us focus now on the transcritical region.

The heat capacity at constant volume can be calculated as the sum of the ideal gas heat capacity, $\tilde{C_v^0}$, and an integral representing the residual part, that can be evaluated from experimental compressibility, Eq. (35).

$$C_v = \tilde{C_v^0} + T \int_{\tilde{V}=\infty}^{\tilde{V}} \left(\frac{\partial^2 p}{\partial T^2} \right)_{\tilde{V}} d\tilde{V} \tag{35}$$

The results for CO_2 are shown in Fig. 8; it is very interesting to see a very pronounced maximum in the neighbourhood of the critical point: the heat capacity tends to increase near the critical point and decrease immediately after. These peaks are less pronounced with temperatures much

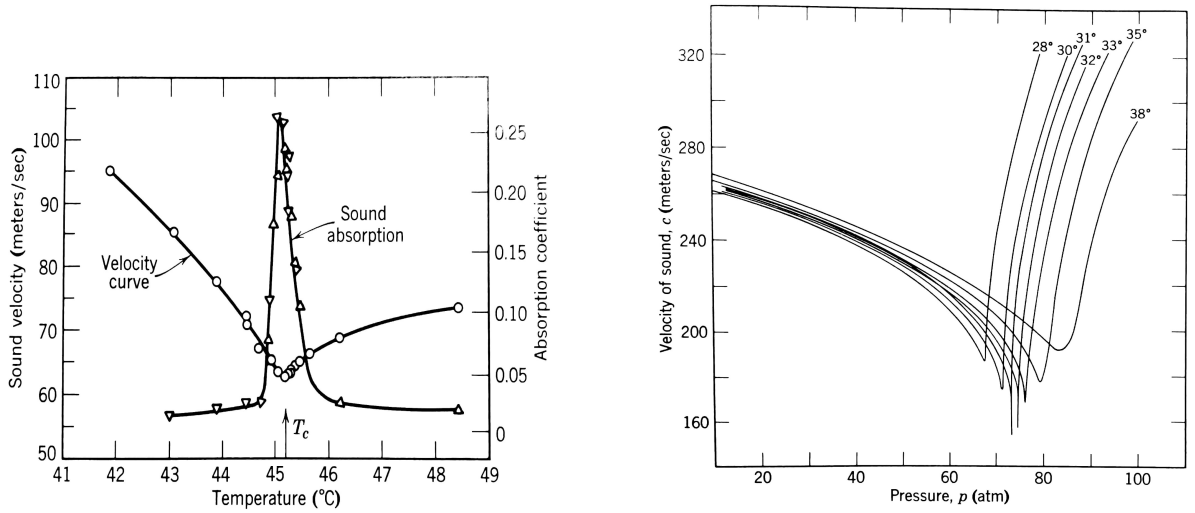

(a) Sound velocity and absorption for SF_6, [4].

(b) Sound velocity for CO_2, [4].

Figure 9: Sound velocity and absorption coefficient in the critical region.

higher than the critical temperature. For what concerns the evaluation of the heat capacity at constant pressure, the case of a liquid system kept at constant pressure is considered. Addition of heat will cause an increment in temperature and volume; by increasing the temperature, at a certain point the vapor pressure becomes equal to the actual pressure of the system, and a vapor phase is generated. Further addition of heat will cause no increment in temperature because it would be absorbed as latent heat of vaporization; so heat capacity is infinite and remains so during the whole phase transition. Then, for any pressure lower than the critical pressure, a range of densities over which c_p is infinite exists. Thus, as a system approaches the critical point from the single phase region, the value of c_p approaches infinite.

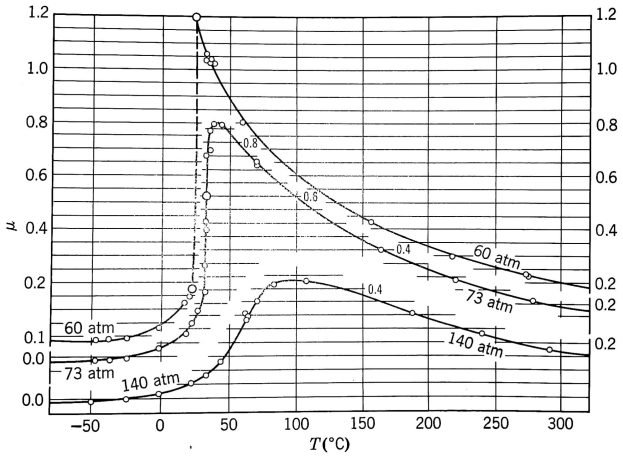

Figure 10: Joule Thomson coefficient for CO_2 in critical region, [4].

A relation for the evaluation of the velocity of sound at zero frequency is reported in [4], but no experimental data are available at frequencies sufficiently low to validate that equation. The results for the experimental evaluations of the velocity of sound in transcritical conditions are reported in Fig. 9; in particular, in Fig. 9a a minimum for the sound velocity, and a maximum for the sound absorption are shown in the proximity of the critical point for Sulfur hexafluoride, SF_6. Instead in Fig. 9b, only the speed of sound is shown but at different temperatures for CO_2; the speed of sound evaluated for temperatures nearer to the critical temperature show a deeper minimum. The Joule-Thomson coefficient at the critical point can be evaluated as, [4]:

$$\mu_{crit} = 1/(\partial p/\partial T)_{\tilde{V}}$$

So it is the reciprocal of the slope of the vapour pressure curve at the critical point. Experiments show a maximum in the critical region, Fig. 10.

Moreover, microscopically, *density fluctuations* become very large in the vicinity of the critical point and this is demonstrated to lead to a scattering of light. In the critical point, this scattering is greater and is referred to as "critical opalescence".

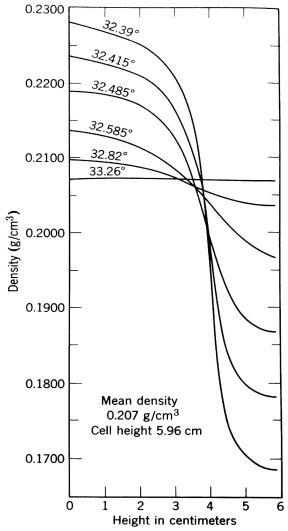

Figure 11: Density gradient of ethane in the critical region, [4].

Up to now, the characteristics of liquid and vapor phases were analyzed, and each phase was described by well-defined properties. The properties of a fluid in the neighbourhood of the critical point instead suffer strong variations across a certain transition region, that becomes progressively broader as the fluid approach and overcome the critical point and at the same time the density difference between the two phases becomes smaller. The lack of a distinct boundary between the liquid and the vapor phases is then augmented by the effect of gravity and the fact that $(\partial p/\partial V)_T$ is small. These two effects, called respectively *diffuseness of the surface* and *importance of gravity*, [4], are experimentally indistinguishable and cause macroscopic density gradients; this gradient has been measured for ethane, with an optical technique, whose results are presented in Fig. 11.

3.4 Phase Behaviour of Two-Component Systems

If, in one-component systems, condensation is directly associated with lowering the temperature and increasing the pressure, and vaporization is the complete opposite process, two-components systems are even more complex due to the possibility of *retrograde condensation*. The complete state behaviour of a binary system is now represented by the four-dimensional surface $p = p(\tilde{V}, T, x)$, where x is the mole fraction of one of the two elements. The 4D surface is studied through different three-dimensional projections; for example, by fixing the molar volume, the vapor pressure surface is obtained, $p_{vap} = p(T, x)$, and is presented in Fig. 12a for a mixture of ethane and epthane.

With Fig. 12a as a reference, some general features of binary mixture can be identified. The curves K_1C_1 and K_2C_2 are the pure components vapor pressure curves of epthane and ethane, respectively. C_1 and C_2 are the pure component critical points, and the line that joins $C_1C_0C_2$ is the locus of critical points. This locus of points divides the surface into two parts: the liquid and the vapor side; any line parallel to the x-axis pierces the surface in two points; these points give the composition of the liquid and the vapor phase at the temperature and pressure at which the line is drawn.

To facilitate the understanding of the three-dimensional surface, three two dimensional projections can be prepared (as it was shown in Fig. 6). Firstly the projection of the isobars on the T-x plane is reported in Fig. 12b. Isobars are created by slicing the 3D surface with planes perpendicular to the pressure axis and obtaining the common liquid-vapor equilibrium curves, used for binary systems. This plot can help us in understanding the phenomenon of *retrograde condensation*, [4]. Consider a liquid system at $200psi$ in point A heated up to point B; here a vapor phase, represented by B', appears. A further increase in temperature results in a greater amount of vapor phase and a smaller amount of liquid phase, represented respectively by D and D'.

At higher pressures, the boundaries between liquid and vapor phase occur at higher temperatures. The boiling point of pure components varies with pressure; it increases with increasing pressure, until the boiling temperature of one component reaches the critical temperature of one of them. For the mixture of ethane-epthane, shown in Fig. 12a, this occurs at approximately 400psi and the corresponding critical temperature is about 250°C; at or above this temperature the composition

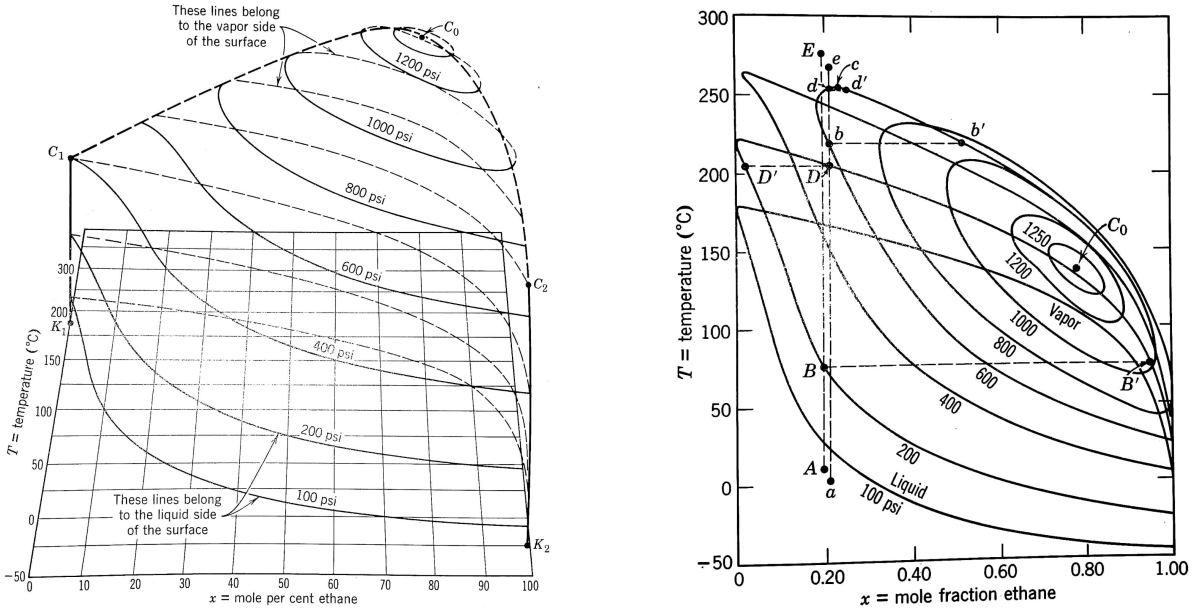

(a) Binary systems at fixed molar volume, [4] **(b)** T-x projection of surface shown in Fig. 12a, [4]

Figure 12: Surface of binary Equation of State

becomes important for the existence of two fluid phases, namely there cannot be two fluid phases beyond some limiting composition.
For example, at pressure of 600psi the heterogeneous area does not extend to the left of $x = 0.18$. So the liquid part of the isobar goes through the lowest ethane mole fraction before joining the vapor part of the curve, in the point named c, which is the critical point of the mixture. This limitation gives rise to one type of retrograde condensation.

Consider a mixture at 600psi whose state is represented by point a, in Fig. 12b; as the temperature is increased the fluid reaches point b, with vapour phase represented by b'. With a further increase of temperature, the system goes from b to d; in doing so, the amount of liquid phase firstly decreases up to a minimum and then increases again until point d is reached, where the last trace of vapor in d' vanishes and the system returns to all liquid state. The initial vaporization is followed by condensation; this is the phenomenon called *retrograde condensation*, and in this case it is of *second kind*, since it is due to a temperature variation. This phenomenon can occur whenever the temperature variation follows a vertical line that lies between the critical point c and the minimum (or in some cases the maximum) mole fraction of one component.

Analogously, the other kind of retrograde condensation can be shown on the p-x plane, where isotherms are shown, and it is caused by a variation of pressure. Consider a system whose state is represented by point α in Fig. 13a, and increase the pressure, until reaching first β and then δ. Initially, condensation can be observed, up to a maximum amount of liquid; then that liquid vaporizes back until in δ all the liquid phase is disappeared. This case is usually referred to as *retrograde condensation of first kind*. Generally, retrograde behaviour are shown whenever the representative path of the system in the three dimensional representation enters and leaves the volume through the same phase boundary surface, which could be either liquid or gaseous. The path does not need to be parallel to the pressure or temperature axis but can mix changes in both the two variables.

The last projection, the p-T plane for constant mole fraction, is also the most common representation of the vapor-liquid equilibria of binary mixture; for this reason, the figure is not taken from the ethane-epthane example of [4] but it is generalized to show all the peculiar characteristics of mixtures phase diagrams, shown in Fig. 13b.

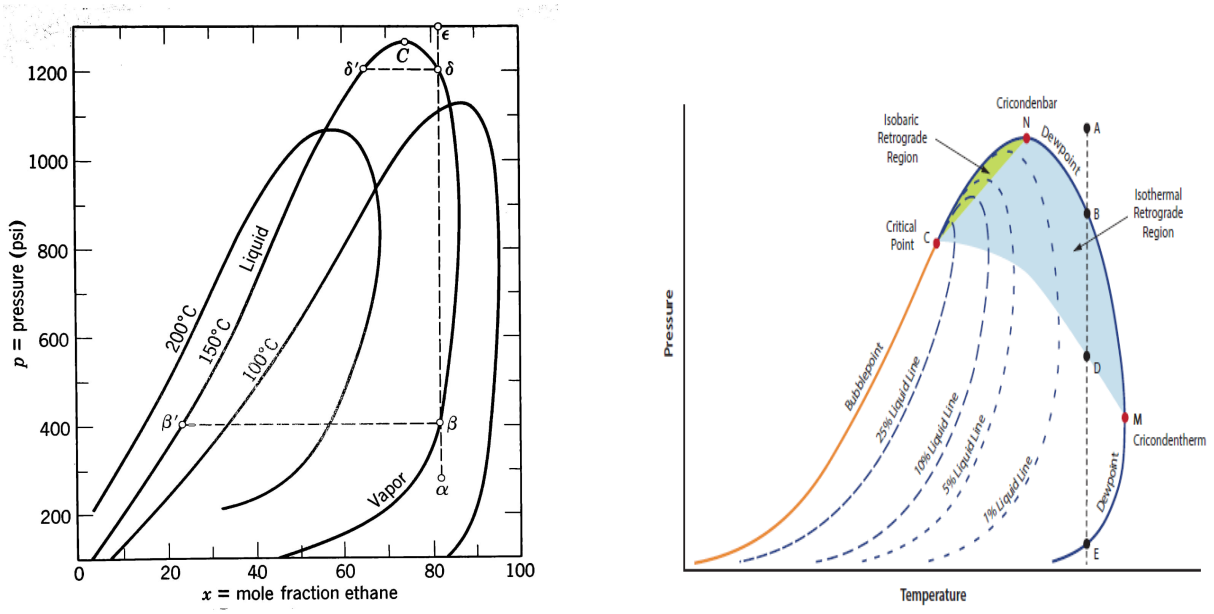

(a) p-x projection of surface shown in Fig. 12a, [4] **(b)** General Vapor-Liquid equilibria of a given binary mixture, taken from [5]

Figure 13: Binary Equation of State

Generally, the portion of the curve which is in contact with the liquidus surface is referred to as "*bubble-point line*" and the portion in contact with the vapor surface is the "*dew-point line*".The critical point of the mixture is the point of juncture of these two lines.

In Fig. 13b, the two types of retrograde phenomena could be presented. As it was pointed out in Fig. 12b, a limiting composition exists for the coexistence of liquid and vapor phases; in the same way, from Fig. 13b, it can be noticed that also a limiting temperature and a limiting pressure exist, beyond which, the coexistence of the two phases is no more possible. These two limiting values are called respectively "*cricondentherm*"(M) and "*cricondenbar*"(N). The position of the critical point with respect to M and N, defines three different cases: cricondentherm and cricondenbar could be both on the bubble line, both on the dew point line, or one on the bubble point line and one on the dew point line. It is important to know their relative position in order to know what will be the behaviour of the mixture when subjected to heating/cooling and compression/expansion processes. Note that in mixtures the critical point no more represents the maximum pressure and temperature at which the two phases coexist. In the last decades, the petroleum industry has given much attention to these problems of retrograde phenomena, since they are of importance in the high-pressure treatment of hydrocarbons.

Let us apply all these considerations to a real case study.

In Fig. 14, the two phase-diagram of a binary mixture composed of methane and propane is shown, with varying compositions.

The representation is made on a p-T diagram; each curve shows the two phases boundary for a different mixture, with varying mole fractions of the same two components. A black geometric symbol is used to identify the position of the mixture critical point, which divides bubble line and dew point line. This mixture is used as example since it will be further studied in this work, because of its pronounced retrograde region.

Firstly it can be noticed the strong variation of the diagram with respect to the composition; secondly the exact position of the critical point is fundamental to properly predict the retrograde condensation behaviour of the mixture. Some coloured lines have been sketched to help in this

analysis.

Starting from the lowest curve, the 95% methane - 5% propane mixture, the critical point is shifted in the bottom part of the curve, making the bubble point line longer than the dew point line. In a case like that (or in the opposite one, with the critical point in the upper part, and a dew point line longer than the bubble line), both the kinds of retrograde condensations could easily be represented. The red line A-B represents a retrograde condensation of second kind, obtained through variation of temperature; it can occur on the right of the mixture critical point (at pressures higher than the critical pressure of the mixture). The green line C-D represents a retrograde condensation of first kind, that occurs with varying pressure and at temperatures higher than the critical temperature (above the critical point). This mixture, in which only a 5% mole fraction of propane is present, shows a wide region where retrograde condensation can occur.

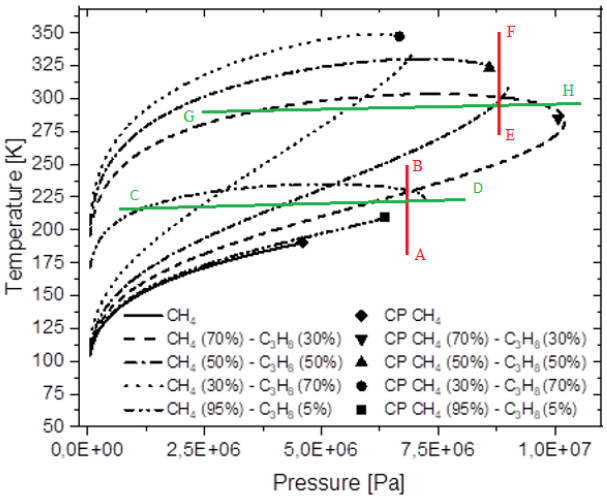

Figure 14: Methane-Propane phase diagram with varying composition. Credits to personal communication with Jaroslaw Shvab.

Moving towards other curves, in which the critical point is approximately equal to the cricondenbar (namely, the critical pressure of the mixture is equal to the maximum pressure of coexistence of the two phases), like the curve of the 70% methane - 30% propane mixture, retrograde condensation of second kind cannot occur, but still, there is the possibility to have retrograde behaviour of first kind (caused by pressure variations). For this reason only the green line G-H has been drawn on that curve.

The opposite case occurs when critical point is approximately equal to the cricondentherm; only retrograde condensation of second kind can exist (due to variations of temperature). This does not exactly happen in the 50%methane -50% propane mixture, but it can be used as example, so only the red line has been drawn.

In industrial applications, the working conditions have to be identified and attention must be paid to these phenomena to avoid the formation of the other phase caused by a decrease of pressure or temperature. In our case, especially the cooling channels for space rocket applications, but also the injection process, can give rise to deep change in the fuel temperature or pressure; then, an accurate evaluation of the vapor liquid boundary is of paramount importance to avoid, or to model, this not intuitive behaviour.

4 The Widom Line

4.1 Phenomenological description

Up to now the development of this discussion has been concentrated in the critical and subcritical domains of the system. In the last few decades, continuously growing attention is paid to the region located after the critical point. In this treatment, the fluid with a pressure and a temperature higher than the critical conditions is called a *supercritical fluid*.
According to many relevant books of the previous century, there exists no physical observable boundary that allows distinguishing a liquid from a gas beyond the critical point, and hence only a single fluid phase exists. However, even if a great effort was made to completely describe fluids behaviour and properties below the critical point, experimental studies in the supercritical region have been limited due to technical difficulties. In 2010 Simeoni et al., [32], were able to demonstrate that some thermophysical quantities have maxima in the critical region, such that a line starting from the critical point and joining these maxima can be drawn. The evidence of these extrema in thermodynamic quantities has been analysed by several authors, [8],[30], [20], [6], [21] in the last decades to give a better understanding of the physical meaning of those peaks. Thanks to many molecular dynamics simulations, a deeper meaning of that behaviour was found; indeed MD allows the evaluation of thermodynamic properties and of the radial distribution function. In statistical mechanics, the radial distribution function, usually indicated as $g(r)$, describes "*how the density of a fluid varies as a function of the distance between particles, or with respect to a reference particle*", [4]. The analysis of this function has shown a quite strong variation in the density when crossing the line of thermodynamic extrema; this strong variation in density resembles the subcritical boiling and was named "*pseudo-boiling*", originally by Kafengauz and Fedorov [22], and later by Oschwald et al. [3], and Okamato et al. [23].

The constant pressure heat capacity is the most frequently chosen response function to find the locus of extrema; depending on the thermophysical property chosen, the obtained line is slightly different. The first definition of this line was given by Sciortino et al. [13], as "*the set of states with a maximum correlation length of the fluid*", but is almost always approximated as "the locus of maximum thermodynamic response functions", since they can be more rapidly calculated from thermodynamic properties. The resulting line is named "*Widom line*", [13].

More precisely in [32] it is carried out an accurate analysis on the sound waves and on the positive dispersion coefficient of fluids; the positive dispersion is an increase of the speed of sound with the wavelength ranging from the continuum limit, with very high wavelengths, to short wavelength limit, reaching interparticle distances. This effect, it is explained in [32], can be generated by the presence of one or more relaxation mechanism that interacts with the dynamics of density fluctuations. Simeoni et al. discovered a different behaviour on the two sides of the Widom line: a liquid-like and a gas-like fluid, with differences very similar to liquid and gases in the subcritical domain (from here, the previous definition of pseudo-boiling).
A first draft of the complete behaviour of a fluid in the different thermodynamic conditions, before and after the definition of the Widom line, is shown in Fig. 15. In particular, in quadrant I, the vapor pressure curve divides the vapor and the liquid state; higher temperatures in II identify gases that cannot be compressed to the liquid state. Fluids in quadrant IV instead, are referred to as compressed liquids, compressible liquids, transcritical liquids or liquids; The last quadrant, III, is the one that identifies supercritical states and in which there is the division between liquid-like (LL) and gas-like (GL). The dotted line is the Widom line.
So far, no quantitative discussion has been given on what happens when crossing the line; it will be the topic of the next sections.

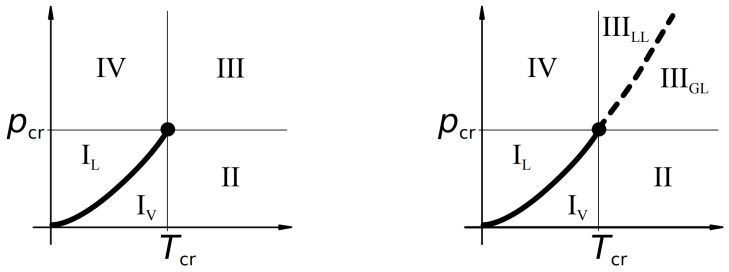

Figure 15: Trans-critical fluid states, taken from [29]

4.2 Widom line equation

As already stated, the original definition of the Widom line was "*the set of states with a maximum correlation length of the fluid*" [13]. However, this property is very hard to evaluate practically. As an approximation, response functions are used by several authors. The most common used thermodynamic functions are the isobaric heat capacity, the isothermal compressibility, and the thermal expansion coefficient.

Banuti et al. found the c_p based Widom line to be well represented by the following equation, [8]:

$$\frac{P}{P_c} = exp\left[\frac{T_c}{\theta_{pb}}\left(\frac{T}{T_c} - 1\right)\right] = exp\left[A\left(\frac{T}{T_c} - 1\right)\right]$$

where the subscripts $_c$ and $_{pb}$ stand for critical and pseudoboiling respectively. Dimensionally, the integration constant $1/\theta_{pb}$ can be interpreted as the inverse of a temperature. In [8], by elaborating the Clapeyron equation near the critical point, it is found that

$$\frac{1}{\theta_{pb}} = \frac{1}{p_c}\left(\frac{dp}{dt}\right)_c$$

thus, the equation of the Widom line can be rearranged as in Eq. (36).

$$\frac{P}{P_c} = exp\left[\frac{T_c}{p_c}\left(\frac{dp}{dt}\right)_c\left(\frac{T}{T_c} - 1\right)\right] \tag{36}$$

The parameter $A = T_c/\theta_{pb}$ in the previous version of the equation was introduced and tabulated in [7] because it is a species dependent constant and has comparable values for simple components.

Eq. (36) tells us *where* to expect some sort of transition phenomenon, but *what* to expect when passing through the Widom line has still to be investigated. This was done in [8]. Let T_- and T_+ be the initial and final temperature of an isobaric transition, such that T_- is smaller than the temperature at which the maximum c_p occurs, and T_+ is larger. In order to overcome the Widom Line, going from a liquid-like to a gas-like fluid, some energy will be required. This energy is quantified as Δh_{pb}.

$$\Delta h_{pb} = \int_{T_-}^{T_+} c_p(T)dT = h(T_+) - h(T_-)$$

The most important finding is that in supercritical conditions, the provided energy is spent to both break molecular bondings *and*, unlikely what happens in subcritical vaporization, raise the temperature of the fluid,[1]. These two contributions are called in [8], structural (st) and thermal (th) contributions.
Δh_{pb} represents the whole area under the $c_P(T)$ curve from T_- to T_+ and so the whole amount of energy required to go from one temperature to the other. The c_p assumes two values: a liquid heat capacity $c_{p,L}$ at low temperatures, while an ideal gas value $c_{p,iG}$ can be used at higher

temperatures. Since no theoretical development can be used for the first, it is assumed to be equal to $c_{p,max}$; for the second, the relation for calorically perfect gas is adopted, $c_{p,iG} = \gamma R/(\gamma - 1)$. Now that all the parameters are defined, it can be considered that the amount of energy needed to heat up the fluid isobarically is $\Delta h_{th} = c_{p,L}\Delta T_{pb}$. The difference between the total amount of energy and the thermal contribution gives the amount of energy needed for the structural contribution, $\Delta h_{st} = \Delta h_{pb} - \Delta h_{th}$.

This is done in [8]. Moreover, Banuti et al. defined two parameters to better visualize the contribution of structural phenomena, and they are presented in Eq. (37) and Eq. (38).

$$B_1 = \frac{\Delta h_{pb}}{\Delta h_L} - 1 \tag{37}$$

$$B_2 = \frac{c_{P,pb}}{c_{P,L}} - 1 \tag{38}$$

The second one is more practical to be used and follows the behaviour of the B_1 with an offset. It has been shown that the values of the parameters can be compared over a range of fluids, especially for the simple fluid. Up to a reduced pressure of 1.5, the structural contribution is higher than the thermal one; this means that the pseudoboiling process raises the amount of energy required to heat the fluid by a factor of two. At $p_r = 3$ there is a 10% of excess energy over liquid heating alone. Towards the critical point, the two parameters diverge since the heating contribution vanishes.
Pseudoboiling is then demonstrated to be a continuous, nonlinear, transcritical process resembling subcritical boiling and that occurs when crossing the Widom line, which has been identified for pure components in Eq. (36). The significant reduction in density that comes during the process strongly resembles classical subcritical vaporization.

4.3 Supercritical transition lines and range of existence

The properties of several fluids have been analyzed during the years with the goal of understanding how the physical transition in supercritical fluids from liquid-like to gas-like can be justified, and which features are shared with the subcritical transition from liquid to vapor.
For supercritical fluids, many transition lines have been suggested; the first was by Fisher and Widom [36], who stated that a transition must exist to explain the difference between the oscillatory decay of the radial distribution function (caused by the predominantly repulsive potential in liquids), and a monotonous decay that characterizes the attractive potential in gases. However, also another treatment based on thermodynamic properties has been carried out. Indeed, it was considered that the subcritical phase transition that occurs across the coexistence line is a first order phase transition; from a thermodynamic point of view, this implies a discontinuity in the slope of the Gibbs free energy, defined as $G = h - Ts$. At supercritical pressures, this jump in the slope has vanished but, it is interesting to see how the Widom line is still strongly related to the Gibbs free energy.
Using the Maxwell relations of classical thermodynamics, several properties can be expressed as a function of the Gibbs free energy, as follows.

$$c_p = \left(\frac{\partial H}{\partial T}\right)_p = -T\left(\frac{\partial^2 G}{\partial T^2}\right)_p \tag{39}$$

$$\alpha_P = \frac{1}{v}\left(\frac{\partial v}{\partial T}\right)_p = \frac{1}{v}\left(\frac{\partial^2 G}{\partial p \partial T}\right)_p \tag{40}$$

$$k_T = -\frac{1}{v}\left(\frac{\partial v}{\partial p}\right)_T = -\frac{1}{v}\left(\frac{\partial^2 G}{\partial^2 p}\right)_T \tag{41}$$

Here, c_p, α_P and k_T are respectively, the isobaric specific heat, the isobaric thermal expansion and the isothermal compressibility. It is evident how all these response functions, that can be used to trace a supercritical transition line, are related to the second derivative of the Gibbs free energy. Thus, Banuti et al. thought that even if the discontinuity in the slope is no more present, a shadow of this transition can be found as a maximum in the curvature of the Gibbs free energy, [29].

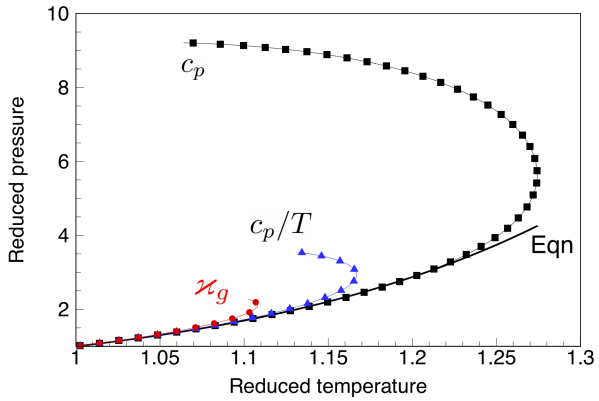

Figure 16: Comparison of Widom lines based on Gibbs free energy, [29].

For this reason, in [29], different functions are evaluated to track their maxima and compare the obtained Widom lines. The selected functions were: c_P, c_P/T (which is equal to the second derivative of the Gibbs free energy) and χ_g, which is the magnitude of the curvature of the Gibbs free energy, defined in Eq. (42).

$$\chi_g = \left| \frac{c_p/T_r}{(1+(-s)^2)^{3/2}} \right| \qquad \text{where} \qquad s = -\frac{\partial G}{\partial T} \tag{42}$$

Fig. 16 shows their results. It is possible to see that the transition temperature does not rise monotonously, but at a certain pressure it curves back to lower temperatures. Up to $p_r \approx 1.5$ all three lines coincide. At higher pressures, first the curvature and then the second derivative of the Gibbs free energy deviate from the c_p-curve. It has been actually shown that even if there is no discontinuity in the slope, there are still pronounced maxima in the curvature. Fig. 16 shows that the loci of maxima deviate from Eq. (36) when they start to curve back; this occurs at reduced pressures of 2, 3, and 4, in the three cases.
The analysis of the curvature is then useful to give a preliminary idea of the endpoint of the Widom line since at higher pressure the peaks of all the thermodynamic properties flatten till losing their physical significance.

Therefore, there is strong evidence for an upper limiting pressure to the thermodynamic Widom line. There is no precise value for it, but a universal flattening in the thermodynamic properties is observed, to the point that any change is negligible, at $p_r \approx 3$, and vanish for $p_r > 10$, [29].

A further complication in the analysis of the supercritical region and identification of the transitional area, is the absence of any reason to justify the choice of the response function that has to be used. For this reason several response functions have been evaluated together, and the resulting Widom Lines were compared with transition lines coming from experimental measures of density or with results coming from MD simulations, [6],[21],[20],[26].
The most relevant feature coming from these works is that all the extrema of the different thermodynamic properties agree over a limited range of temperature and pressure, but for reduced pressure higher than 1.5, the Widom Lines coming from different response functions slightly diverge from the each other. This can be seen for example in Fig. 17, where Banuti et al. presented

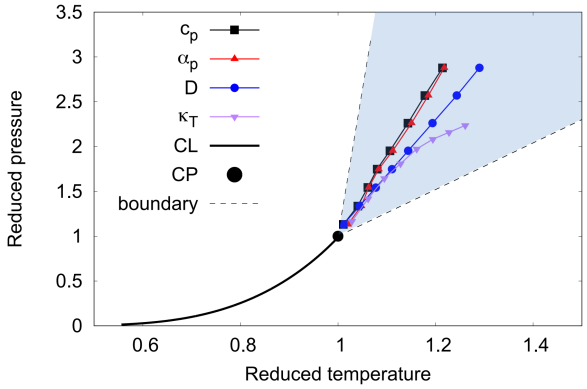

Figure 17: Different Widom Lines for Argon, [29]

the transition lines for pure Argon, [29]. All the lines clearly sketch a transition area, more than a precise boundary between the two states. However, as it is already explained, this region is limited; no more peaks are distinguishable for reduced pressure higher than 3, and moreover, the fluid behaves almost like an ideal gas when heated up to reduced temperature of 2.

4.4 Unified Criterion

As it has been shown, the extrema of the response functions have weakened at a reduced pressure of 3 and completely vanished at 10. However, a more accurate criterion on the endpoint of the Widom Line has been proposed, finding a much smaller transition region.

In [20], Zeròn et al. evaluated the extrema of several response functions and used the coincidence of these curves to determine the end-point of the Widom line. Since the coincidence of the lines can be influenced by the scale used to show the coordinates of the maxima, in their work they chose to present the data in the $T^* - p^*$ plane. Using analytical equations of state, the Widom lines for both a Square-Well and a Hard-Core Lennard-Jones potentials were obtained. In both cases the most separated lines were always those coming from the isobaric specific heat and the isothermal compressibility, and for this reason, the following criterion was adopted: the Widom Line exists till the point in which the condition in Eq. (43) is no more satisfied.

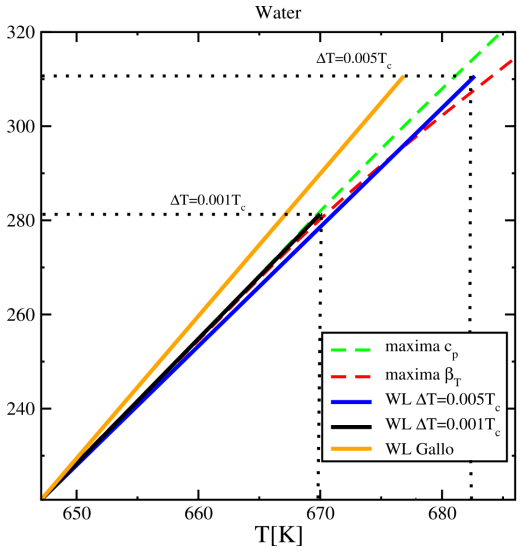

Figure 18: Widom Lines for water, [21].

$$|T_{k_T,max} - T_{c_p,max}| \approx 0.001 T_c \qquad (43)$$

Note that it depends on the critical temperature of the substance considered.
In [21], De Jesus et al. adopted the Zeròn criterion for several calculations. In Fig. 18 their results are shown. The two dashed lines represent the maxima of the two response functions, isobaric specific heat and isothermal compressibility, while the black line is drawn taking as end-point the one suggested by Zeròn in Eq. (43) (note that the black line always lies between the two dashed lines). Instead, the blue one is presented with a 'more-relaxed' criterion:

$$|T_{k_T,max} - T_{c_p,max}| \approx 0.005 T_c$$

With this assumption, the Widom line can not be considered a straight line anymore because in that case, it exits the region defined by the two response functions, so it is surely less accurate. Note that this relaxed criterion makes the Widom line following more the curve of the isothermal compressibility.

In this work, little attention will be paid to the criterion to find the end-point of the Widom Line, since the main goal is to define that region in which strong gradients are found, independently from the exact definition of the end-point of the WL.

4.5 Widom line in binary mixture

How does this description change when talking about mixtures? A good description is given for binary mixture in the work of Raju et al., [30].
A first theoretical differentiation of the different mixing behaviour was given by van Konynenburg and Scott, [24]; starting from the van-der-Waals equation of state, they defined six types of phase behaviour for binary mixtures. In [30], types I and III are considered. The first type includes those mixtures with a continuous gas-liquid critical line connecting the critical points of the pure components and that exhibit complete miscibility; in this category substances of similar species and/or with comparable critical properties are placed (ex. methane/ethane). Type-III mixtures are those mixtures for which the region of liquid-liquid immiscibility goes up to the gas-liquid critical line generating a discontinuity. The difference in intermolecular forces is particularly relevant for the two constituents in this class (ex. nitrogen/heavy hydrocarbons).

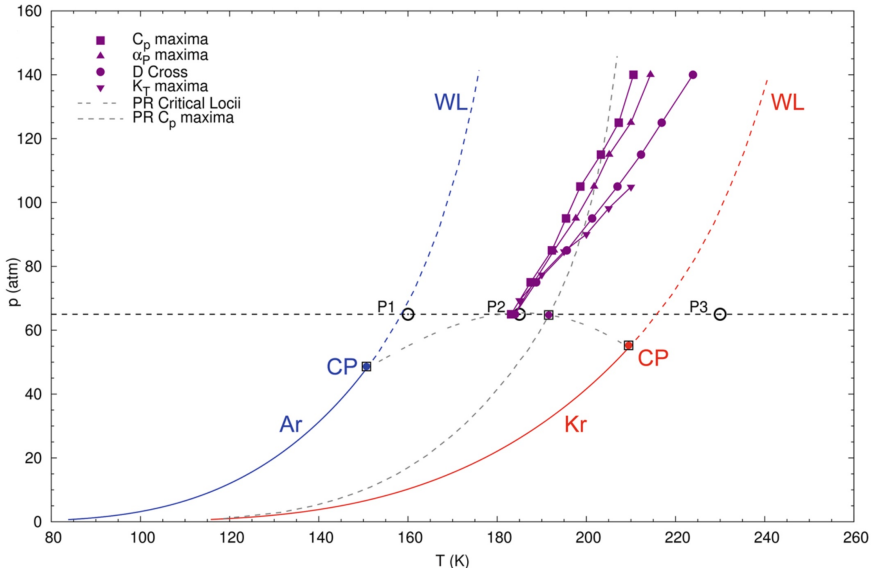

Figure 19: Widom lines for a binary mixture of Argon-Krypton, [30].

Raju et al. [30] conducted experiments and calculations for mixtures of type I using argon and krypton; simulations were performed at temperatures between T=115K and T=275K, at increments of 5K, and for various pressures between p=65atm and p=140atm. The Widom lines for the same three response functions previously used are evaluated and shown in Fig. 19, where also the Peng-Robinson equation for the mixture is presented (dotted line), to show how good it can describe the behaviour of the system, even in supercritical conditions.
The Ar/Kr mixture exhibits a single set of Widom lines that emanate from the critical point of the mixture. This behaviour is extremely similar to the one of a pure component, and to understand this similarity, Raju et al. investigated the structure of the mixture. The argon/krypton radial

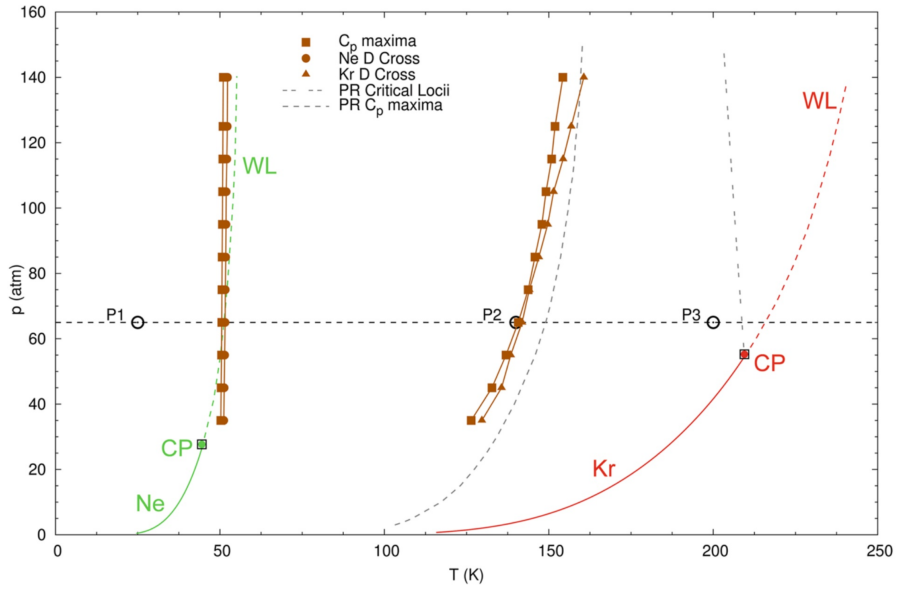

Figure 20: Widom lines for a binary mixture of Argon-Krypton, [30].

distribution functions have perfectly similar behaviour across the phase transition; this suggests that the mixture is homogeneous and that both the components turn from a liquid-like to gas-like phase together. The homogeneity and the miscibility of the mixture generate a pure fluid-like behaviour.

Then, simulations were carried out for a neon/krypton mixture, which has type-III behaviour. Because of the difference in critical properties between the two components, these kinds of mixtures are characterized by a discontinuous gas-liquid critical curve and liquid-liquid immiscibility. To examine the behaviour and the resulting Widom lines, simulations of an equimolar mixture were performed. Fig. 20 shows the results.
A drastically different phase-transition behaviour is observed for this type-III mixture. In particular, it can be noticed that thermodynamic properties like enthalpy or isobaric specific heat show the presence of two distinct phase transitions, namely two distinct peaks at two distinct temperatures. The presence of two different transitions creates two sets of Widom Lines at two distinct locations in the projected p-T state diagram. Therefore, it demonstrates separately the phase transition of each component.

It is important to appreciate that the two distinct phase transitions in this mixture are not identical to the Widom lines of pure components. This shows that there is an interaction between molecules even though the mixture components are immiscible and this affects the transition point of the mixture.
In comparison, the Widom Line obtained from Peng Robinson EoS predicts (and not very well) only the Widom Line that occurs at higher temperature and completely misses the other.

Raju et al. [30] showed that in the second case the mixture is not homogeneous because the radial distribution functions for the pure components are significantly different, showing a transition to a gas-like regime at appreciably different temperatures.
Therefore, the supercritical region in mixtures can no longer be considered as a uniform and homogeneous fluid phase, but it has to be referred to as a complex state space where components transition, from a liquid-like to a gas-like state, can occur simultaneously or separately.

5 Evaluation of thermo-physical properties and Widom Lines

5.1 Starting Point

Since the use of chemical pure methane would lead to extremely high costs, real operations are supposed to implement liquefied natural gas (LNG) which is significantly more cost-efficient. This propellant will include different impurities, as shown for example in common mixtures used in DLR in Tab. 1; these impurities can significantly influence the thermodynamic properties of the fuel. Actually, the little understanding in the field of thermodynamic and transport properties of mixtures in supercritical states limits their application because those properties are fundamental to determine the behaviour of the propellant and heat transport processes under rocket engine operation conditions, like during cooling or injection.

Chem. Name	**Mol.%**	**Mol.%**	**Mol.%**
CH_4	95.6320	99.5481	99.4985
C_2H_6	3.9922	0.1279	0.0477
C_3H_8	0.2232	-	0.0067
$i-C_4H_{10}$	0.0396	-	-
$n-C_4H_{10}$	0.0347	-	-
$i-C_5H_{12}$	0.0014	-	-
$n-C_5H_{12}$	0.0005	-	-
N_2	0.0764	0.3077	0.429
CO_2	-	0.0163	0.0181

Table 1: Three typical mixtures of LNG in conventional storage facilities and used for tests at Institute of Space Propulsion, German Aerospace Center.

In this work, many aspects of methane-based mixtures are covered; starting from the evaluation of the critical point and the vapor-liquid equilibrium curve, and then moving to the supercritical environment.
It has to be noticed that this work is just a part of a bigger project whose results will be submitted to be published, [15]. The authors of this project are: Dr. N. Slavinskaya, J. Shvab, D. Suslov, Prof. Dr.-Ing. O.J. Haidn, and the author of this thesis, T. Santese.

This is important because some of the results obtained from other co-authors will be introduced before the results obtained in the frame of this specific thesis.

In Tab. 2 some major properties of substances available in relevant quantities in LNG are collected. The clear differences in the Lennard Jones parameters and in the critical and triple point properties, underline a possible problem in the EoS of mixtures since it can cause appreciable deviations of the mixture critical properties from the methane ones. It can be a root for possible retrograde condensation, but also can cause the critical region to be nearer to the prescribed operating space conditions.

In particular for carbon dioxide, the triple point connecting the three phases has much higher values than methane's triple point; therefore, solid carbon dioxide could exist within the liquid or gaseous methane. Also, its critical point is higher in pressure and temperature than the one of methane and could affect the boiling line of the mixtures. Thus, for safety reasons, the CO_2 should be avoided completely.

In this work then, mixtures of methane, ethane, propane, nitrogen and hydrogen have been considered. The three hydrocarbons have critical properties comparable in magnitude, nitrogen-methane is a type-I binary mixture [30], and exhibit complete miscibility at all temperatures. Hydrogen instead, has critical parameters much lower than methane; therefore it cannot influence

Chem. Name	$T_c[K]$	$P_c[MPa]$	T_{tr} [K]	P_{tr} [MPa]	Ac. factor ω	$\epsilon/k[K]$	$\sigma[A]$
Methane	190.56	4.6	90.69	11.7	0.011	141.40	3.746
Ethane	305.32	4.9	90.37	0.001	0.099	252.30	4.302
Propane	369.83	4.2	85.52	$1.7 \cdot 10^{-7}$	0.152	266.90	4.982
Nitrogen	126.19	3.4	63.15	12.6	0.037	38.00	2.290
Hydrogen	33.18	1.3	13.80	7.04	-0.22	244.00	3.763
Carb. Dioxide	304.18	7.4	216.59	15.37	0.225	97.53	3.621

Table 2: Critical point, triple point and LJ parameters for investigated components, taken from [10], [4], [41],[48],[2].

vapor-liquid equilibria of mixtures, but its impact on the critical point and supercritical behaviour of mixtures should be analyzed.

All the possible combination of mixture were considered among these 5 components, with a concentration of each impurity that was varied in 0.5% steps until the maximum proportion of 5% of mole fraction was reached.

5.1.1 Results from Co-Authors

In [15], the Soave modification of Redlich-Kwong cubic EoS has been used, together with the algorithm described in detail in the work of Zizin and Slavinskaya, [37], for the evaluation of the critical point of mixtures. This algorithm was based on the work of Heidemann and Khalil [16] and Michelsen and Heidemann [31]; since the critical point is placed on the stability curve of the stable phase, it was found by expanding in Taylor series the Helmholtz free energy around a test point. Based on these works, the critical point was achieved if both the quadratic and cubic terms in Taylor series were equal to zero. All the information are given in [37].

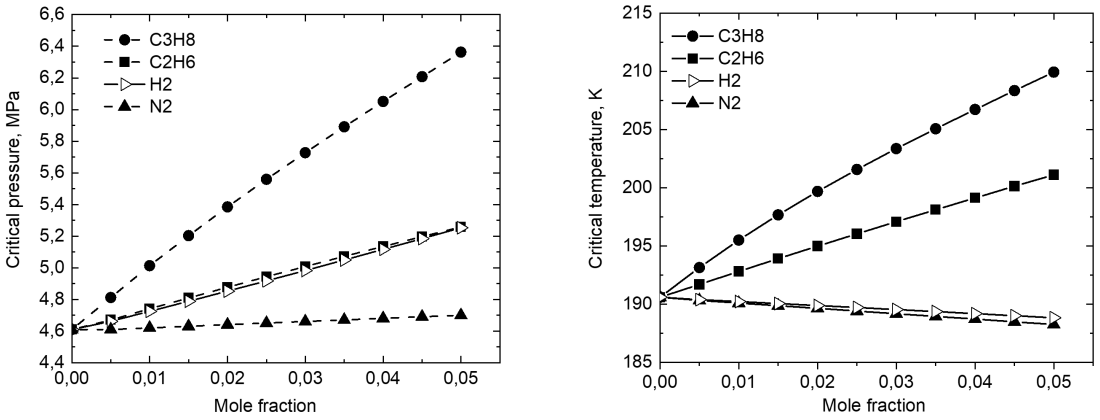

Figure 21: Critical pressure and temperature of a mixture of methane containing variable mole fractions of Propane (C_3H_8), Ethane (C_2H_6), Nitrogen (N_2) or Hydrogen (H_2), taken from [15].

The results show drastic changes in the coordinates of the critical point as the composition is varied. Particularly interesting are the charts showed in Fig. 21. In this figure, the variation of the critical pressure (on the left) and temperature (on the right) is presented , for a binary mixture containing methane and a second component whose mole fraction goes from 0 to 0.05. Propane is the component that has a maximal impact on critical parameters; a 0.05 mole fraction of propane leads to an increase in critical pressure of 39% and of the critical temperature of 10% with respect to the methane critical constants. Also, the other elements have a non-negligible influence on the critical point mixture, in particular hydrogen and ethane.

From all the gathered data about the influence of impurities on the critical point of the mixture, in [15], a very accurate linear approximation has been extrapolated to evaluate the critical point of methane-based mixtures containing the other four components under investigation. In particular critical temperature and pressure can be evaluated as in Eq. (44).

$$\begin{cases} T_c = a_{t0} + a_{t1}x_{CH4} + a_{t2}x_{C2H6} + a_{t3}x_{C3H8} + a_{t4}x_{N2} + a_{t5}x_{H2} \\ P_c = a_{p0} + a_{p1}x_{CH4} + a_{p2}x_{C2H6} + a_{p3}x_{C3H8} + a_{p4}x_{N2} + a_{p5}x_{H2} \end{cases} \tag{44}$$

where x_i is the mole fraction of the i-th component, while the coefficients a_i can be found in Tab. 3.

	a_0	a_{CH4}	a_{C2H6}	a_{C3H8}	a_{N2}	a_{H2}
T_c	91.76334	99.27925	305.31115	514.01379	53.02326	65.95531
P_c	22.21207	23.84545	158.4874	410.07809	50.37995	170.27066

Table 3: Coefficients for Eq. (44), taken from [15].

The accuracy of this linear approximation was measured taking as the exact result the one given by the long mathematical process explained in [37]. It has a mean error of 0.126% for the critical temperature and 0.422% for the critical pressure.

Using the algorithm described in [37], it was possible to construct the vapor-liquid diagrams from low pressure to critical point for mixtures composed of up to 20 compounds.
As for the critical properties, also the vapor-liquid diagram presents strong variations with respect to the composition. The mixtures of hydrocarbons present the phenomenon of retrograde condensation, which was previously explained. This phenomenon can be more or less pronounced, depending on the components and their mole fraction.

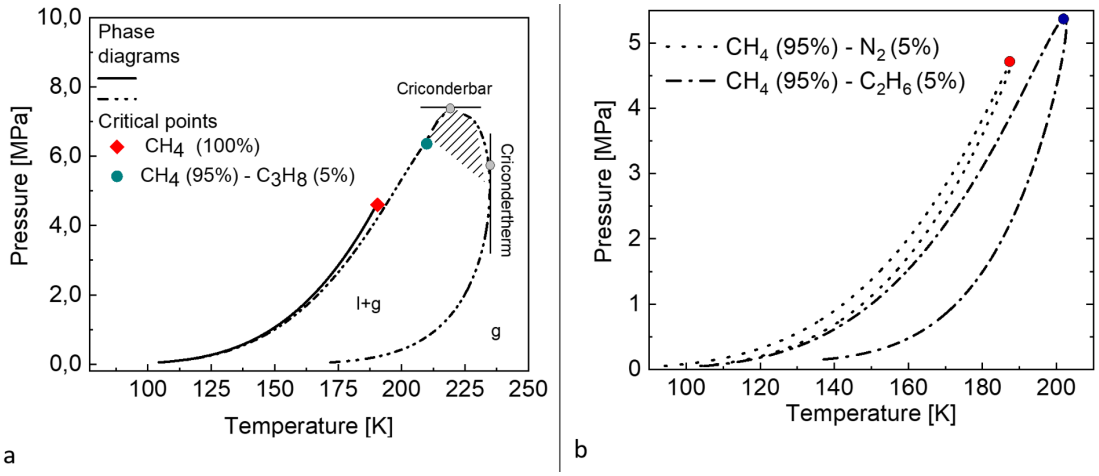

Figure 22: Vapor-liquid equilibria for different mixture; a) methane 95% - propane 5% b) methane 95% - ethane 5% and methane 95% - nitrogen 5%, taken from [15].

Some results are here reported, in Fig. 22. In the left part, it can be seen the vapor pressure curve of pure methane, compared with the vapor liquid equilibria for the binary mixture with a 0.05 mole fraction of propane. Making a comparison with the right part, where the second element is ethane or nitrogen, it is clear the presence of a much more pronounced region where retrograde condensation can occur, highlighted with oblique grey lines.
The blend with propane is again the mixture whose properties are the most influenced, and for this reason, it will be better treated in the following.

5.2 Supercritical Region - The Equation of State

When moving to the supercritical domain, some problems with the validity of Redlich-Kwong EoS and with the applied mixing rules may arise. For this reason, it has been chosen to use a much more complex and recent model, the GERG-2008, proposed by Kunz and Wagner in [19] and updated in [25], where all the problems are comprehensively solved.

GERG-2008 is a wide-range model mainly for mixtures of natural gases or similar gases but that involves some other elements. It is based on pure components EoS of each element present in the mixture (with 21 natural gases available) and correlations developed for binary blends of these components, up to a total of 210 binary mixtures.

Thus, applying modern optimization methods and using experimental data covering the whole fluid region, namely the homogeneous gas, liquid and supercritical region, the fitting parameters were evaluated and an empirical equation of state was formulated. This model can predict the properties of several natural gases and multicomponent mixtures in a prescribed range of validity with the declared accuracy, [25]. The fitting of GERG-2008 parameters was based on a database composed of more than 125 000 experimental data for many thermodynamic properties in different fluid regions.
The normal range of validity of GERG-2008 includes temperatures from 90 to $450K$ and pressures up to $35MPa$ where the most accurate experimental data are represented within their accuracy. For this model, it has been also defined an extended validity range in which the accuracy is slightly lower, but allows to make calculation up to temperatures of $700K$ and pressure of $70MPa$.

GERG-2008 is explicit in the Helmholtz free energy which is treated as a function of density, temperature and composition vector. Let $a(\rho, T, \bar{x})$ be the Helmholtz free energy; it is split into "ideal gas" contribution (indicated with superscript ^{o}) and "residual" contribution (superscript ^{r}). It is then used in its dimensionless form, $\alpha = a/RT$, obtaining Eq. (45).

$$\alpha(\delta, \tau, \bar{x}) = \alpha^o(\rho, T, \bar{x}) + \alpha^r(\delta, \tau, \bar{x}) \tag{45}$$

where δ and τ are respectively the reduced mixture density and the inverse reduced mixture temperature according to:

$$\delta = \rho/\rho_r \qquad \tau = T_r/T \tag{46}$$

Here, ρ_r and T_r are composition-dependent parameters, and are defined as follows:

$$\frac{1}{\rho_r(\bar{x})} = \sum_{i=1}^{N} x_i^2 \frac{1}{\rho_{c,i}} + \sum_{i=1}^{N-1} \sum_{j=i+1}^{N} 2x_i x_j \beta_{v,ij}\gamma_{v,ij} \frac{x_i + x_j}{\beta_{v,ij}^2 x_i + x_j} \frac{1}{8} \left(\frac{1}{\rho_{c,i}^{1/3}} + \frac{1}{\rho_{c,j}^{1/3}} \right)^3$$

$$T_r(\bar{x}) = \sum_{i=1}^{N} x_i^2 T_{c,i} + \sum_{i=1}^{N-1} \sum_{j=i+1}^{N} 2x_i x_j \beta_{T,ij}\gamma_{T,ij} \frac{x_i + x_j}{\beta_{T,ij}^2 x_i + x_j} (T_{c,i} + T_{c,j})^{0.5}$$

The binary parameters $\beta_{v,ij}$,$\gamma_{v,ij}$, $\beta_{T,ij}$ and $\gamma_{T,ij}$ are given in [25]; $\rho_{c,i}$ and $T_{c,i}$ are the critical density and temperature of the i-th component according to [25] and N is the number of components.
Now, for what concerns the ideal-gas contribution it is expressed as:

$$\alpha^o(\rho, T, \bar{x}) = \sum_{i=1}^{N} x_i \left[\alpha_{oi}^o(\rho, T) + \ln x_i \right]$$

where

$$\alpha^o_{oi}(\rho,T) = \ln\left(\frac{\rho}{\rho_{c,i}}\right) + \frac{R^*}{R}\left[n^o_{oi,1} + n^o_{oi,2}\frac{T_{c,i}}{T} + n^o_{oi,3}\ln\frac{T_{c,i}}{T} + \sum_{k=4,6} n^o_{oi,k}\ln\left(\left|\sinh\left(\theta^o_{oi,k}\frac{T_{c,i}}{T}\right)\right|\right)\right.$$
$$\left. - \sum_{k=5,7} n^o_{oi,k}\ln\left(\cosh\left(\theta^o_{oi,k}\frac{T_{c,i}}{T}\right)\right)\right]$$

Here, $n^o_{oi,k}$ and $\theta^o_{oi,k}$ depend on the i-th component and are tabulated in [25]. the ratio R^*/R is necessary to correct some old data; $R^* = 8.314510$, while R is the universally accepted value of 8.314472.
The residual part of the dimensionless Helmholtz free energy is instead developed in the following way:

$$\alpha^r(\delta,\tau,\bar{x}) = \sum_{i=1}^{N} x_i\alpha^r_{oi}(\delta,\tau) + \sum_{i=1}^{N-1}\sum_{j=i+1}^{N} x_i x_j F_{ij}\alpha^r_{ij}(\delta,\tau) \tag{47}$$

The first sum in this equation is the "linear contribution", instead the second term is the so-called "Departure Function" and it is evaluated only for those couple of components for which a departure function was available. For other couples, F_{ij} is taken as zero (F_{ij} values can be found in [25]). The second term is evaluated as the sum of all binary specific departure functions of the involved binary subsystems; these departure functions are based on quadratic mixing rules, which are reasonably connected to physically well-founded mixing rules. To define the two terms of the residual Helmholtz free energy, the following relations are necessary.

$$\alpha^r_{oi}(\delta,\tau) = \sum_{k=1}^{K_{pol,i}} n_{oi,k}\delta^{d_{oi,k}}\tau^{t_{oi,k}} + \sum_{k=K_{pol,i}+1}^{K_{pol,i}+K_{exp,i}} n_{oi,k}\delta^{d_{oi,k}}\tau^{t_{oi,k}}e^{-\delta^{c_{oi,k}}}$$

All the parameters $n_{oi,k}$,$d_{oi,k}$,$t_{oi,k}$,$c_{oi,k}$,$K_{pol,i}$ and $K_{exp,i}$ are given in [25] for each i-th component. Moreover:

$$\alpha^r_{ij}(\delta,\tau) = \sum_{k=1}^{K_{pol,ij}} n_{ij,k}\delta^{d_{ij,k}}\tau^{t_{ij,k}} + \sum_{k=K_{pol,ij}+1}^{K_{pol,ij}+K_{exp,ij}} n_{ij,k}\delta^{d_{ij,k}}\tau^{t_{ij,k}}$$
$$\cdot\exp\left[-\eta_{ij,k}(\delta-\epsilon_{ij,k})^2 - \beta_{ij,k}(\delta-\gamma_{ij,k})\right]$$

Also in this case all the parameters $n_{oi,k}$,$d_{oi,k}$,$t_{oi,k}$,$\eta_{oi,k}$,$\epsilon_{ij,k}$,$\beta_{ij,k}$,$\gamma_{ij,k}$, $K_{pol,ij}$ and $K_{exp,ij}$ are given in [25] for each couple of components for which the departure function is known (and so F_{ij} is different from zero, otherwise the term α^r_{ij} is not even evaluated).

α^r_{ij} was developed in [25] for either a specific binary mixture (specific departure function) or a certain group of binary mixtures (generalized departure function).
Once all these relations are implemented, the dimensionless Helmholtz free energy is completely defined by Eq. (45). In the homogeneous gas, liquid and supercritical region, a more common pressure explicit equation of state can be retrieved from the Helmholtz free energy with a simple relation.

$$P(\delta,\tau,\bar{x}) = \rho RTZ = \rho RT(1+\delta\alpha^r_\delta) \tag{48}$$

Where a simplified notation, that will be used also in the next sections, is implemented:

$$\alpha^r_\delta = \frac{\partial\alpha^r}{\partial\delta}$$

5.3 The code

The model is implemented in MATLAB, [35].
The code allows the evaluation of mixtures of eight components, even if in this work only 5 of them are considered. The input is then an 8-numbers vector, containing the mole fraction of the 8 allowed components. It is important to give this vector respecting the order of the elements; in particular, the positions are: 1-Methane, 2-Ethane, 3-Propane, 4-i-Butane, 5-n-Butane, 6-Nitrogen, 7-Hydrogen and 8-Carbon Dioxide. So for example, if the mixture is a 95% Methane and 5% Propane, the right input vector would be:

$$x = [0.95, 0, 0.05, 0, 0, 0, 0, 0]$$

As it was said, all the evaluations in this work are done considering only mixtures of methane, ethane, propane, nitrogen and hydrogen, which are the most common components that would be found in LNG for space applications. Butane and Carbon Dioxide were excluded from the work after the implementation of the EoS.

The first step to build the code has been writing some functions in which all the data coming from tables, [25] are stored. In this way, calling a function, giving the right indexes, all the parameters are retrieved. This is the reason for which the mixture has to be given in a precise order, because the position in the composition vector is used to identify which component is that and to pick the right parameters from tables.
Having now all the parameters, the relations in the previous section can be used to define the Helmholtz free energy. A very peculiar MATLAB feature is the *symbolic toolbox* that allows the user to define some variables, use them to create functions and derive them with respect to those variables.
At the beginning of the code, twelve variables are defined: T, ρ, τ, δ, x_1, x_2, x_3, x_4, x_5, x_6, x_7 and x_8. Even if a mixture composition is defined as an input, all the calculations are done keeping the composition as a variable and substituting the composition only at the end; this because some thermodynamic properties require the derivation with respect to the mole number (ex. for fugacity coefficient).
Once the Helmholtz free energy and pressure are retrieved by means of Eq. (45) and Eq. (48), all the needed thermodynamic properties can be evaluated. The isobaric heat capacity is linked to α through Eq. (49), which comes from [25].

$$c_p(\delta, \tau, \bar{x}) = R\left[-\tau^2(\alpha^o_{\tau\tau} + \alpha^r_{\tau\tau}) + \frac{(1 + \delta\alpha^r_\delta - \delta\tau\alpha^r_{\delta\tau})^2}{1 + 2\delta\alpha^r_\delta + \delta^2\alpha^r_{\delta\delta}} \right] \tag{49}$$

It can be noticed from Eq. (45), that α^r is actually a function of δ and τ so all its derivatives are easy to be developed in MATLAB thanks to the symbolic toolbox; instead, α^o is a function of ρ and T so it cannot be directly derivated with respect to τ. The right procedure to take this derivative is reported in [25] and accounts for the following passages.

$$\alpha^o_{\tau\tau} = \frac{\partial^2 \alpha^o}{\partial \tau^2} = \sum_{i=1}^{N} x_i \left(\frac{T_{c,i}}{T_r}\right)^2 \left(\frac{\partial^2 \alpha^o_{oi}}{\partial (T_{c,i}/T)^2}\right)$$

and

$$\left(\frac{\partial^2 \alpha^o_{oi}}{\partial (T_{c,i}/T)^2}\right) = R^*/R\left[-n^o_{oi,3}\left(\frac{T}{T_{c,i}}\right)^2 - \sum_{k=4,6} n^o_{oi,k} \frac{(\theta^o_{oi,k})^2}{(\sinh(\theta^o_{oi,k} \cdot T_{c,i}/T))^2} \right.$$
$$\left. - \sum_{k=5,7} n^o_{oi,k} \frac{(\theta^o_{oi,k})^2}{(\cosh(\theta^o_{oi,k} \cdot T_{c,i}/T))^2} \right]$$

A similar formulation is given in [25] for the evaluation of the isochoric heat capacity, presented in Eq. (50).

$$c_v(\delta,\tau,\bar{x}) = R\Big[-\tau^2(\alpha^o_{\tau\tau}+\alpha^r_{\tau\tau})\Big] \tag{50}$$

For what concerns the thermal expansion coefficient, α_p, and the isothermal compressibility, k_T, they can be expressed as a function of ρ and T through the following relations found on [9].

$$\alpha_p = \frac{1}{\rho}\frac{\partial P/\partial T}{\partial P/\partial \rho} \tag{51}$$

$$k_T = \frac{1}{\rho}\frac{1}{\partial P/\partial \rho} \tag{52}$$

These derivatives of the pressure are evaluated after the evaluation of P through Eq. (48) and the substitution of the reduced variables δ and τ with T and ρ according to the relation Eq. (46).
The last property that will be used in this work is the speed of sound, whose evaluation is performed in Eq. (53), according to [25].

$$w^2(\delta,\tau,\bar{x}) = \frac{RT}{M}\left[1+2\delta\alpha^r_\delta+\delta^2\alpha^r_{\delta\delta}-\frac{(1+\delta\alpha^r_\delta-\delta\tau\alpha^r_{\delta\tau})^2}{\tau^2(\alpha^r_{\tau\tau}+\alpha^o_{\tau\tau})}\right] \tag{53}$$

Other thermodynamic properties like Joule-Thomson coefficient or isentropic exponent could be easily evaluated just by implementing the relations explained in [25]; here only the process required to evaluate the fugacity coefficient φ_i of the i-th component is reported since it explains the choice of leaving the composition as a variable of the process.

$$\ln\varphi_i = \left(\frac{\partial n\alpha^r}{\partial n_i}\right) - \ln(1+\delta\alpha^r_\delta) \tag{54}$$

The process to evaluate the derivative with respect to the mole number n_i of the i-th component is explained in [25] and it is the following:

$$\left(\frac{\partial n\alpha^r}{\partial n_i}\right) = \alpha^r + n\left(\frac{\partial \alpha^r}{\partial n_i}\right)$$

where

$$n\left(\frac{\partial \alpha^r}{\partial n_i}\right) = \delta\alpha^r_\delta\left[1-\frac{1}{\rho_r}n\left(\frac{\partial\rho_r}{\partial n_i}\right)\right]+\tau\alpha^r_\tau\frac{1}{T_r}n\left(\frac{\partial T_r}{\partial n_i}\right)+\alpha^r_{x_i}-\sum_{k=1}^{N}x_k\alpha^r_{x_k}$$

The derivatives α^r_τ,α^r_δ and $\alpha^r_{x_i}$ are of easy evaluation in `MATLAB` if the composition is kept as variable, since α^r is actually a function of δ, τ and $\bar{x}$. Instead, to get the derivatives with respect to the mole number the following relations are needed.

$$n\left(\frac{\partial\rho_r}{\partial n_i}\right) = \left(\frac{\partial\rho_r}{\partial x_i}\right) - \sum_{k=1}^{N}x_k\left(\frac{\partial\rho_r}{\partial x_k}\right)$$

$$n\left(\frac{\partial T_r}{\partial n_i}\right) = \left(\frac{\partial T_r}{\partial x_i}\right) - \sum_{k=1}^{N}x_k\left(\frac{\partial T_r}{\partial x_k}\right)$$

5.4 Validation of Pure Components

In this paragraph, not all the details of the computations will be given, but the logic of the process and the method are explained. More details will be given later on, during the presentation of the final results.
After the implementation of all the component specific parameters and all the relations explained in the previous paragraph, the thermodynamic quantities result to be expressed in the code as a function of δ,τ, ρ, T and the vector $\bar{x}$ of the composition. At this point, δ and τ can be substituted, following Eq. (46), and also the vector $\bar{x}$ is replaced by the actual mixture. The result gives all the thermodynamic properties as a function of ρ and T only.

The final goal of this analysis is to evaluate the behaviour of the selected response functions at given reduced pressure values, in order to identify the coordinates of the extrema, and then fitting these points to get Widom Lines.
In order to compare the results with the already existent literature regarding the Widom Line, our results should be expressed in Pressure-Temperature diagrams and, as anticipated, the evaluation of the thermodynamic properties should be performed at fixed pressure values. Since all the thermodynamic properties implemented up to now are functions of ρ and T only, in order to fix the pressure, the corresponding density has to be found.
For each reduced pressure, a temperature vector is created started from the critical point of the mixture and a loop is implemented: at each value of the temperature vector, the equation of state shown in Eq. (48) is solved to find the density at that temperature and that fixed pressure. To solve the equation of state, given the pressure and the temperature, the implicit equation solver "*fsolve*" is used, which is a built-in function of MATLAB, [35].
so to sum up: for a given pressure value, at each step of the loop, the temperature is taken from the vector, the density is retrieved, and the value of the thermodynamic property is evaluated at those T and ρ.

NOTE: Solving the implicit equation in the density is possible for reduced pressure starting from approximately 1.1; this happens because if the same procedure was applied too near the critical point, the result would be unreliable, because of the extremely high density fluctuation occurring at the critical point. To better understand this, Fig. 23 is used; as it can be seen there, even a small error in the evaluation of critical pressure and/or temperature would lead to a big error in the calculation of the critical density because of the meniscus shown near the critical point. Starting with reduced pressure of 1.1 allows to avoid the region where the results could be extremely altered by small errors in the evaluation of the critical point.

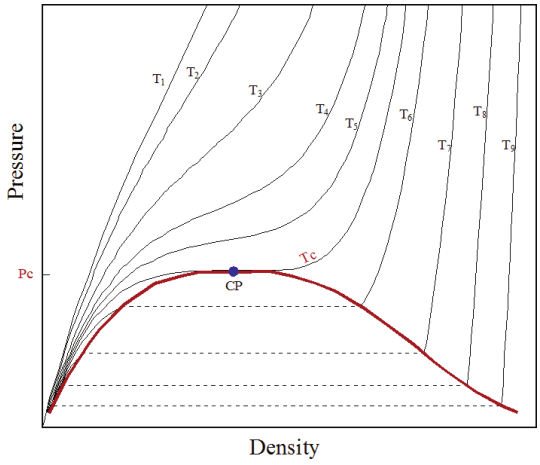

Figure 23: Pressure - Density behavior near critical point. The image is taken from [34].

The procedure of evaluating thermodynamic quantities at constant pressure, is implemented in a double-loop (on pressure and temperature), and a draft of it is here reported:

```
for each  Pr (1.1, 1.2, 1.5, 1.75, 2, 2.25, 2.5, 3, 3.5)
    for each T (from T_crit to  T_crit+150)
    % given the temperature and the pressure at each step, find rho
```

```
    rho = fsolve ( EoS )
    % evaluate TD properties @(T,rho)
    cp(T,rho) =
    cv(T,rho) = ...
    then store the values of TD properties in a vector, at fixed P and varying T
    end
end
```

As it has already been shown, the implementation of the GERG-2008 EoS is not trivial and involves hundreds of parameters for each component of the mixture. Moreover, starting from a dimensionless Helmholtz free energy, several mathematical rearrangements are needed to get the results in pressure-temperature diagrams. In order to verify that the implementation of the EoS and the evaluation of the properties has been successful, the results for pure components coming from the code are compared with the most important database for thermo-physical properties, the NIST database, [45]. In particular, the NIST-Webbook, [10], allows downloading many data for pure components, selecting the range of temperature and pressure of interest. In this validation process, data for methane and propane have been used to verify the correctness of the code.

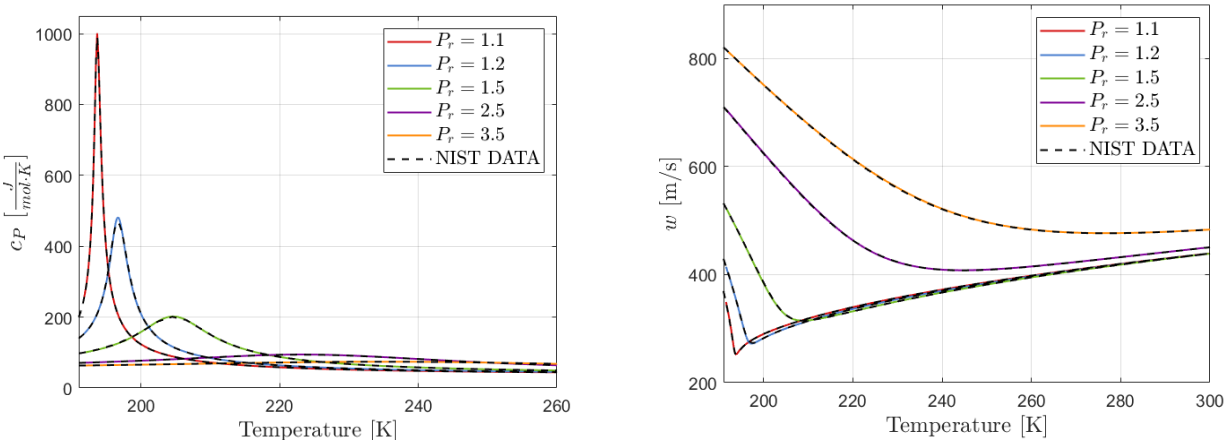

Figure 24: Comparison of isobaric heat capacity, c_p and speed of sound w in supercritical methane between this work (coloured lines) and NIST database (black dashed lines).

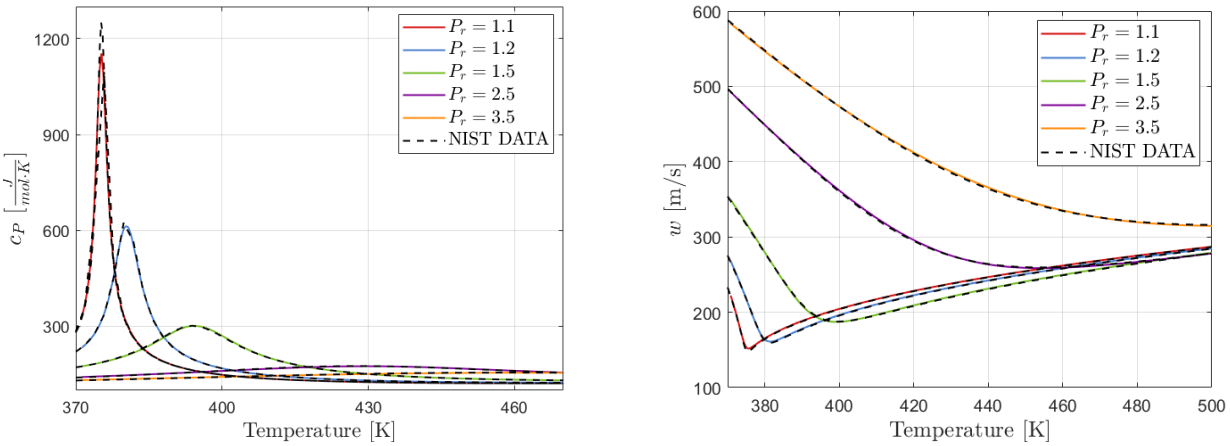

Figure 25: Comparison of isobaric heat capacity, c_p and speed of sound w in supercritical propane between this work (coloured lines) and NIST database (black dashed lines).

Here the comparison is reported only for pure methane and pure propane; this is because methane is the basic constituent of the analysed mixtures, and propane is the only element that shows a slight deviation from NIST data. Fig. 24 and Fig. 25 show the comparison for two differ-

ent properties; on the left the isobaric heat capacity and on the right the speed of sound.

The results are outstanding. The data from NIST are taken with a temperature step of 0.2 K, which means with very high accuracy; nevertheless, the results of this work follow them perfectly at every pressure value, especially for methane. As anticipated, only a slight deviation for propane occurs, in the case of the peak for reduced pressure equal to 1.1. However, the temperature at which the peak occurs is well predicted, and it will be used later in our calculations. For all the other elements, the thermodynamic properties are predicted extremely good, when compared with NIST data.

5.5 Results for Pure Components

All the results presented from this section, will be submitted for publication; hence, a different software for plotting has been used, which is ORIGIN, [38].

Once the thermodynamic functions are evaluated, the vector containing all the values will be manipulated to obtain the position of the extrema that will be used to draw the Widom Line.
As it has been shown in Section 4, the isobaric heat capacity is the most used quantity to individuate the first Widom Line, in order to find the region in which the phenomenon presented as "pseudo-boiling" occurs, that separates a liquid-like from a gas-like region.
In literature, different results can be found for pure component Widom Line; for this reason, it has been chosen to compare our results with previously presented Widom Lines for pure components. One of the most relevant studies about these lines has been carried out by D.Banuti; starting from the Clayperon equation, he found that the Widom Line can be drawn for pure components using a simple exponential relation, here presented in Eq. (55), [7].

$$P_r = exp[A_s(T_r - 1)] \tag{55}$$

where A_s is defined as $\frac{T_c}{P_c}\left(\frac{dP}{dT}\right)_c$, and it has been tabulated for pure components, as it can be seen in Fig. 26.

Species	ω	A_s
He	−0.382	3.516
H_2	−0.219	4.137
Ne	−0.0387	5.028
Ar	−0.00219	5.280
Kr	−0.0009	5.307
Xe	0.00363	5.326
O_2	0.0222	5.428
N_2	0.0372	5.589
F_2	0.0449	5.686
CO	0.050	5.750
CH_4	0.01142	5.386
C_2H_6	0.0993	5.687
C_3H_8	0.1524	5.882
C_4H_{10}	0.201	6.257
C_5H_{10}	0.251	6.117
C_6H_{12}	0.299	6.688
CO_2	0.22394	6.470
NH_3	0.25601	6.235
R124	0.28810	6.597
H_2O	0.3443	6.479

Figure 26: Tabulated coefficients for Banuti equation in Eq. (55), taken from [7].

Again, the validation has been conducted for methane and propane, using the peak of the c_p; the resulting Widom Lines are shown in Fig. 27.

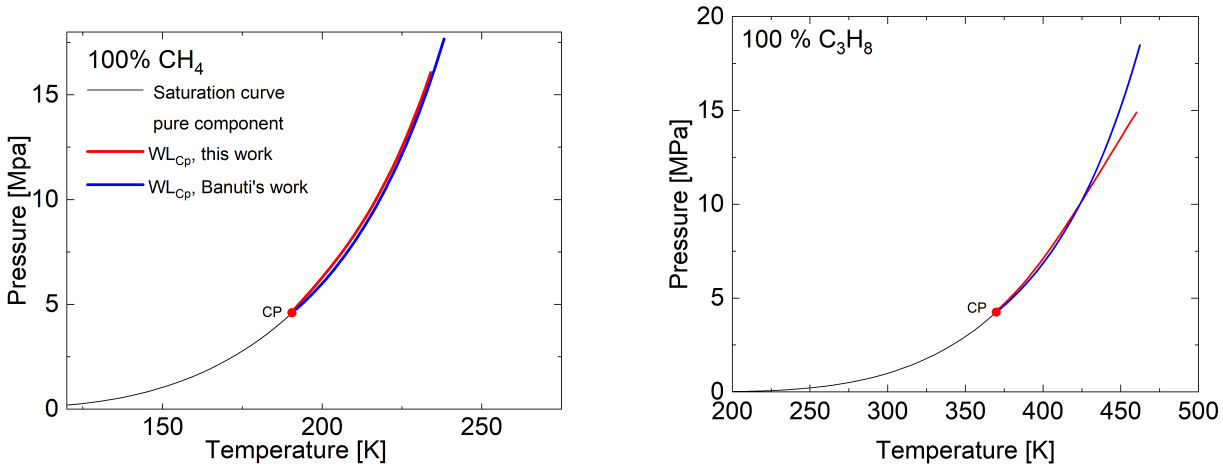

Figure 27: Widom Line comparison between this work and analytical extrapolation from Banuti equation Eq. (55), for methane on the left and propane on the right.

It is evident the extremely good agreement also in this case; for a more complex molecule like the propane there is a slight deviation between the two results for higher reduced pressure, but since the isobaric heat capacity has been computed correctly, obtaining the same values of the NIST database, this result may reveal a more accurate prediction than the mathematical extrapolation of D.Banuti, which can suffer the complexity of heavier molecules.

It is still missing how those Widom Lines, presented in Fig. 27, are evaluated.
It has been said that they come from the extrema of the corresponding response functions, the c_p in that case. But it is needed to be more precise on the method of evaluation of the extrema's coordinates.
Everything starts with the evaluation of the critical point of the mixture, which is done with the linear approximation described earlier in Eq. (44), taken from Shvab's work. Once critical temperature and pressure have been determined, all the thermodynamic properties can be evaluated for several reduced pressure values, over a prescribed temperature range. The considered pressures are, as already stated: $P_r = 1.1, 1.2, 1.5, 1.75, 2, 2.25, 2.5, 3$ and 3.5. These values have been chosen properly to satisfy some conditions: firstly, the highest reduced pressure is chosen to be 3.5 since at that value, the properties of methane, which is the main constituent, do not show anymore any relevant extremum. This is also in good agreement with previous works, [8], [29], where it is shown that peaks in thermodynamic properties exist up to reduced pressure of 3. Secondly, great attention is given to low reduced pressures values (1.1, 1.2 and 1.5) because in that region retrograde condensation could occur, and more detailed monitoring of properties is desirable.
For what concerns the temperature range it starts from the critical temperature and extends for 150 degrees, with a step of $0.001T_c$; it will be clear shortly why such a small step is needed.
All the thermo-physical properties of pure methane are here presented in Fig. 28; these properties are used to track the Widom Line corresponding to each property, as it has been done for the c_p in Fig. 27. Note that the properties are not plotted at every reduced pressure considered in the code just to have clearer images. Later on, a comparison with the same properties for a mixture will be done.

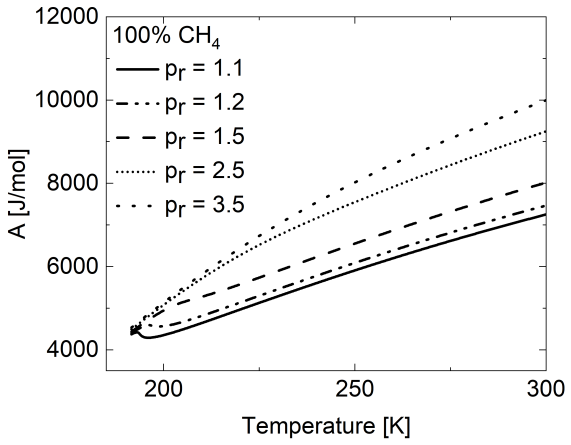

(a) Helmholtz free energy.

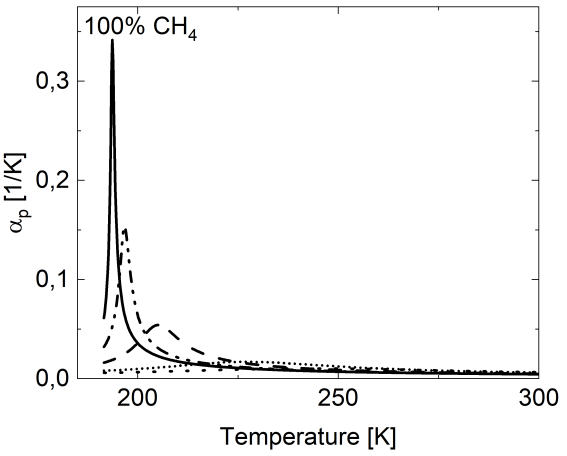

(b) Thermal expansion coefficient.

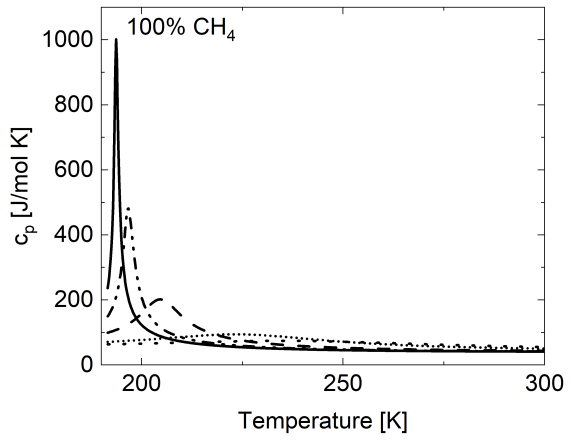

(c) Isobaric heat capacity.

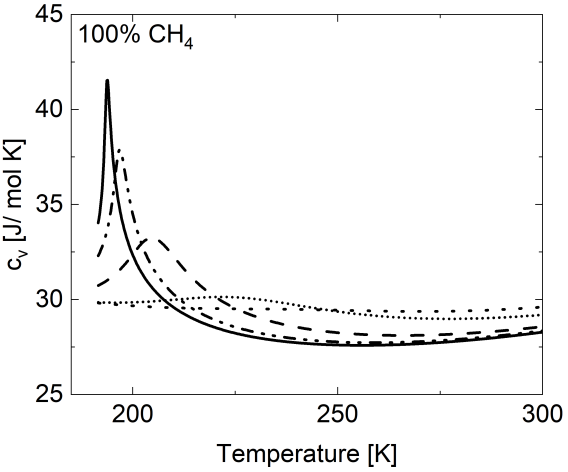

(d) Isochoric heat capacity.

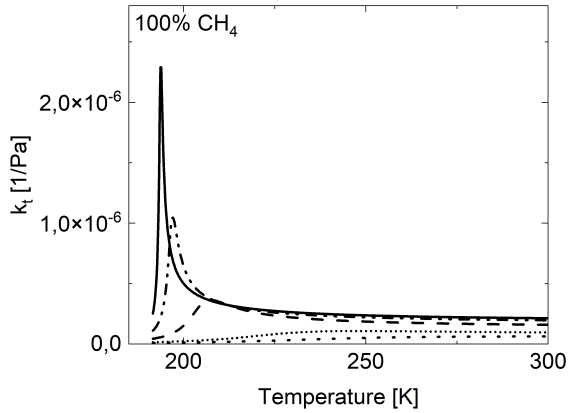

(f) Isothermal compressibility.

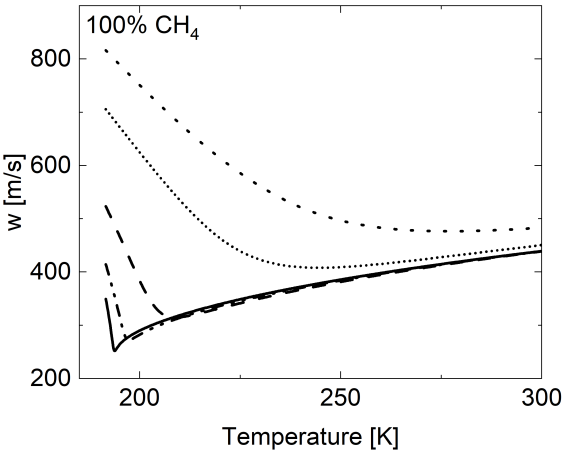

(g) Speed of sound.

Figure 28: Thermo-physical properties for pure methane.

5.6 Results for Mixtures

Since pure methane would be extremely expensive for space applications, the evaluation of thermophysical properties for pure components is not of great interest in this work. It is essential to understand how the properties of methane are changed when little portions of other light hydrocarbons, nitrogen or hydrogen are present in the mixture.

The great advantage of the developed code is that all the process shown in the previous section, validated for pure substances, is implemented to be repeated for any methane-based mixture, and not only for the Widom Line coming from the isobaric heat capacity, but for 5 Widom Lines coming from different response functions. As anticipated during the explanation of the GERG-2008 EoS, the chosen response functions for this work are: isobaric heat capacity c_p, isochoric heat capacity c_v, thermal expansion coefficient α_p, isothermal compressibility k_t, and speed of sound w, respectively evaluated with Eq. (49), Eq. (50), Eq. (51), Eq. (52), and Eq. (53).

Of course, not all the results coming from any of the combinations of the interesting elements will be shown, but the attention is given to those blends that can result as the most dangerous for practical applications. Indeed, from Fig. 22 it has been noticed that a 5% mole fraction of propane will cause a significant area of retrograde condensation, that lies at temperature and pressure slightly higher than the critical point of the mixture.
Hence, the 95% methane - 5% propane mixture is taken as a case-study.

After the evaluation of the critical point for the given mixture with the linear approximation expressed in Eq. (44), from [15], the only missing detail in the algorithm that has been implied in this work is how the coordinates of the extrema are found. This can be explained by looking at Fig. 29, where all the response functions, plus the Helmholtz free energy, are plotted at different reduced pressure values for the mixture under investigation.
As in Fig. 28, where the same properties for pure methane were plotted, all the response functions in Fig. 29 show, as expected, pronounced maxima, or minima, right after the critical point, that move at a higher temperature when the pressure is increased.

The coordinates of the extremum point, for each reduced pressure value, are found by taking the derivative of the property and looking at the temperature at which it changes sign. For example, when a maximum is present, the derivative of the considered property will be initially positive and then it will become negative right after the maximum.
The opposite will happen for a minimum.

This is done because solving the derivative to find the point in which it is zero would be much more time consuming from a computational point of view; moreover, a very good accuracy in the location of the maxima is obtained by taking the temperature step very small. This is the reason for which the temperature range is divided into steps of $0.001T_c$, which is approximately equal to steps of 0.2 degrees for the considered mixtures.
Once that all the coordinates of the extrema are found and saved, those points are fitted with a third-order polynomial to sketch the line.

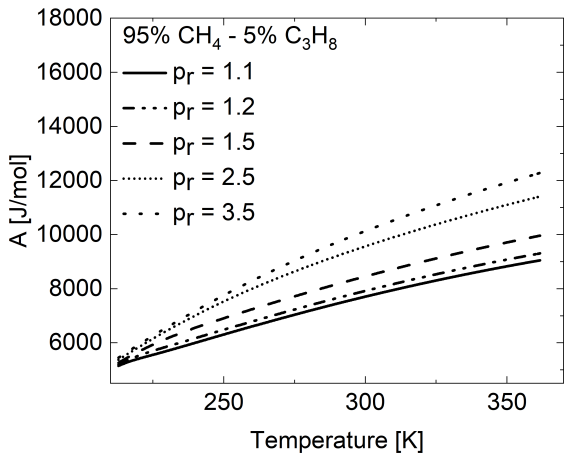

(a) Helmholtz free energy.

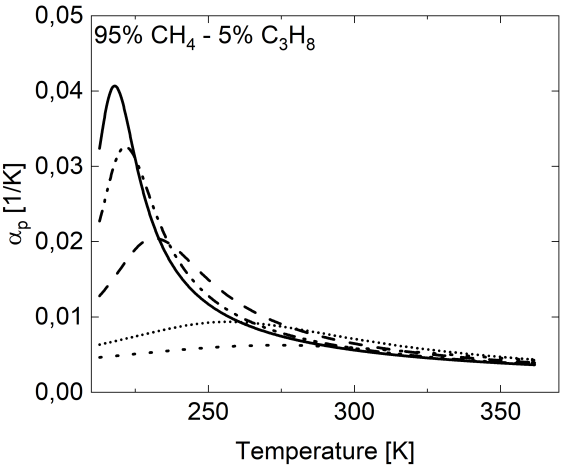

(b) Thermal expansion coefficient.

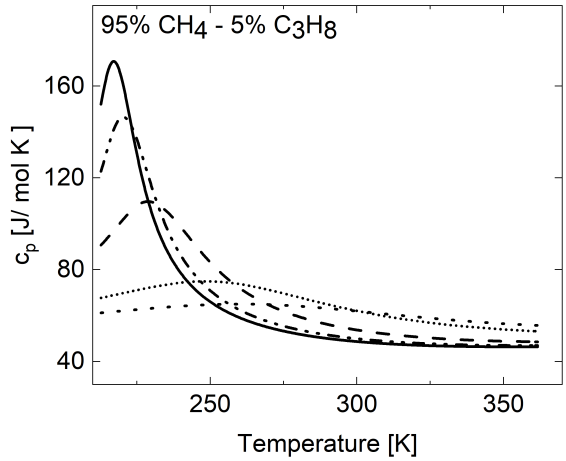

(c) Isobaric heat capacity.

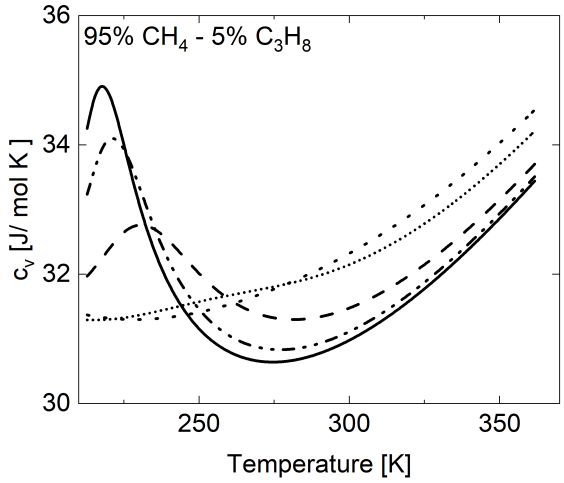

(d) Isochoric heat capacity.

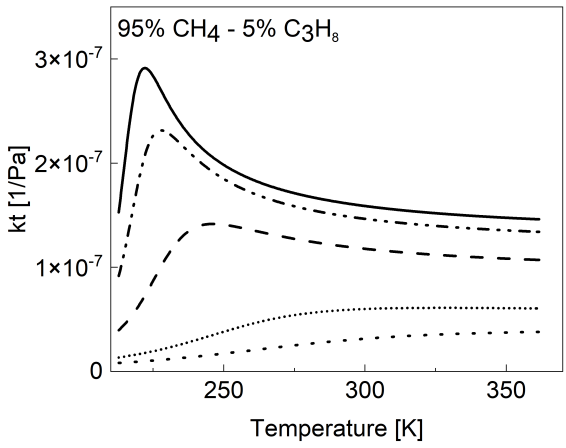

(e) Isothermal compressibility.

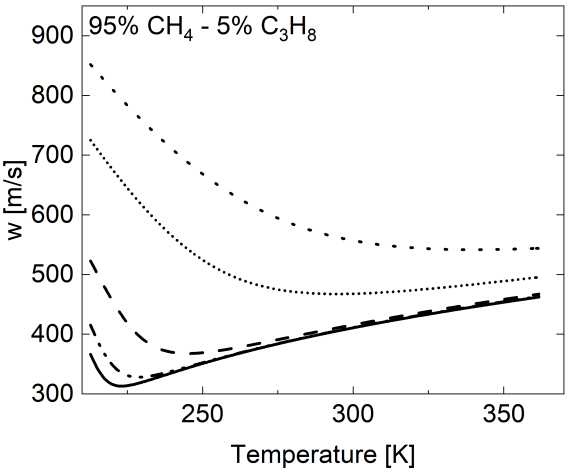

(f) Speed of sound.

Figure 29: Thermo-physical properties for the 95% methane - 5% propane mixture.

Now that both the evaluation of the thermo-physical properties and the definition of the coordinates of the extrema are explained, all these data can be used to draw the Widom Lines corresponding to those response functions. The c_p Widom Line was already presented in Fig. 27 for pure components; now in Fig. 30 the picture is completed with Widom Lines coming from the other response functions.

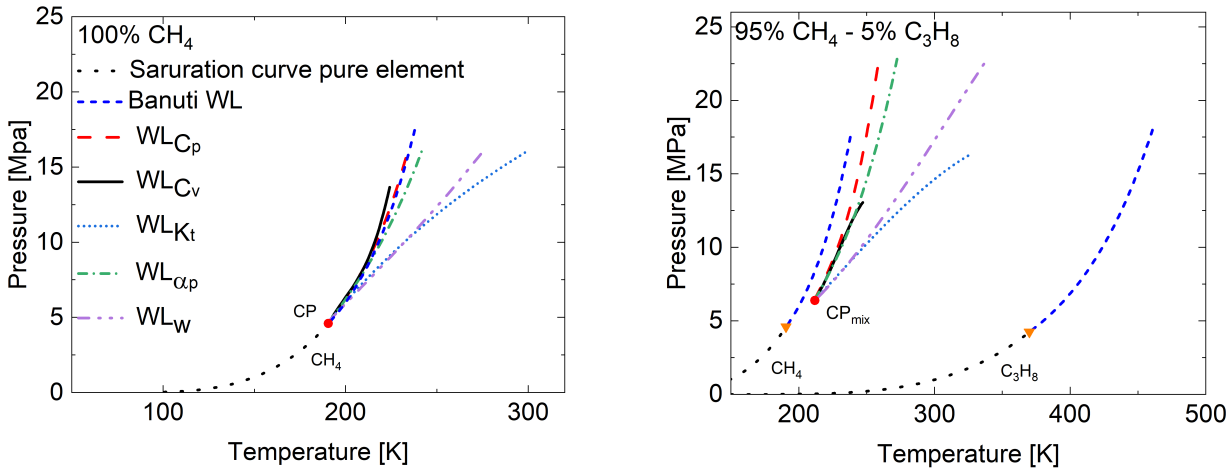

(a) Widom Lines for pure methane.

(b) Widom Lines for a mixture of 95% methane and 5% propane.

Figure 30: Widom Lines coming from the five selected response functions plus saturation curves of pure components [45], and Banuti et al. c_p Widom Line, [7]. The coordinates of the extrema of each function are evaluated and fitted with a third-order polynomial.

In Fig. 30a all the five Widom Lines for pure methane can be appreciated. It will be a common pattern that: the Widom lines coming from the isobaric heat capacity, isochoric heat capacity and thermal expansion coefficient will be very similar with each other. A different path is taken from the other two lines, for the isothermal compressibility and the speed of sound. As already stated when presenting the Widom Line, there is no precise reason to chose one line over the other as the boundary between liquid-like and gas-like; hence, all the five lines are always evaluated in this work, and the distinction between these two paths is always confirmed. The same happens in Fig. 30b, where a 5% mole fraction of propane is mixed with 95% of methane. Here, the critical point of the mixture is characterized by much higher pressure and slightly higher temperature. This causes that a reduced pressure of 3.5 is equal to a much higher absolute pressure, and then longer Widom Lines are present because the extrema are still detectable above $20MPa$. In Fig. 30, and more generally in all the following figures presenting mixtures, also the saturation curve of the pure components is presented; its values are taken directly from NIST database, [45]. Lastly, the saturation of curve each pure component is continued with a dashed blue line that represents the c_p Widom Line taken from the work of Banuti et al., [7]. This will be done for every representation of Widom Lines for mixtures. Following the same procedure, just changing the initial composition, the Widom Lines for other mixtures can be found; in Fig. 31 a couple of binary mixtures, a three-components mixture and a four-components mixture are shown, to give some examples of results that can be obtained with the developed algorithm.

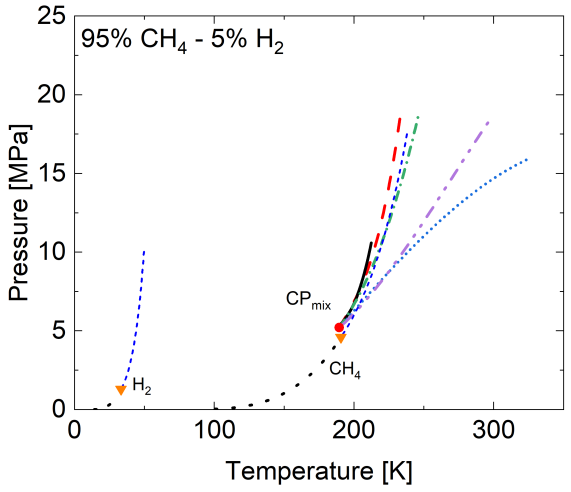

(a) Widom Lines for a mixture of 95% methane and 5% hydrogen.

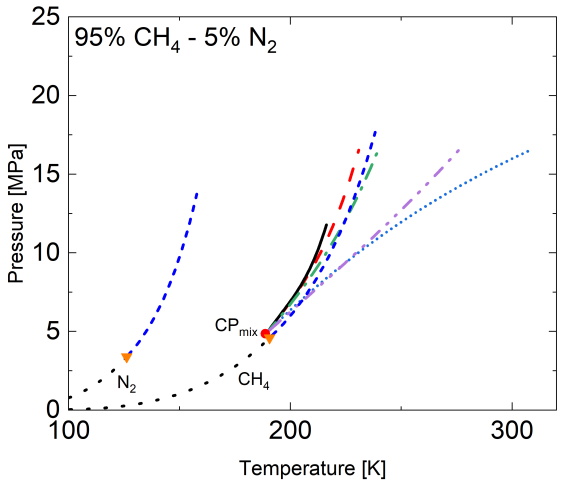

(b) Widom Lines for a mixture of 95% methane and 5% nitrogen.

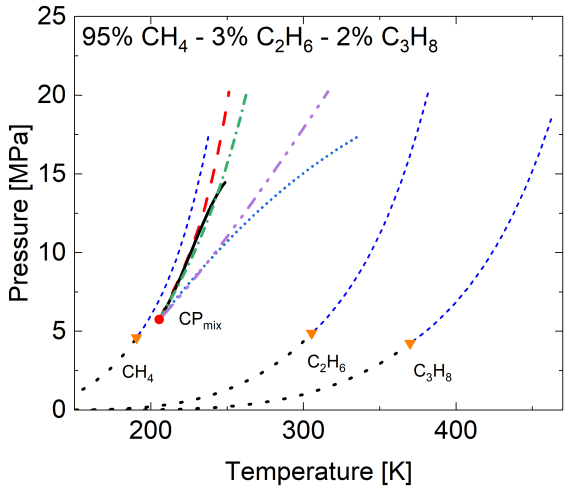

(c) Widom Lines for a mixture of 95% methane, 3% ethane and 2% propane.

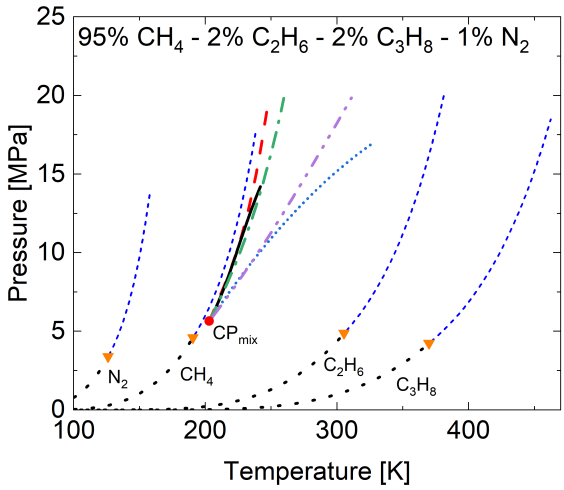

(d) Widom Lines for a mixture of 95% methane, 2% ethane, 2% propane and 1% nitrogen.

Figure 31: Widom Lines for other mixtures coming from the five selected response functions plus saturation curves of pure components [45], and Banuti et al. c_p Widom Line, [7]. The coordinates of the extrema of each function are evaluated and fitted with a third-order polynomial.

5.7 Widom Area

As it was stated at the beginning, the goal of this work is to evaluate the thermo-physical properties of methane mixtures in order to understand where strong gradients can occur; this goal aims at describing the dangerous region, that can be crossed during the operative conditions of space applications. For example, when the fuel, namely the methane mixture itself, is used to cool down the nozzle, its temperature and pressure decrease, moving its status from an initial condition to a different final state on a Temperature-Pressure diagram.
It is clear now that crossing a Widom Line means crossing this potentially dangerous area. However, this description is not accurate, since it has been demonstrated that the extrema of each thermodynamic response function flatten with increasing reduced pressure; this decrease in the extrema causes then a lower gradient in the properties.
To make it clear, crossing the Widom Lines at a reduced pressure of 1.1 involves a much stronger

gradient than crossing the same Widom Line at a reduced pressure of 3.
To determine the region in which strong gradients in properties should be expected, the rate of change ε, for the response functions was calculated. The threshold for this rate, ε_f, was assumed equal to 0.05 times the average value of the property f, along with the studied temperature interval.

$$\varepsilon_f = 0.05 f \qquad \text{where} \qquad f = \text{average value of} \quad c_p,\ c_v,\ \alpha_p,\ k_T,\ \text{or}\ w. \tag{56}$$

In this contest, the "*Widom Area*" is defined as a surface, of parameters p and T, in which the threshold defined in Eq. (56) is exceeded.

$$\varepsilon > \varepsilon_f \tag{57}$$

The rate of change of the property f is evaluated across a temperature interval of $5K$, for all the evaluated temperatures, given by the step of $0.001T_c$ previously described. All the temperatures at which the threshold rate of change is exceeded are saved in a vector until the next point in which the gradient is lower than ε_f is found. Doing so, a map of the region in which the gradient ε of each property f is higher than the threshold rate of change ε_f was obtained. The Widom Area defines the temperature and pressure range in which a strong gradient for thermodynamic properties should be accounted during applications. As expected, the region nearer to the critical point shows changes in properties very high, with respect to the changes that occur at higher pressure, even if peaks are still detectable. The process is repeated for each Widom Line.

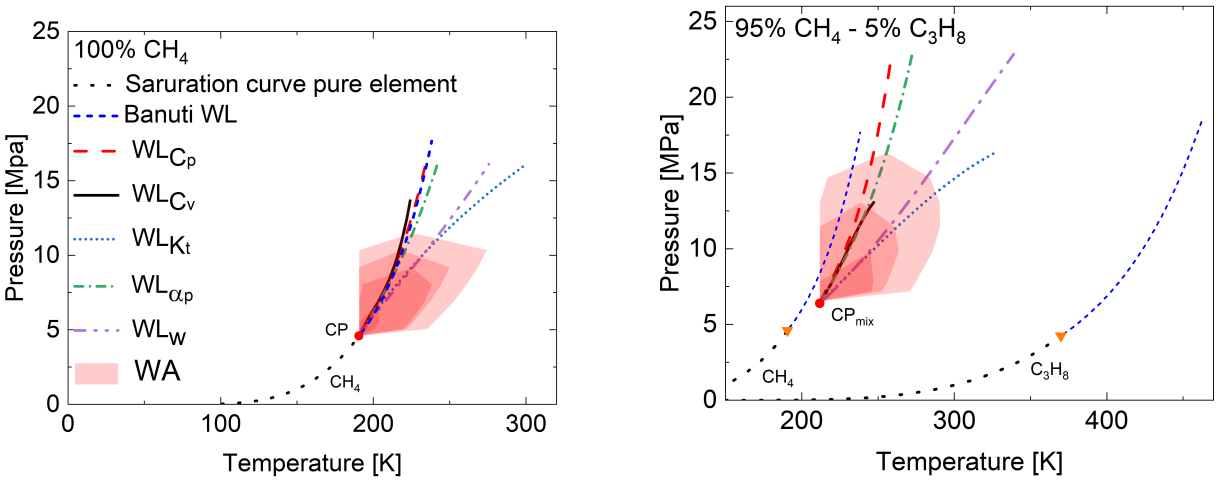

(a) Widom Area for pure methane.

(b) Widom Area for a mixture of 95% methane and 5% propane.

Figure 32: Widom Area for the mixtures in Fig. 30. Also, saturation curves [45], and Banuti et al. c_p Widom Line, [7], are shown. The surface is composed of those points characterized by a rate of change that exceeds the threshold defined in Eq. (56).

As in Fig. 30, the first results presented in Fig. 32 are those for pure methane and a mixture of 95% methane and 5% propane. In Fig. 32a, it can be seen that the Widom Area is found as the superposition of the dangerous surfaces coming from each Widom Line. Almost every property shows a region near the critical point in which the threshold rate of change is exceeded. The Widom Area stops at reduced pressure well below the 3.5; this confirms that even if peaks are still detectable, the actual change in properties is limited, as it could be appreciated in Fig. 29.
Again, the same procedure is applied to other compositions, which are shown in Fig. 33.
Now that both the Widom Lines and the Widom Area are obtained, an interesting comparison can be made. In Fig. 32b, the Widom Area seems to be bigger.

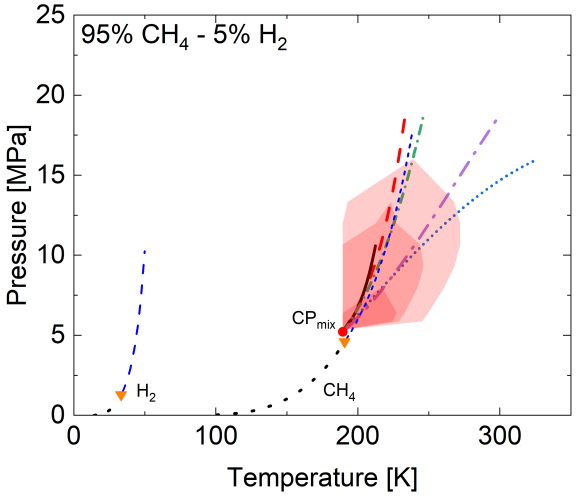

(a) Widom Area for a mixture of 95% methane and 5% hydrogen.

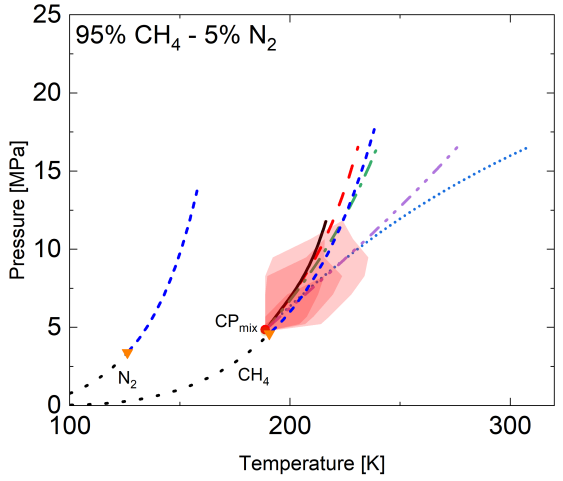

(b) Widom Area for a mixture of 95% methane and 5% nitrogen.

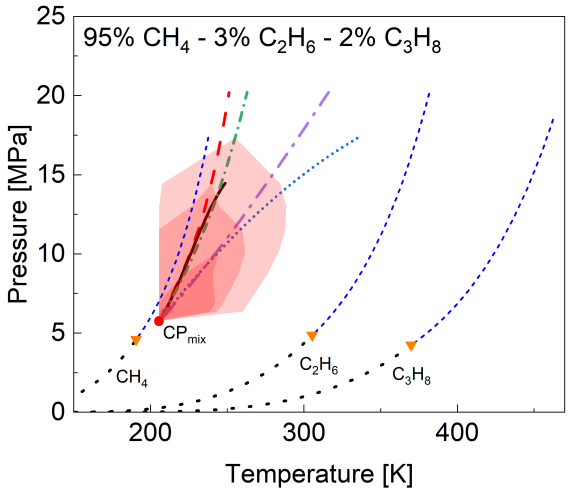

(c) Widom Area for a mixture of 95% methane, 3% ethane and 2% propane.

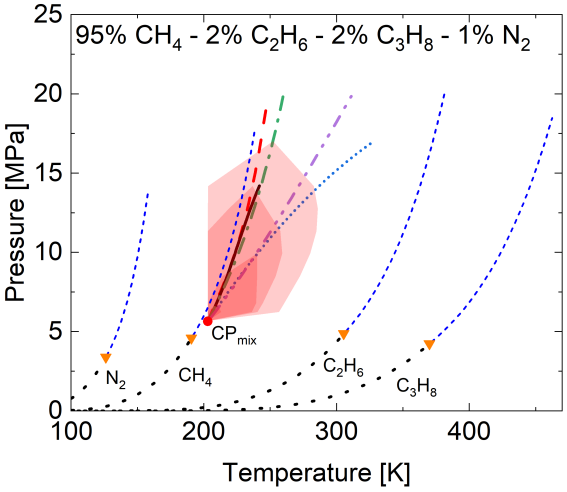

(d) Widom Area for a mixture of 95% methane, 2% ethane, 2% propane and 1% nitrogen.

Figure 33: Widom Area for the mixtures shown in Fig. 31, coming from the five selected response functions. Also, saturation curves of pure components [45], and Banuti et al. c_p Widom Line, [7], are shown. The surface is composed of those points characterized by a rate of change that exceeds the threshold defined in Eq. (56).

This happens for two reasons: firstly the mixture has higher critical properties, but, it has also to be considered that pure methane has more pronounced peaks that are felt in a narrower range of temperatures; in mixtures instead, the extrema are usually lower and the variations occur in a wider temperature range. This can be appreciated in Fig. 34, where the isobaric heat capacity is reported at different reduced pressure for pure methane and the usual mixture of 95% methane and 5% propane. These two images were already presented previously, but putting them next to the other, the difference is obvious.

For pure methane an incredibly pronounced maximum is present for a reduced pressure of 1.1; at the same pressure, the mixture with propane shows a maximum but with an absolute value which is much lower and with the whole variation occurring in a wider temperature range. The steady-state value, at higher temperatures is instead almost the same.
Due to this difference, if the threshold had been chosen much higher, the Widom Area of pure

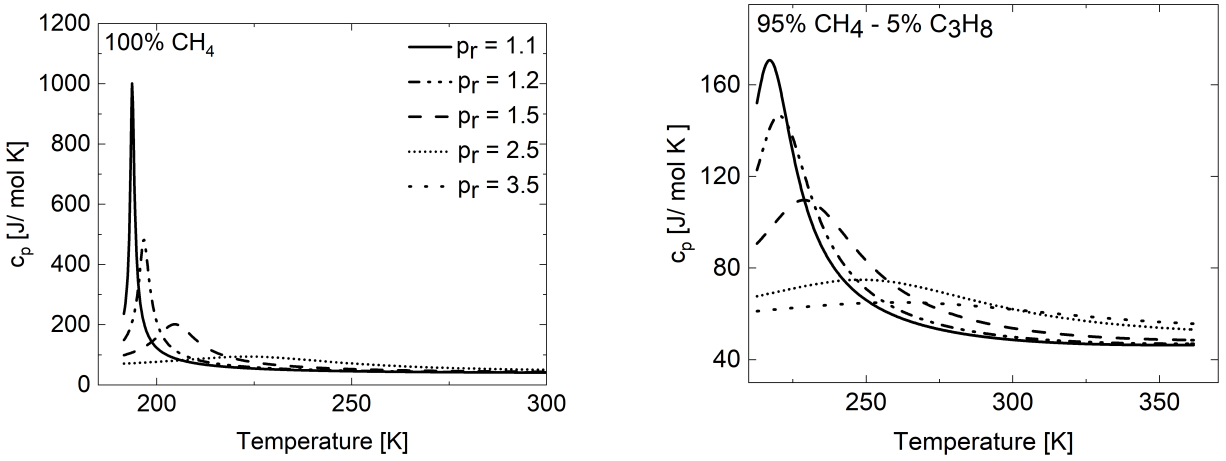

Figure 34: Comparison of the isobaric heat capacity between pure methane (on the left) and 95% methane - 5% propane (on the right).

methane would have been still visible, due to the extremely high gradient, while probably the Widom Area of the mixture would have resulted smaller or not appearing at all, since the average gradient is lower.
These variations in thermo-physical properties when going from pure components to mixture occur even for a very small mole fraction of impurities and are different for every compound that is added. The effect of 5% of propane can be seen comparing Fig. 28 with Fig. 29.
Besides, also the representation given in this work called "Widom Area" cannot present all the changes that occur when dealing with mixtures instead of pure components, because if a different threshold rate of change had been chosen, a different Widom Area would have been obtained. However a preliminary idea of the location where to expect stronger gradients is given in these figures and furthermore, the threshold can be changed in the code in order to show the dangerous area for a certain application.

6 The Frenkel Line

The chemical interpretation of the extrema of thermodynamic properties that has been shown and their localization did not have any relevant theoretical explanation and nowadays are the subject of many investigations due to their large impact on engineering process, especially for the large heat transfer that is caused.
The phenomenological explanation for this strange behaviour of properties near the critical point starts from the analogy with the local structure transformation that occurs across the vapor-liquid coexistence line in the subcritical region: in the liquid phase, the reason is the destruction of fluid structure as the temperature is increased or as pressure is decreased; in the gas phase, molecule clusters are built, leading to density change. Following this description, in the vicinity of the critical point, peaks in the thermodynamic functions may be explained with this structure transformation, which disappears far from the critical point. The lines of the set of extrema ("ridges") of properties were referred to as extensions of the vapor-liquid coexistence line, called pseudo-boiling line and, as it has already been presented, divided two states of the fluid, a liquid-like and a gas-like. Later the definition of Widom Line was introduced.

Two main roads are now under investigation regarding the demarcation line between liquid-like and gas-like supercritical states. The first has already been described in Section 5 and assumes the Widom Line as the locus of ridges, evaluated from thermodynamic quantities.
The question here to be answered is, where is the end-point of this WL?
Many authors agree with the assumption that the Widom line exists up to the point where the locations of all extrema coincide. Depending on the EoS and calculated properties this point can be between $1.05T_r$ and $2T_r$, and $1.2p_r$ and $3p_r$.
The other approach, suggested by Brazhkin et al. [42], is based on the microscopic description of the viscoelastic theory provided by Frenkel [14].
In this new section, the second road is shortly presented.

6.1 Frenkel's theory

This description is carried out by introducing the liquid relaxation time, τ_{rt}, a fundamental flow property of a liquid that Brazhkin et al. define as "*the average time between two consecutive atomic jumps in a liquid at one point in space; each jump can approximately be viewed as a jump of an atom from its neighbouring cage into a new equilibrium position with subsequent cage relaxation*", [42]. Moreover, it defines liquid viscosity η and diffusion coefficient D.
Brazhkin et al. in [42] proposed that, for the liquid phase, an equally important change in the system behaviour exists, and that it is related to the change in its dynamics rather than thermodynamics, as it is described for WL.
In this frame, all liquids have two qualitatively different states and a new additional crossover line (or narrow zone) should be added to the phase diagram which separates the two liquid states, as shown in Fig. 35.

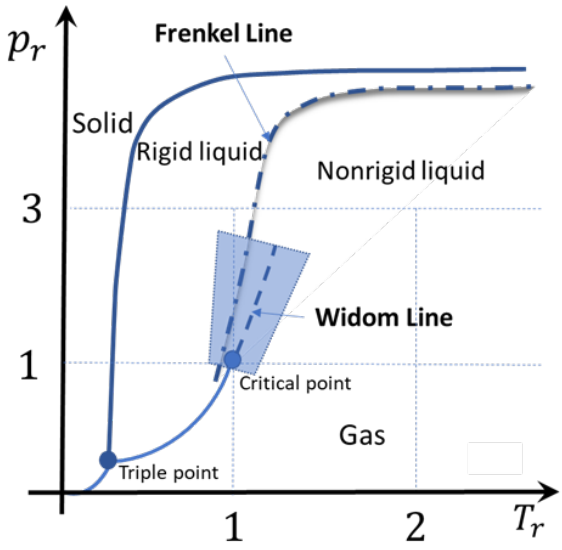

Figure 35: New proposed state diagram.

This line does not correspond to any thermodynamic phase transition, namely it is a crossover

and not a discontinuity of any physical properties. Brazhkin et al. [42] called it the "Frenkel line".

Fig. 35 presents the actual state of the art in the fundamental thermodynamic phase structure diagram. The fundamental difference between the Widom and the Frenkel line is that while the Widom line in the phase diagram is defined by the locus of the extrema of the thermodynamic functions, the Frenkel line is associated with a transition of microscopic structural and dynamical features in supercritical fluids.
The above description of dynamical/structural crossover is seen by Brazhkin et al. [42] in terms of the motion of an atom: they distinguished between a quasiharmonic vibrational motion around an equilibrium position for a *rigid-liquid* and a diffusive motion between two neighbouring positions for *non-rigid liquids* and searched for the point in which the oscillatory motion ceases, leaving only non-rigid liquid motion.

Lastly, Brazhkin et al. were able to understand the link between the dynamic transition and the transport properties of the fluid: diffusion coefficient D, viscosity η and thermal conductivity λ. They noticed that the transition occurs when the relaxation time τ_{rt} is comparable to the minimal (Debye) vibrational period τ_0 ($\tau_0 \approx 0.1 - 1ps$).

$$\tau_{rt} \approx \tau_0 \tag{58}$$

In [42] it is shown that the condition in Eq. (58) gives the transition of D from exponential to power-law temperature dependence. Looking at the viscosity instead, the crossover is even easier to recognize because the condition in Eq. (58) brings to an evident change in the temperature behaviour of viscosity since it goes from the exponential decrease, when $\tau_{rt} > \tau_0$ (solid-like vibration character), to the power-law increase when $\tau_{rt} < \tau_0$ (non-rigid diffusive character).
It has been shown previously, in the Chapman-Enskog theory that the thermal conductivity behaves very similar to the viscosity coefficient.
Lastly, in [42], it is shown that also the speed of sound decreases before the Frenkel line, and starts increasing right after. Then, three important properties have been shown to have their minima on the Frenkel crossover line: viscosity coefficient, thermal conductivity and speed of sound.
From here, the importance of an accurate evaluation of these properties comes.

6.2 Evaluation of viscosity

The evaluation of transport properties is of paramount importance for any engineering application, in order to model and measure the exchange of mass, momentum, and heat in the system due to gradients in concentration, velocity and temperature, respectively.
In Sec.1.2, the evaluation of these three transport properties is presented, using an ultra simplified theory, with rigid non-attracting spherical molecules that travel all with the same speed in few directions. In Sec. 1.7 the results from a more accurate theory are presented in the Chapman-Enskog theory.

However, for real components and mixtures, these quantities are extremely difficult to evaluate theoretically and several ways have been proposed, [9]. It would be also extremely expensive to evaluate the transport properties experimentally.
Here a simple model for the evaluation of the viscosity of mixtures is presented; the model is based on the work of Lötgering-Lin, [17], [27] in which a third-order polynomial function of the residual entropy was used to predict a dimensionless viscosity. This work was performed using a PCP-SAFT equation of state, using then characteristic parameters of that model; however, this model has been very recently adapted to the EoS that has been used in this work, namely the GERG-2008. In [33], Jonas Mairhofer uses the same approach but with adjusted coefficients in order to fit the method to the new EoS.

Adapting this prediction method to GERG-2008, excellent results are achieved for natural gas mixtures. The averaged deviation is evaluated in [33] to be as low as 3.09%. For its simplicity and good results, this merely predictive approach is one of the best models for natural gas mixtures. The proposed approach is not limited to natural gas viscosity, but accurate predictions are also obtained for multicomponent mixtures over a wide temperature and pressure intervals.

The following explanation of the prediction method makes reference to [33], so it can be consulted for further information.
The entropy scaling approach that will be used here, goes back to Rosenfield, [47], who demonstrated that for simple monoatomic molecules, dimensionless transport properties can be expressed as a function of the residual entropy alone. In their work, Lötgering-Lin et al. [17][27] used this methodology, compared their results for pure components with experimental values and proposed a predictive model for mixtures, using PCP-SAFT EoS. Lastly, Jonas Mairhofer fitted the method for a different EoS, the GERG-2008.

Within this method, a dimensionless viscosity is defined in Eq. (59), and to do so, the Chapman-Enskog viscosity of the pure component is used, from Eq. (22).

$$\eta_i^* = \frac{\eta_i}{\eta_{CE,i}} \qquad \text{where} \qquad \eta_{CE,i} = \frac{5}{16}\frac{\sqrt{M_i kT/(N_a\pi)}}{\sigma^2\Omega^{(2,2)*}} \tag{59}$$

where to evaluate $\Omega^{(2,2)}$ the Neufeld correlation has been used, Eq. (24), while to evaluate the Lennard-Jones parameters the correlations from Chung et al. [43] is adopted, where critical constants are employed to evaluate the coefficients:

$$\sigma = 0.809 V_c^{1/3}$$

$$\epsilon/k = T_c/1.2593$$

Then, in Eq. (60), the residual entropy is defined. It is particularly easy to retrieve this quantity due to the nature of GERG-2008 that is built on the ideal and residual part of the Helmholtz free energy, as it can be recalled in Eq. (45).

$$s_i^r(\rho, T, \bar{x}) = -\frac{\partial a^r}{\partial T} \tag{60}$$

In Eq. (60), a^r is the residual Helmholtz free energy, that can be recovered from the dimensionless residual Helmholtz free energy in Eq. (47). Lastly, the dimensionless viscosity can be evaluated with a third-order polynomial, like in Eq. (61).

$$\ln \eta_i^* = A_i + B_i s_i^r/R + C_i(s_i^r/R)^2 + D_i(s_i^r/R)^3 \tag{61}$$

where A_i to D_i are pure substance viscosity parameters.
In our work, each component parameter has been taken from the 'Supporting Information' document, attached to [33].

Furthermore, this prediction model is expanded for mixtures, [33]. Based on the work of Lötgering-Lin et al., the coefficient A to D are evaluated by making a simply mole fraction average of the pure component specific parameters, like in the following:

$$\psi^{mix} = \sum_{i=1}^{N} x_i \psi_i$$

where N is the number of components of the mixture, x_i the i-th mole fraction and psi_i is any parameter from A to D of the i-th component.

For a mixture of N components, it yields Eq. (62).

$$\ln \eta_i^* = \sum_{i=1}^{N} x_i A_i + \sum_{i=1}^{N} x_i B_i (s^r/R) + \sum_{i=1}^{N} x_i C_i (s^r/R)^2 + \sum_{i=1}^{N} x_i D_i (s^r/R)^3 \tag{62}$$

Therefore, no adjustable interaction parameter is introduced, since the objective is purely predictive.

Moreover, J. Mairhofer does not adimensionalize the residual entropy s^r,[33] , as it has been done in the work of Lötgering-Lin et al. [17], where the s^r is divided by the segment number (a PCP-SAFT parameter); but Mairhofer did not apply this technique because no improvements are found with it.

Lastly, when dealing with mixtures, the viscosity has to be adimensionalized with respect to a Chapman Enskog viscosity for mixtures, for which the approximation of Wilke is used, [46].

$$\eta_{CE,mix} = \sum_{i=1}^{N} \frac{x_i \eta_{CE,i}}{\sum_{j=1}^{N} x_j \phi_{ij}} \qquad \text{where} \qquad \phi_{ij} = \frac{\left(1 + (\eta_{CE,i}/\eta_{CE,j})^{1/2} (M_j/M_i)^{1/4}\right)^2}{(8(1 + M_i/M_j))^{1/2}}$$

For what concerns the validity of the process, it has been taken into account the fact that the GERG-2008 EoS has two different validity ranges, normal and extended; then results will be less accurate when pressures of $35MPa$ or temperatures of $450K$ are overcome; as it will be shown later on.

6.3 Pure Components Results and Validation

As it was already done previously to validate the correct implementation of the EoS, here, the prediction method for viscosity is validated for pure methane, taking as reference the viscosity data coming from the NIST database, [10].
The algorithm just presented has been used for pure methane on a temperature interval that spans from the critical temperature to $625K$, which is the maximum temperature available on the NIST database. The pressure is varied starting from a value of $1.2p_r$ up to $15p_r$. The results are presented in Fig. 36.

The prediction of the viscosity for pure methane shown in Fig. 36 is outstanding. Up to a reduced pressure of 8, results follow almost exactly the NIST data. A little deviation from the reference curve is present for a reduced pressure of 10, and only for a reduced pressure of 15, the method starts failing.
Moreover, along a single curve, it can be noticed that for temperatures higher than $450K$, the curve starts deviating from the reference but still keeping a very good accuracy.
These two kinds of deviations are due to the validity range of the EoS itself. The GERG-2008 has indeed two different validity ranges, how it was stated when the model has been presented. For temperatures higher than $450K$ and/or pressures higher than $35MPa$ (in this case approximately $p_r = 8$) the normal validity range is overcome, entering the extended validity range, characterized by slightly lower accuracy.

Since the aim of this work is only a prediction of where to expect a structural/dynamical change, the accuracy obtained with the simple method explained above is more than enough to start searching for the Frenkel Line. As explained in [42], the coordinates of the minima of the viscosity can be used to identify the line where this crossover is likely to happen.

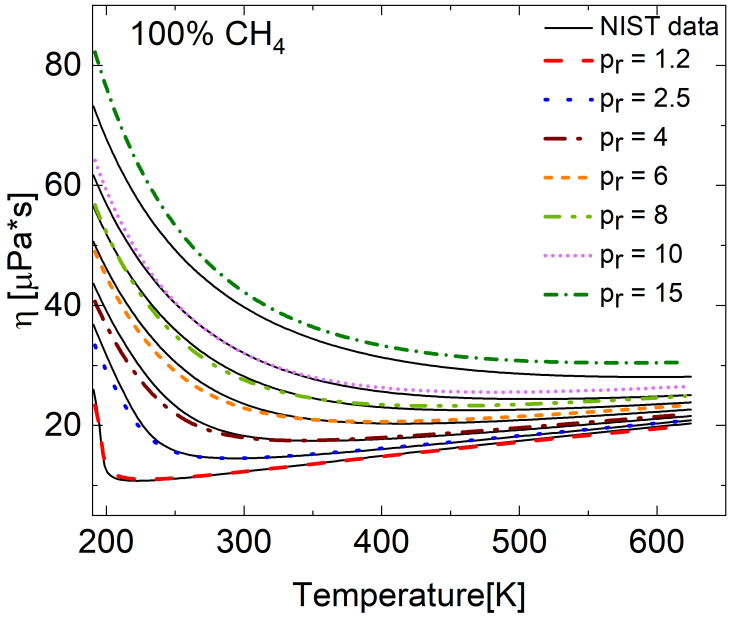

Figure 36: Comparison between the viscosity values of this work and the NIST database, [10], for pure methane.

6.4 Evaluation of Frenkel Line

As it has been explained previously, the structural change in the fluid that occurs across the Frenkel Line can be identified by looking at the behaviour of transport properties and speed of sound. In particular, the viscosity coefficient, the thermal conductivity and the speed of sound present a minimum along with their temperature variation. In this work, only two of these properties have been used: the speed of sound because of its simple evaluation, with Eq. (53); and the viscosity coefficient that can be evaluated with the predictive method explained in Sec.6.2, [33]. Thermal conductivity has not been evaluated due to its complex evaluation, but also because it was proposed by Chapman-Enskog theory that the thermal conductivity can approximately be linked to the viscosity through the isochoric heat capacity, having then a similar behaviour (refer to Eq. (22) and Eq. (23)).
Viscosity and speed of sound are evaluated at the same reduced pressure shown in Fig. 36, namely: $p_r = 1.2, 2.5, 4, 6, 8, 10, 15$.

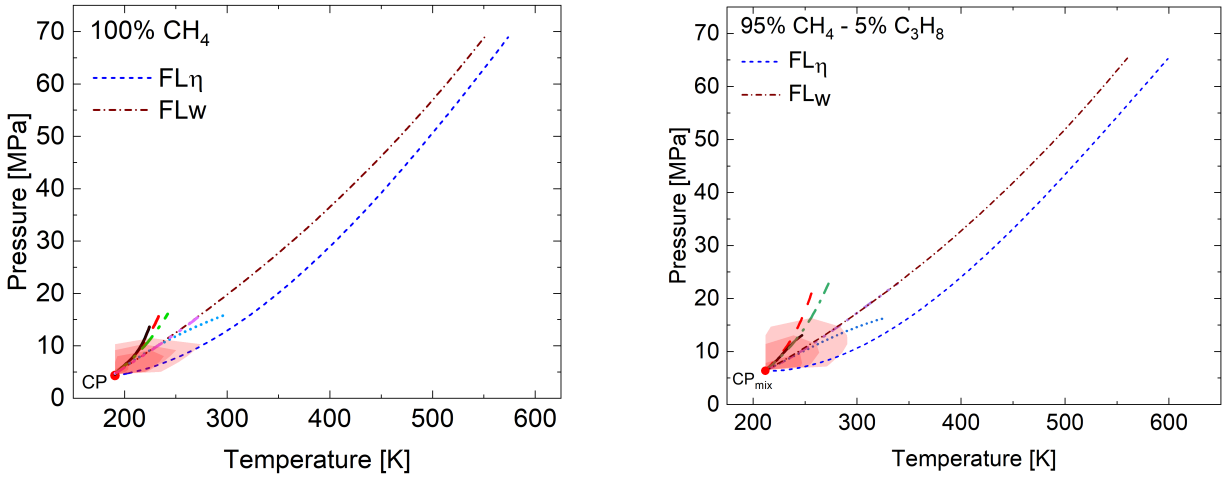

Figure 37: The Frenkel Lines coming from speed of sound and viscosity coefficient for pure methane, on the left, and a mixture of 95% methane and 5% propane, on the right.

Their minima are found with the same code that is used to find extrema for Widom Lines; this means that the derivative of the function is taken, and the point in which the derivative changes its sign is saved as the position of the extremum; since it is looked for a minimum, the derivative has to change its sign from negative to positive.
Again a good accuracy is achieved in the individuation of the coordinates of the extrema thanks to a small temperature step, $0.001T_c$. Following the same procedure used for Widom Lines, the point of extrema are fitted using a third-order polynomial to obtain the Frenkel Line. Results for pure methane and the usual mixture of methane and propane are shown in Fig. 37. Also in this case, different demarcation lines are obtained for different properties. In Fig. 37 the two obtained Frenekel Line are plotted together with Widom Lines and Widom Area of the corresponding mixture to give a better understanding of the magnitude of these transitions.
However, if in the case of Widom Lines the calculations were performed in the best validity range of the implemented EoS, now the accuracy could be lower, especially at very high pressures. Then the evaluation of the Frenkel Line coming from the diffusion coefficient and the thermal conductivity would be of great help in identifying the transition region, and simulation of molecular dynamics could be used to confirm the results.

7 Further Improvement and Conclusion

The goal of this work was to provide a complete view of the behaviour of commercially available methane mixtures, that includes several impurities, like light hydrocarbons, nitrogen or hydrogen. The supercritical state of fluids is nowadays a hot topic of research, even more for hydrocarbons, due to their huge commercial impact and use in several fields.
The GERG-2008 EoS is the most recent and updated equation of state for hydrocarbons and was developed with the same aim, namely to provide a unified model to describe their behaviour during engineering technical applications. In space application the supercritical part of the state diagram has paramount importance, and the localization of strong gradients in properties is fundamental for the safe and correct use of fuels. For this reason, drawing the Widom Lines and highlighting the Widom Area, which is identified as a dangerous area, has been the greatest achievement of the present work, and it was also its primary goal.

However, the picture is not complete, and for an accurate description of the supercritical transitions that occur in a fluid, a more accurate description of the Frenkel Line will be needed. This is required for some applications that work at very high pressure, like the Raptor engine from SpaceX, whose combustion chamber works at almost $30MPa$, a value well beyond the extension of Widom Lines.
To do so, the last essential tile is the knowledge of transport properties.
Those properties are extremely difficult to be evaluated experimentally and the theoretical approach is equally hard. Some simpler prediction methods exist and one of them has been used in the present work. However, the lower accuracy of the extended validity range of GERG-2008 plus the approximations made with a simple prediction method, make our calculations unreliable above a reduced pressure of 10.

A good way to overcome these problems would be running molecular dynamics simulations.
MD simulations have been widely employed in the last decades, thanks to the increase of the available power of computers and software developed with the aim of simulating chemical reactions and thermodynamic properties. In MD simulations, a box containing N molecules of the prescribed fluid can be simulated under whatever thermodynamic condition, in a costless and quick way.
The drawback of this road is that to simulate such a box of molecules, clear instruction on the shape, bonds, angles and interatomic forces has to be given. Of course, there is plenty of libraries with models that can be used, but the setting of the different coefficients needed by each model has to be performed based on literature, and experience.
Of course, even if it is hard and expensive, but the other way to get more information is running experimental tests; this would give this project some values to compare, in order to have an idea of the mean deviation of the obtained results.

All that has been said up to now would be useful to reach a much better understanding of the thermodynamic and transport properties of the methane mixtures. Even once this point will be reached, other work will be requested before a complete knowledge of these mixtures could be reached. In fact, for each application that aims at using liquid methane mixtures, specific tests or simulations will be required. For example, for space applications, methane mixtures present problems during the cooling and injection phases.
Due to the huge amounts of heat transferred, steep temperature and speed gradients occur in the cooling channels of rocket engines. The result is that all thermo-physical material properties are subject to changes. If the fluid is characterized by both near-critical temperature and pressure, the so-called "*Heat Deterioration*" could occur, that is a phenomenon capable of endangering the integrity of the whole structure, [28].

In a case like this one, further analysis is needed and can be carried on with CFD analysis, accounting for all the characteristic dimensions, materials and conditions of the specific application.

Methane is a valuable and green resource, that still presents some unknowns that have to be solved. Nowadays, many technology fields aim at using new green sources of power to pursue the worldwide challenge of a cleaner ecosystem, and methane could be the answer for future space propellants. An engine working with LOx and CH_4 is totally green, and this feature would also be joined to the extremely good technical properties, as storability and good performance. In these years the space market is continuously growing, and the number of missions will increase exponentially in the following decades. In 2021 the first touristic-space flight has been launched, and if the will of having up to 3 touristic-space flights per day will become true, environmental issues could emerge, forcing the industries to go for green and safe propellants, where this has to be intended not only for the launch phase, but also for the production and transport processes.
To conclude, the study of supercritical methane mixtures does not provide only an environmental challenge, but a real technological inquiry that pushes further the limits of engineering. It is a question that can be answered with cooperative work between companies and universities, in order to provide new solutions and new technologies for future space missions, but also to leave our planet a better place than we found it.

References

[1] M.Oschwald A.Schik. "Supercritical nitrogen free jet investigated by spontaneous Raman scattering". In: *Experiments in Fluids 27, 497–506* (1999).

[2] D. Ambrose and C. Tsonopoulos. "Vapor-Liquid Critical Properties of Elements and Compounds. 2. Normal Alkanes". In: *J. Chem. Eng. Data, 40, 3, 531–546* (1995).

[3] M. Oschwald J.J. Smith R.Branam J. Hussong A.Schik B.Chehroudi and D. Talley. "Injection of fluids into supercritical environment". In: *Combustion Science and Technology, 178(1-3), 49-100* (2006).

[4] J.O.Hirschfelder C.F.Curtiss and R.B.Bird. *Molecular Theory of Gases and Liquids*. Wiley, 1954.

[5] J.M. Campbell. *Gas Conditioning and Processing, Volume 1: The Basic Principles*. Hubbard, R. and Snow–McGregor, 2014.

[6] P. Gallo D. Corradini and M. Rovere1. "Widom line and dynamical crossovers as routes to understand supercritical water". In: *Nature Communication 5, 5806* (2014).

[7] M. Raju D. T. Banuti and M. Ihme. "s". In: *Physical review E 95, 052120* (2017).

[8] D.Banuti. "Crossing the Widom Line - Supercritical pseudo-boiling". In: *Journal of the Supercritical Fluids, 98, 12-16* (2015).

[9] M. L. Huber E. W. Lemmon Ian H. Bell and M. O. McLinden. "NIST Standard Reference Database 23: Reference Fluid Thermodynamic and Transport Properties-REFPROP, Version 10.0, National Institute of Standards and Technology". In: (2018).

[10] Mark O. McLinden Eric W. Lemmon and Daniel G. Friend. "Thermophysical Properties of Fluid Systems in NIST Chemistry WebBook, NIST Standard Reference Database Number 69, Eds. P.J. Linstrom and W.G. Mallard, National Institute of Standards and Technology, Gaithersburg MD, 20899". In: (retrieved August 26, 2021).

[11] Seif-Eddeen K. Fateen, Menna M. Khalil, and Ahmed O. Elnabawy. "Semi-empirical correlation for binary interaction parameters of the Peng–Robinson equation of state with the van der Waals mixing rules for the prediction of high-pressure vapor–liquid equilibrium". In: *Journal of Advanced Research, 4, 2, 137-145* (2013).

[12] Claudio A. Faúndez and José O. Valderrama. "Modeling associating hydrocarbon+alcohol mixtures using the Peng-Robinson equation of state and the Wong-Sandler mixing rules". In: *Comptes Rendus Chimie,16,2,135-143* (2013).

[13] Ulrich Essmann Francesco Sciortino Peter H. Poole and H.E. Stanley. "Line of compressibility maxima in the phase diagram of supercooled water". In: *Phys. Rev. E 55, 727* (1997).

[14] J. Frenkel. *Kinetic Theory of Liquids*. New York: Oxford University Press, 1946.

[15] N. Slavinskaya - J. Shvab - D. Suslov - O.J. Haidn and T. Santese. "Investigation of the impurities influence on liquid methane boiling behavior at the rocket engine typical operation conditions". In: *TO BE PUBLISHED* (2021).

[16] R. Heidemann and A. Khalil. "The calculation of critical point". In: *AIChE Journal, 5, 769-779* (1980).

[17] Lötgering-Lin Matthias Fischer Madlen Hopp and Joachim Gross. "Pure Substance and Mixture Viscosities Based on Entropy Scaling and an Analytic Equation of State". In: *Ind. Eng. Chem. Res., 57, 40954114* (2018).

[18] J.E.Meyer and M.G.Meyer. *Statistical Mechanics*. Wiley, 1940.

[19] O. Kunz - R. Klimeck - W. Wagner - M. Jaeschke. *The GERG-2004 Wide-Range Equation of State for Natural Gases and Other Mixtures*. 2007. ISBN: 978-3-18-355706-6.

[20] I.M. Zerón J. Torres-Arenas E.N. de Jesús B.V. Ramírez A.L. Benavides. "Discrete potential fluids in the supercritical region". In: *Journal of Molecular Liquids 293, 111518* (2019).

[21] E.N. de Jesús J. Torres-Arenas A.L. Benavides. "Widom line of real substances". In: *Journal of Molecular Liquids 322, 114529* (2021).

[22] N. L. Kafengauz and M. I. Fedorov. "Excitation of High-Frequency Presssure Oscillations during Heat Exchange with Diisopropylcyclohexane". In: *Inzhenerno-Fiztcheski Zhurnal, 11,1, 99-104* (1966).

[23] Jun Ota Katsumi Sakurai Koji Okamoto and Haruki Madarame. "Transient Velocity Distributions for the Supercritical Carbon Dioxide Forced Convection Heat Transfer". In: *Journal of Nuclear Science and Technology, 40(10), 763-767* (2003).

[24] R. L van Konynenburg P. H. Scott. "Critical lines and phase equilibria in binary van der Waals mixtures". In: *Philosophical Transactions of the Royal Society of London A: Mathematical, Physical and Engineering Sciences 298,1442, 495–540* (1980).

[25] O. Kunz and W. Wagner. "The GERG-2008 Wide-Range Equation of State for Natural Gases and Other Mixtures: An Expansion of GERG-2004". In: *J. Chem. Eng. Data, 57, 30323091* (2012).

[26] James Losey and Richard J. Sadus. "The Widom Line and the Lennard-Jones Potential". In: *J. Phys. Chem. B, 123, 82688273* (2019).

[27] Lötgering-Lin and Joachim Gross. "Group Contribution Method for Viscosities Based on Entropy Scaling Using the Perturbed-Chain Polar Statistical Associating Fluid Theory". In: *Ind. Eng. Chem. Res., 54, 79427952* (2015).

[28] M. Onofri M. Pizzarelli F. Nasuti. "CFD analysis of transcritical methane in rocket engines cooling channels". In: *J. Supercrit. Fluids 62, 79–87* (2012).

[29] D.Banuti M.Raju M.Ihme. "On the characterization of transcritical fluid states". In: *Cent. Turbul. Res. Annu. Res. Briefs , 165–178* (2017).

[30] M.Raju D.Banuti M.Ihme. "Widom Lines in Binary Mixtures of Supercritical Fluids". In: *Sci Rep 7, 3027* (2017).

[31] M.Michelsen and R.Heidemann. "Calculation of critical points from cubic two-constant equations of state". In: *AIChE Journal, 3, 521-523* (1981).

[32] G.Simeoni T.Bryk F.Gorelli M.Santoro. "The Widom Line as the crossover between liquid-like and gas-like behaviour in supercritical fluids". In: *Nature Phys 6, 503–507* (2010).

[33] Jonas Mairhofer. "A Residual Entropy Scaling Approach for Viscosity Based on the GERG-2008 Equation of State". In: *Ind. Eng. Chem. Res., 60, 26522662* (2021).

[34] Vânia Maria et al. "Carbon Dioxide Use in High-Pressure Extraction Processes Provisional chapter Carbon Dioxide Use in High-Pressure Extraction Processes". In: 2018. DOI: 10.5772/intechopen.71151.

[35] MATLAB. *9.9.0.1467703 (R2020b)*. Natick, Massachusetts: The MathWorks Inc., 2020.

[36] Fisher Michael E. and B. Widom. "Decay of Correlations in Linear Systems". In: *The Journal Of Chemical Physics, Vol.50, number 9* (1969).

[37] A.Zizin N.A Slavinskaya and A.M. "On model Design of a Surrogate Fuel Formulation". In: *J.Eng. Gas Turbines Power, 132, 11, 111501* (2010).

[38] Origin(Pro). "Version 2021b". In: *OriginLab Corporation, Northampton, MA, USA* (2021).

[39] Ding-Yu Peng and Donald B. Robinson. "A New Two-Constant Equation of State". In: *Ind. Eng. Chem. Fundamen., 15, 1, 59–64* (1976).

[40] A.R. Janzen Philip D. Neufeld and R.A. Aziz. "Empirical Equations to Calculate 16 of the Transport Collision Integrals $\Omega^{(l,s)*}$ for the Lennard-Jones (12-6) Potential". In: *J. Chem. Phys. 57, 1100; https://doi.org/10.1063/1.1678363* (1972).

[41] R. B. Stewart R. T. Jacobsen and M. Jahangiri. "A thermodynamic property formulation for nitrogen from the freezing line to 2000 K at pressures to 1000 MPa". In: *International Journal of Thermophysics, 7, 3, 503-511* (1986).

[42] V. V. Brazhkin Yu. D. Fomin A. G. Lyapin V. N. Ryzhov and K. Trachenko. "Two liquid states of matter: A dynamic line on a phase diagram". In: *Physical Review E 85, 031203* (2012).

[43] Lloyd L. Lee Ting-Horng Chungó Mohammad Ajlan and Kenneth E. Starling. "Generalized Multiparameter Correlation for Nonpolar and Polar Fluid Transport Properties". In: *Ind. Eng. Chem. Res., 27, 671-679* (1988).

[44] O.A. Hougen K.M. Watson. *Chemical Process Principles*. Wiley, 1952.

[45] NIST Chemistry WebBook. "NIST Standard Reference Database". In: *National Institute of Standards and Technology, Gaithersburg, MD, USA* (2016).

[46] C.R. Wilke. "A Viscosity Equation for Gas Mixtures". In: *J. Chem. Phys. 18, 517* (1950).

[47] Rosenfield Y. "Relation between the transport coefficients and the internal entropy of simple systems." In: *Phys. Review A,15, 25452549.* (1977).

[48] K. Yamada Y. Suehiro M. Nakajima and M. Uematsu. "Critical parameters of xCO2+ (1 x)CHF3 forx= (1.0000, 0.7496, 0.5013, and 0.2522)". In: *The Journal of Chemical Thermodynamics, 28, 10, 1153-1164* (1996).